B V RAJU COLLEGE

VISHNUPUR

BHIMAVARAM

FACULTY RESEARCH PUBLICATIONS

ACADAMIC YEAR 2021-22

INDEX

JETIR.ORG ISSN: 2349-5162 | ESTD Year : 2014 | Monthly Issue

JOURNAL OF EMERGING TECHNOLOGIES AND INNOVATIVE RESEARCH (JETIR)

An International Scholarly Open Access, Peer-reviewed, Refereed Journal

Breaking a Stick to form a Polygon with Positive Integers using Python

[1]S N R G BHARAT IRAGAVARAPU, [2]SATYA VAMSI KUMAR APPALA

[1]Assistant Professor, [2]Lecturer

[1] Department of Mathematics, [2] Computer science department

[1]Gayatri Vidya Parishad College of Engineering (Autonomous), Visakhapatnam, India

[2]B V Raju College, Vishnupur, Bhimavaram, India.

Abstract: In this paper, using a computer programming language, we determine the number of polygons (e.g. triangle/pentagon/decagon etc.) that can be formed by using a stick of given length say n units, n being a positive integer greater than 2.

Keywords **- Triangle Inequality, Polygon, Inequality Condition, Python**

I. INTRODUCTION

In [1, 2, 3, and so on] we formed a triangle, quadrilateral and pentagon, etc. through breaking a stick using programming language. In this paper, by using Python language we form all possible polygons by generalizing with positive integers through breaking stick, for any such n. For example, suppose we take a stick of length 15 units and cut this stick at 5 places to form 6 parts of the stick. Let a, b, c, d, e, f be the lengths of the six parts of the stick and assume that a, b, c, d, e, f are positive integers. Hence we have the basic relation a + b + c+ d + e + f = n. Here number n is given but a, b, c, d, e, f are variable numbers. For formation of a hexagon having side lengths a, b, c, d, e, f we need to see that the condition a + b + c + d + e > f and f is the largest side length compare to others i.e. the sum of the remaining side lengths is greater than the largest side length. Here (a, b, c, d, e, f) = (b, c, d, e, f, a) = (c, d, e, f, a, b) = (d, e, f, a, b, c) = (e, f, a, b, c, d) = (f, a, b, c, d, e).

This is very difficult if the numbers of our selection are considerably large. Now our aim is to form any polygon with Positive Integers using Python language

II. MAIN RESULT

2.1Algorithm

Step 1: start
Step 2: import combinations and chain modules from itertools package
Step 3: Read the length of the stick
Step 4: Read number of parts you want to breakdown stick
Step 5: Find possible permutations and combinations (where permutations and combinations == no of parts+1) which equals to stick length.
Step 6: consider only the combinations list after removing permutations from the list.
Step 7: Each side in the combinations list can form a valid polygon or not by checking some of the conditions like
a. Sum of n-1 sides is greater than nth side
b. nth side should be greater than all other sides
return the sides which satisfy above conditions
Step 8: print number of polygons that can be formed and their possible sides.
Step 9: stop

2.2 Python program

```
from itertools import combinations, chain
length = int(input("Enter the stick length:"))
# length = int(length)
parts = int(input("Enter number of parts you want to breakdown stick:"))
# parts = int(parts)
def perm_comb(n):
    """
    :param n:
    :return: a list of permutations and combinations of values equal to n
    Generate the series of +ve integer lists which sum to a +ve integer, n.
    """
    from operator import sub
    b, mid, e = [0], list(range(1, n)), [n]
    splits = (d for i in range(n) for d in combinations(mid, i))
    return (list(map(sub, chain(s, e), chain(b, s))) for s in splits)
perm_comb_lst = []
for p in perm_comb(length):
    """
    possible permutations and combinations(where permutations and combinations == no of parts+1) which equals to stick length
    :return: permutations and combinations list
    """
    if len(p) == parts+1:
        perm_comb_lst.append(p)
def remove_perm(perm_comb_lst):
    """
    :return: combinations list
    """
    return([list(i) for i in {*[tuple(sorted(i)) for i in perm_comb_lst]}])
comb_lst = remove_perm(perm_comb_lst)
# print("combinations list having length equals to no of parts+1 is :\n", comb_lst)
def check_valid_polygon(sides):
    """
    each side in the comb_lst can form a valid polygon or not by checking some of the conditions like
        a. Sum of n-1 sides is greater than nth side
        b. nth side should be greater than all other sides
    :return: sides which satisfy above conditions
    """
    try:
        for side in sides:
            other_sides = (sum(sides) - side)
            if side > other_sides:
                return ''
            elif side == other_sides:
                return ''
        else:
```

```
        # print("sides in check polygon",sides)
        last_element = sides[len(sides)-1]
        last_element_index=len(sides)
        for i in sides[0:last_element_index-1]:
            if last_element > i:
                flag = True
                pass
            else:
                flag = False
                break
        if flag == True:
            return sides
        else:
            return ''
        return sides
    except Exception as err:
        raise err
sides = comb_lst
res_list = []
for i in sides:
    res_list.append(check_valid_polygon(i))
print("Response list is", res_list)
polygon_list=[]
for i in res_list:
    if i != '':
        polygon_list.append(i)
    else:
        continue;
print("No of polygons that can be formed are: " + str(len(polygon_list)) + " and their sides list are:\n", polygon_list)
```

2.2 Result analysis

We are required to display all the combinations that follow the polygon inequality. This can be achieved with help of the following steps.
Step 1: Write all permutations in form of triads for a given integer.
Step 2: Eliminate equivalent permutations so that only the combinations remain.
Step 3: Display only the combinations that satisfy the triangle inequality.
The above procedure can be explained below:

For example,

- Consider a stick length 12.
- Let the combinations are (1, 1, 1, 1, 3, 5), (1, 1, 1, 2, 2, 5), (1, 1, 1, 2, 3, 4), (1, 1, 2, 2, 2, 4), (1, 2, 2, 2, 2, 3).
- The total number of hexagons with stick length 12 are 5

We can represent this result in outputs

2.3 Outputs

We will get different outputs for different stick lengths.

Output-1

Enter the stick length:12

Enter number of parts you want to breakdown stick: 5

No of polygons that can be formed are: 5 and their sides list are:

[[1, 1, 1, 2, 3, 4],
[1, 1, 2, 2, 2, 4],
[1, 1, 1, 1, 3, 5],
[1, 1, 1, 2, 2, 5],
[1, 2, 2, 2, 2, 3]]

By using above combinations we can form a hexagon.

Output-2

Enter the stick length: 12
Enter number of parts you want to breakdown stick:4
No of polygons that can be formed are: 6 and their sides list are:

[[1, 1, 1, 4, 5],
[1, 1, 2, 3, 5],
[1, 1, 3, 3, 4],
[1, 2, 2, 2, 5],
[1, 2, 2, 3, 4],
[2, 2, 2, 2, 4]]

By using above combinations we can form a pentagon

Output-3

Enter the stick length:25

Enter number of parts you want to breakdown stick:2

No of polygons that can be formed are: 12 and their sides list are:

[[8, 8, 9],
[6, 8, 11],
[7, 7, 11],
[6, 9, 10],
[4, 9, 12],
[6, 7, 12],
[5, 9, 11],
[5, 8, 12],
[7, 8, 10],
[3, 10, 12],
[2, 11, 12],
[4, 10, 11]]

By using above combinations we can form a triangle.

III. CONCLUSION

By using this program, we can easily find the number of polygons that can be formed through breaking a stick using python, it becomes novel and easy process.

REFERENCES

[1] S.N.R.G.Bharat Iragavarapu, M.Anuraag Chandra 2016. Breaking a Stick to form a triangle, Journal of Computational Mathematics and Ap-plied Mathematics, Mantech Publications 1,(1), 1-10.

[2] S.N.R.G.Bharat Iragavarapu, J. kushwanth, 2017. Formation of a Integer Quadrilateral through Breaking a Stick, International Journal of Innovative research and Advanced Studies, 4(3): 350-352.

[3] S.N.R.G.Bharat Iragavarapu, Chandolu Somarjun, 2017.Breaking a Stick to form a Hexagon with Positive Integers using Programming Language Python, International Research Journal of Engineering and Technology (IRJET), 4(8): 95-97.

[4] S.N.R.G.Bharat Iragavarapu, Konathala Chetan, 2017. Breaking a Stick to form a Nonagon with Positive Integers using Programming Language MATLAB, International Research Journal of Engineering and Technology (IRJET), 4(9): 37-40.

Publications

Available Online

J. Sci. Res. **14** (3), 931-941 (2022)

JOURNAL OF SCIENTIFIC RESEARCH

www.banglajol.info/index.php/JSR

Excess Thermodynamic Properties of Binary Mixtures of Dimethyl Malonate with some Branched Alkanols

K. P. Krishna[1,5], P. B. Sandhyasri[2], K. Anitha[3], G. R. Babu[1], K. R. Kumar[4], R. R. Raju[1*]

[1]Department of Chemistry, AcharyaNagarjuna University, Nagarjunanagar, Gunturu-522510, AP, India

[2]Department of Physics, Govt. Degree College, Avanigadda -521121, AP, India

[3]Department of Chemistry, Sri Krishna Devaraya University, Ananthapur-515003, AP, India

[4]Department of Chemistry, Vasavi College of Engineering, Hyderabad-500031, Telangana, India

[5]Department of M.Sc Chemistry, B.V. Raju College, Bhimavaram-534201, AP, India

Received 1 February 2022, accepted in final revised form 16 June 2022

Abstract

The intermolecular hydrogen bond interactions in the dimethyl malonate with some branched alkanols (2-methyl-1-propanol, 2-propanol, and 2-butanol) binary mixture have been studied experimentally and theoretically. The ultrasonic velocities U, densities ρ of binary mixtures of dimethyl malonate with 2-methyl-1-propanol, 2-propanol, 2-butanol from 303.15 K to 318.15 K were measured. Excess molar volume (V^E), deviation in adiabatic compressibility ($\Delta\beta_{ad}$) and excess intermolecular free length (L_f^E) have been calculated from the measured experimental data. It is observed that the order of interactions in dimethyl malonate – branched alkanols mixtures is 2-methyl-1-propanol > 2-propanol > 2-butanol.

Keywords: Dimethyl malonate; Branched alcohols; Deviation in adiabatic compressibility; Excess molar volumes; Excess intermolecular free lengths.

doi: http://dx.doi.org/10.3329/jsr.v14i3.57976 J. Sci. Res. **14** (3), 931-941 (2022)

1. Introduction

Optical and ultrasonic techniques have been used to investigate complex formations in liquid mixtures. The formation of hydrogen bonds in solutions and their impact on mixture physical characteristics have gotten much attention. Even though many experimental and theoretical investigations have been conducted to understand hydrogen bonding better, it is still a topic of current research. Theoretical and process design considerations necessitate knowledge of the physicochemical properties of liquid mixes generated by two or more components linked by hydrogen bonds. Volumetric features of

* *Corresponding author*: rrraju1@gmail.com

these mixes are key sources of information for characterization of the interactions between the components and for comprehending the liquid state theory from a theoretical standpoint. Furthermore, alcohols and amines are frequently employed in various industrial and consumer applications; thus, understanding their physical properties is crucial from a practical standpoint. The liquids used in this study were chosen because of their industrial significance. Dimethyl malonate is employed as a reagent in the manufacturing of barbiturates, artificial flavorings, vitamin B1, and vitamin B6. Alcohols are employed as hydraulic fluids in pharmaceuticals and cosmetics, as well as in animal remedies, perfumes, paint removers, flavors, and dyestuffs, as well as for defrosting and antibacterial purposes.

We report here the excess molar volume V^E, Deviation in adiabatic compressibility $\Delta\beta_{ad}$ and excess intermolecular free length L_f^E of the binary systems: dimethyl malonate with (2-propanol, 2-butanol, and 2-methyl-1-propanol). These findings have been used to analyze the branching effect in the alkanol and hydroxyl group's position in the interaction with the dimethyl malonate in terms of hydrogen bonding and dipole-dipole interaction. According to a literature review, these parameters are not provided for the selected systems.

The goal of this study was to see how the position of an alcohol molecule's -OH group affects the sign and amplitude of numerous thermodynamic functions when mixed with dimethyl malonate. Recently, substantial research work has been reported on the excess properties of 2-butanol + Monoethanol amine [1], Formamide + 1-propanol, 2-propanol, 1-butanol, 2-methyl-1-propanol [2], 2-propanol + *n*-alkanes (C6-C10) systems [3], nitro methane with 2-propanol, 2-butanol and 2-pentanol [4], benzyl alcohol with 1-butanol, 2-butanol, 2-methyl-1-butanol and 30-butanol [5] butyl acetate with 2-propanol, 2-butanol and 2-pentanol [6], N-propylamine + 2-alkanols (2-propanol, 2-butanol, 2-pentanol) [7], aniline and nitro benzene with 2-methyl-1-propanol [8] and N,N-dimethylformamide with 2-butanol and 2-pentanol [9]. In terms of hydrogen bonding, dipole-dipole interaction, proton-acceptor interaction, and dispersive forces, the findings have been utilized to explain the nature of the interaction between dissimilar molecules.

2. Experimental Techniques

2.1. *Material and methods*

Using a single crystal variable-path multi-frequency ultrasonic interferometer operating at 3 MHz, the ultrasonic velocities in pure liquids and in their binary mixtures were measured. Using conductivity water, the double-arm pycnometer is optimized with as density of 995.61 kg m^{-3} at 303.15 K. To hold the temperature constant, a thermostat with an accuracy of ±0.01 K is used. The weighings are carried out using the digital balance of Mettler Toledo (Switzerland make) ABB5-S /FACT with a precision of ±0.01 mg. The liquid samples; (dimethyl malonate, 2-propanol, 2-methyl-1-propanol, 2- butanol) used for the present investigation are of analytical grade quality, obtained from Loba chemicals, with > 99 % purity.

2.2. *General procedure*

2.2.1. *Ultrasonic velocity measurement*

In the cell, which is mounted on the pedestal, the liquid mixture in which the ultrasonic speed must be overcome is taken. The micrometer head is gradually shifted so that the reflector is as far away from the crystal as possible. The reflector is now gently rotated towards the crystal by gently rotating the micrometer head. The current in the micrometer is highest at a particular location of the reflector. The 0^{th} peak corresponds to this reading. Micrometer readings for the 1^{st}, 2^{nd}, 3^{rd}, 4^{th}, 5^{th}, 6^{th}, 7^{th}, 8^{th}, 9^{th}, and 10^{th} peaks are taken similarly by turning the head in the same direction, removing backlash error. The distance shifted by the reflector for five peaks is calculated by subtracting the micrometer readings corresponding to the 0^{th} and 5^{th} peaks. Similarly, the difference between the readings for the 1^{st} and 6^{th}, 2^{nd} and 7^{th}, and 3^{rd} and 8^{th} peaks are noted, followed by the average value of the distance moved by the reflector for 5 peaks.

2.2.2. *Density measurements*

The density of the liquids was used as one of the purity requirements. The density (ρ) of pure liquids and all liquid mixtures is determined in this study using a 10^5 m^3 double-arm pycnometer at 303.15, 308.15, 313.15, and 318.15 K. At 303.15 K, as described by Nikkam *et al.* [10,11]. The pycnometer is calibrated using conductivity water with a density of 995.61 kg m^3. A moving microscope with a resolution of 0.01 mm records the location of the liquid levels in the two arms of the air bubble-free pycnometer. The density values obtained from triplicate replication at each temperature are repeatable within 2×10^{-1} kg/m^3, with a measurement uncertainty of 2 parts in 10^4 parts. To achieve thermal equilibrium, the pycnometer was placed in the thermostat for 20 min.

3. Result and Discussion

The investigational values of speed of sound and densities, deviation in adiabatic compressibility, excess molar volume, the excess intermolecular free length of liquid mixtures of DMM with 2-methyl-1-propanol, 2-propanol, 2-butanol over the entire composition range expressed in mole fraction X_1 of DMM ($0\leq X_1\leq 1$), at different temperatures, are listed in Table 2. From Table 1, it is clear that experimental values are in strong agreement with the literature values.

Table 1. Comparison of experimental values with literature data at 303.15 K.

Liquid	Ultrasonic velocity (U)m/s		Density (ρ) Kg/m^3	
	Experimental	Literature	Experimental	Literature
Dimethyl malonate	1365.2	1365.2 [12]	1.1423	1.1423[12]
2-Methyl-1-propanol	1104.7	1105.6 [15]	0.7895	0.7902[14]
2- Propanol	1105.0	1115.1 [15]	0.7715	0.7724[16]
2-Butanol	1141.0	1140.5 [13]	0.7936	0.7941[16]

Studying the excess parameters is necessary to substantiate the existence of interaction among the molecules. Excess liquid mixture parameters are used to calculate the deviation from ideality in liquid mixture behavior. The molecular interactions are explained by considering both a positive and a negative contribution of the excess parameters.

The excess values of molar volume (V^E) and intermolecular free length (L_f^E), and deviation in adiabatic compressibility ($\Delta\beta_{ad}$) are shown in Table 2. They are calculated by using the following standard relations:

Excess volume (V^E) : $V^E = \left(V - (V_1X_1 + V_2X_2)\right)$ (1)

Deviation in adiabatic compressibility ($\Delta\beta_{ad}$) : $\Delta\beta_{ad} = \beta_{ad1}X_1 + \beta_{ad2}X_2$ (2)

Excess intermolecular free length (L_f^E) : $L_f^E = L_f - \left(L_{f1}X_1 + L_{f2}X_2\right)$ (3)

Table 2. Ultrasonic velocity (U), density (ρ), deviation in adiabatic compressibility ($\Delta\beta_{ad}$), excess molar volume (V^E) and excess intermolecular free length L_f^E of DMM + 2-M1-P, +2-propanol, +2-butanol systems at 303.15, 308.15, 313.15, and 318.15 K.

Mole fraction X_1	Velocity U m/s	Density ρ gm/cm^3	$\Delta\beta_{ad}$ X10^{-12} m^{2}N^{-1}	V^E cm^3 mol^{-1}	L_f^E Å
2-Methyl-1-propanol					
303.15 K					
0.0000	1111.0	0.7933	0.0000	0.0000	0.0000
0.0824	1125.2	0.8298	-3.6532	-0.1837	-0.0291
0.1680	1140.8	0.8657	-6.5399	-0.2929	-0.0523
0.2572	1158.1	0.9013	-8.7284	-0.3630	-0.0699
0.3500	1177.5	0.9367	-10.2282	-0.4084	-0.0819
0.4469	1199.2	0.9720	-11.0281	-0.4466	-0.0882
0.5479	1223.7	1.0070	-11.0255	-0.4510	-0.0879
0.6534	1251.7	1.0415	-10.0938	-0.4011	-0.0802
0.7637	1283.9	1.0756	-8.1166	-0.3182	-0.0641
0.8791	1321.3	1.1091	-4.8401	-0.1732	-0.0379
1.0000	1365.20	1.1423	0.0000	0.0000	0.0000
308.15 K					
0.0000	1104.7	0.7895	0.0000	0.0000	0.0000
0.0824	1118.9	0.8268	-3.6909	-0.2711	-0.0295
0.1680	1134.3	0.8630	-6.5423	-0.3936	-0.0525
0.2572	1151.3	0.8989	-8.7351	-0.4804	-0.0703
0.3500	1170.1	0.9345	-10.2624	-0.5295	-0.0826
0.4469	1191.4	0.9701	-11.0633	-0.5754	-0.0890
0.5479	1215.5	1.0052	-11.0394	-0.5660	-0.0886
0.6534	1243.0	1.0399	-10.1188	-0.5175	-0.0809
0.7637	1274.1	1.0740	-8.2241	-0.3952	-0.0654
0.8791	1311.2	1.1075	-4.8638	-0.2219	-0.0384
1.0000	1354.50	1.1405	0.0000	0.0000	0.0000
313.15 K					
0.0000	1096.0	0.7853	0.0000	0.0000	0.0000
0.0824	1108.9	0.8230	-3.7020	-0.2923	-0.0299
0.1680	1123.2	0.8598	-6.5497	-0.4686	-0.0531
0.2572	1138.6	0.8960	-8.7419	-0.5542	-0.0710
0.3500	1155.8	0.9321	-10.2901	-0.6266	-0.0838

0.4469	1175.2	0.9680	-11.1208	-0.6750	-0.0906
0.5479	1197.6	1.0035	-11.0520	-0.6647	-0.0900
0.6534	1222.8	1.0383	-10.1618	-0.5808	-0.0826
0.7637	1252.0	1.0728	-8.2623	-0.4651	-0.0669
0.8791	1287.3	1.1069	-4.8894	-0.3039	-0.0393
1.0000	1328.25	1.1396	0.0000	0.0000	0.0000
			318.15 K		
0.0000	1089.5	0.7800	0.0000	0.0000	0.0000
0.0824	1101.7	0.8181	-3.7092	-0.3302	-0.0300
0.1680	1115.2	0.8553	-6.5563	-0.5254	-0.0534
0.2572	1129.4	0.8919	-8.8279	-0.6462	-0.0722
0.3500	1145.6	0.9282	-10.3228	-0.7111	-0.0846
0.4469	1163.8	0.9645	-11.1586	-0.7685	-0.0916
0.5479	1185.0	1.0006	-11.1087	-0.7898	-0.0913
0.6534	1209.0	1.0359	-10.2105	-0.7278	-0.0838
0.7637	1236.8	1.0707	-8.2927	-0.5977	-0.0679
0.8791	1270.4	1.1045	-4.9020	-0.3699	-0.0399
1.0000	1309.65	1.1370	0.0000	0.0000	0.0000
			2-Propanol		
			303.15 K		
0.0000	1110.0	0.7763	0.0000	0.0000	0.0000
0.0692	1127.7	0.8145	-2.9030	-0.1599	-0.0229
0.1434	1146.6	0.8524	-5.1290	-0.2859	-0.0406
0.2229	1166.9	0.8898	-6.6784	-0.3574	-0.0530
0.3086	1188.7	0.9268	-7.6121	-0.3937	-0.0604
0.4010	1212.3	0.9638	-8.0024	-0.4331	-0.0634
0.5010	1237.9	1.0003	-7.7564	-0.4238	-0.0614
0.6097	1265.6	1.0364	-6.8791	-0.3791	-0.0543
0.7281	1295.8	1.0719	-5.3026	-0.2750	-0.0416
0.8576	1328.9	1.1070	-3.0060	-0.1294	-0.0235
1.0000	1365.2	1.1423	0.0000	0.0000	0.0000
			308.15 K		
0.0000	1105.0	0.7715	0.0000	0.0000	0.0000
0.0692	1122.3	0.8105	-3.0475	-0.2231	-0.0241
0.1434	1140.8	0.8489	-5.3316	-0.3753	-0.0424
0.2229	1160.6	0.8865	-6.8956	-0.4538	-0.0549
0.3086	1182.0	0.9239	-7.8518	-0.5052	-0.0625
0.4010	1205.0	0.9615	-8.2795	-0.5730	-0.0659
0.5010	1230.0	0.9982	-8.0110	-0.5582	-0.0637
0.6097	1257.1	1.0342	-7.0441	-0.4649	-0.0559
0.7281	1286.7	1.0700	-5.4407	-0.3524	-0.0430
0.8576	1319.0	1.1052	-3.0911	-0.1802	-0.0243
1.0000	1354.5	1.1405	0.0000	0.0000	0.0000
			313.15 K		
0.0000	1097.0	0.7676	0.0000	0.0000	0.0000
0.0692	1113.0	0.8073	-3.1973	-0.2838	-0.0255
0.1434	1130.2	0.8462	-5.5461	-0.4630	-0.0444
0.2229	1148.6	0.8840	-7.1091	-0.5388	-0.0571
0.3086	1168.4	0.9219	-8.0990	-0.6138	-0.0652
0.4010	1189.8	0.9597	-8.4917	-0.6698	-0.0684
0.5010	1213.0	0.9963	-8.1460	-0.6167	-0.0656
0.6097	1238.1	1.0329	-7.1991	-0.5486	-0.0579
0.7281	1265.5	1.0689	-5.5510	-0.4183	-0.0446

0.8576	1295.5	1.1049	-3.2358	-0.2813	-0.0259
1.0000	1328.5	1.1396	0.0000	0.0000	0.0000
			318.15 K		
0.0000	1090.0	0.7625	0.0000	0.0000	0.0000
0.0692	1105.2	0.8027	-3.3071	-0.3271	-0.0264
0.1434	1121.5	0.8418	-5.6934	-0.5187	-0.0457
0.2229	1139.0	0.8803	-7.3458	-0.6426	-0.0593
0.3086	1157.8	0.9183	-8.3145	-0.7077	-0.0673
0.4010	1178.1	0.9562	-8.6779	-0.7519	-0.0704
0.5010	1200.0	0.9934	-8.3606	-0.7262	-0.0679
0.6097	1223.9	1.0300	-7.3547	-0.6299	-0.0597
0.7281	1249.9	1.0667	-5.7428	-0.5387	-0.0466
0.8576	1278.4	1.1025	-3.3265	-0.3419	-0.0269
1.0000	1309.7	1.1370	0.0000	0.0000	0.0000
			2-Butanol		
			303.15 K		
0.0000	1150.0	0.7984	0.0000	0.0000	0.0000
0.0819	1167.6	0.8342	-2.0037	-0.1567	-0.0155
0.1671	1186.0	0.8695	-3.4670	-0.2579	-0.0269
0.2560	1205.1	0.9045	-4.4598	-0.3240	-0.0347
0.3486	1225.0	0.9396	-5.0648	-0.3905	-0.0394
0.4453	1245.8	0.9744	-5.2526	-0.4281	-0.0409
0.5463	1267.6	1.0087	-5.0015	-0.4134	-0.0390
0.6519	1290.3	1.0427	-4.3570	-0.3693	-0.0340
0.7625	1314.1	1.0762	-3.2926	-0.2746	-0.0256
0.8784	1339.0	1.1091	-1.7981	-0.1211	-0.0140
1.0000	1365.2	1.1423	0.0000	0.0000	0.0000
			308.15 K		
0.0000	1141.0	0.7936	0.0000	0.0000	0.0000
0.0819	1158.5	0.8300	-2.0887	-0.2111	-0.0162
0.1671	1176.7	0.8659	-3.6148	-0.3553	-0.0282
0.2560	1195.6	0.9014	-4.6386	-0.4459	-0.0363
0.3486	1215.4	0.9367	-5.2217	-0.5037	-0.0409
0.4453	1236.1	0.9720	-5.4356	-0.5623	-0.0426
0.5463	1257.6	1.0066	-5.1747	-0.5438	-0.0406
0.6519	1280.2	1.0406	-4.4722	-0.4614	-0.0351
0.7625	1303.8	1.0743	-3.3820	-0.3474	-0.0265
0.8784	1328.5	1.1074	-1.8685	-0.1767	-0.0146
1.0000	1354.5	1.1405	0.0000	0.0000	0.0000
			313.15 K		
0.0000	1137.5	0.7896	0.0000	0.0000	0.0000
0.0819	1153.1	0.8266	-2.2617	-0.2612	-0.0176
0.1671	1169.4	0.8630	-3.9071	-0.4428	-0.0305
0.2560	1186.3	0.8987	-4.9504	-0.5248	-0.0388
0.3486	1204.0	0.9345	-5.5880	-0.6099	-0.0439
0.4453	1222.5	0.9700	-5.7794	-0.6588	-0.0455
0.5463	1241.7	1.0046	-5.4444	-0.6045	-0.0430
0.6519	1261.9	1.0391	-4.7212	-0.5305	-0.0373
0.7625	1283.0	1.0730	-3.5654	-0.4011	-0.0282
0.8784	1305.1	1.1070	-2.0592	-0.2737	-0.0163
1.0000	1328.3	1.1396	0.0000	0.0000	0.0000
			318.15 K		
0.0000	1132.4	0.7845	0.0000	0.0000	0.0000

0.0819	1146.9	0.8221	-2.4187	-0.3224	-0.0188
0.1671	1162.0	0.8587	-4.1089	-0.5102	-0.0320
0.2560	1177.8	0.8950	-5.2471	-0.6397	-0.0411
0.3486	1194.2	0.9308	-5.8531	-0.7008	-0.0460
0.4453	1211.3	0.9665	-6.0279	-0.7422	-0.0476
0.5463	1229.3	1.0017	-5.7271	-0.7213	-0.0453
0.6519	1248.0	1.0363	-4.9588	-0.6319	-0.0394
0.7625	1267.6	1.0709	-3.8130	-0.5320	-0.0303
0.8784	1288.1	1.1047	-2.1848	-0.3415	-0.0174
1.0000	1309.7	1.1370	0.0000	0.0000	0.0000

4. Discussion

There is interdependence between the intermolecular free length and ultrasonic velocity. As a consequence of combining materials, the ultrasonic velocity decreases if the intermolecular free length increases or vice versa. This is found for DMM + 2-methyl-1-propanol, DMM + 2-propanol, and DMM + 2-butanol systems in the present investigation. With an increase in temperature, we also see a drop in velocity due to splitting hetero and homo molecular clusters.

In a binary liquid mixture, the relative degree of expansion or contraction is responsible for the sign of(V^E). In this investigation, the V^E values for all binary mixtures of DMM with sub-alkanols are negative over the entire composition spectrum and are shown in Figs. 1A, 1B, and 1C. The negative V^E values suggest that volume contraction occurs when dimethyl malonate is combined with sub-alkanols due to the formation of hydrogen bonds between different molecules.

The negative algebraic V^E values of dimethyl malonate with alkanols fell in the order of: 2-methyl-1-propanol>2-propanol>2-butanol 2-methyl-1-propanol has two $–CH_3$ groups on its -carbon atom; hence its negative V^E value grows as the number of $–CH_3$ groups increases [17]. V^E plots against mole fractions are of parabolic shape characterized by well-defined minima occurring at around 0.5 mole fractions suggesting the existence of complex formation.

Deviation in adiabatic compressibility is observed to be negative over the mole fraction of DMM from Figs. 2A, 2B, and 2C, indicating the existence of strong interactions among the molecules. As a consequence of molecular interaction between the component molecules in the liquid mixtures, the sign, and magnitude of $\Delta\beta_{ad}$ play a vital role in determining molecular structure. The negative $\Delta\beta_{ad}$ in the studied mixtures can be explained by hydrogen bonding between the oxygen atom of dimethyl malonate and the hydrogen atom of the hydroxyl group of 2-alkanol molecules based on the complex formation between dimethyl malonate and 2-alkanol molecules. This is in line with the view put forward by Fort and Moore [18] that liquids of different molecular sizes typically combine with volume decreases that yield negative values in intermolecular free length, adiabatic compressibility.

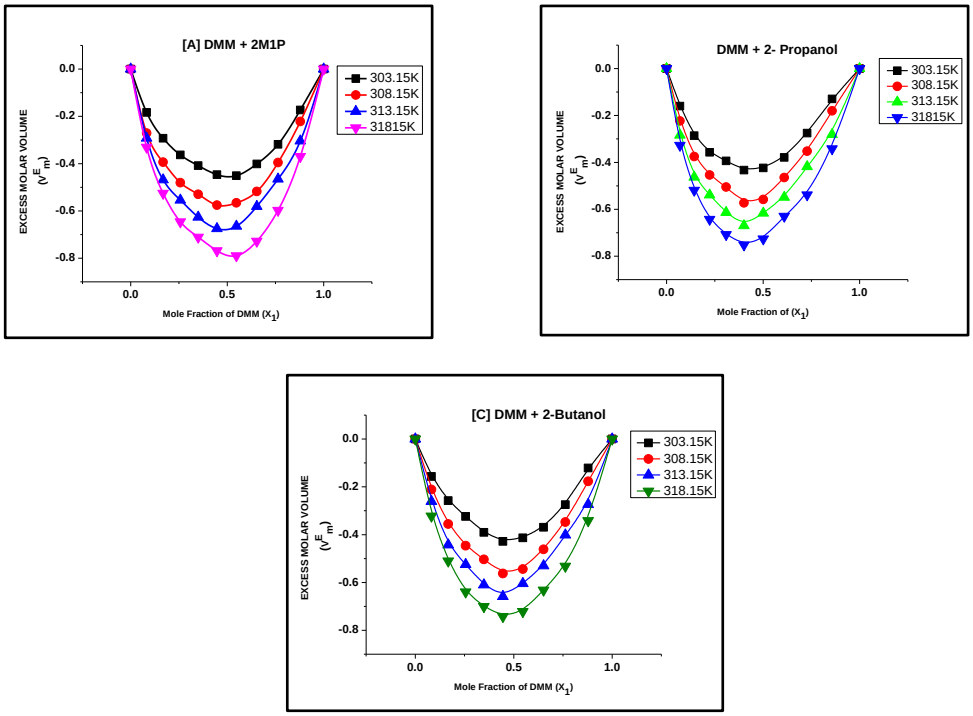

Fig. 1. Variation of excess molar volume with the mole fraction of DMM for the systems [A] DMM + 2-M1-P, [B] DMM + 2-propanol and [C] DMM + 2-butanol.

According to Jacobson, the intermolecular free length refers to the distance among the surfaces of neighboring molecules [19]. Due to the mixing phase, an increase in free length contributes to a decrease in sound velocity. This implies that free duration is the primary factor in evaluating the essence of the variance of ultrasonic velocity in the liquid mixture. Even the structural changes are observed to affect the intermolecular free length variation. Figs. 3A, 3B, and 3C show the variance of excess intermolecular free length for the whole dimethyl malonate composition spectrum for the three systems under analysis. The negative L_f^E values suggest that the sound wave has a longer distance to travel [20]. It is due to the prevailing existence of interactions among molecules that are not identical. The occurrence of β_{ad} and L_f^E minima at the same concentrations confirms the occurrence of molecular interactions [21].

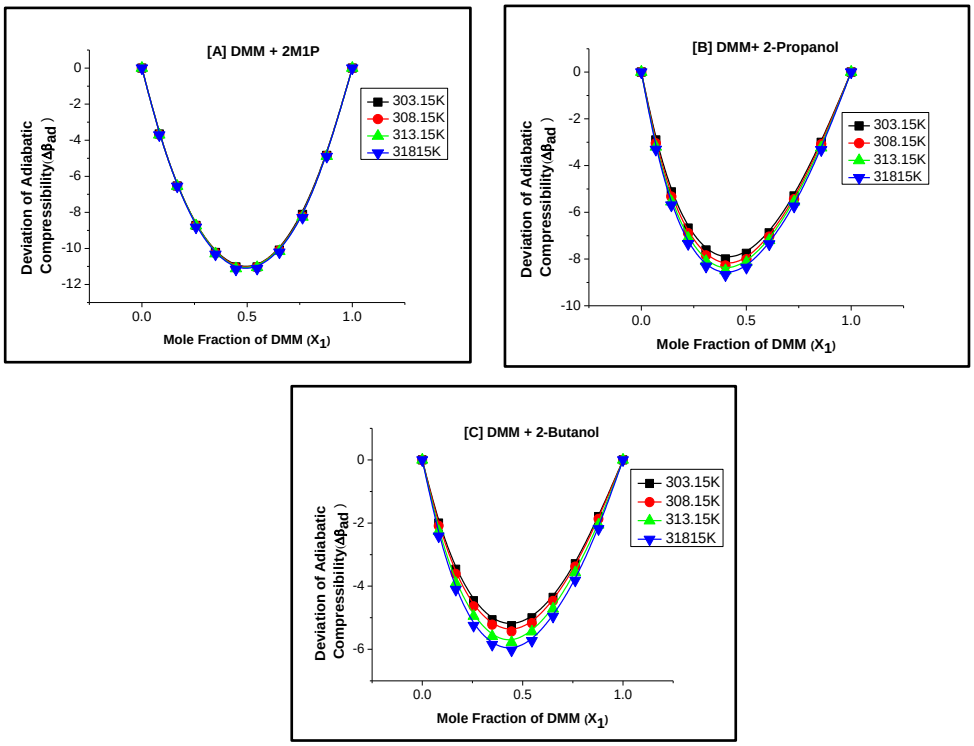

Fig. 2. Variation of Adiabatiac Compressibility with the mole fraction of DMM for the systems [A] DMM + 2-M1-P , [B] DMM + 2-propanol and [C] DMM + 2-butanol.

DMM is a substance that is polar and linked to it. Sub Alkanols are polar liquids, closely connected by hydrogen bonding to the degree of polymerization, which may vary depending on the OH group, temperature, chain length, and location. The probability of intramolecular hydrogen bonding within 2-alcohol molecules and their property to bind hydrogen bonds with other molecules generates fascinating solution behavior. When mixing certain highly-associated alcohols with extremely polar solvents, the H-bonds break, and complicated interactions ensue. When describing the interaction between DMM and alkanol mixtures, it is crucial to consider the length of the alkanol chain and the position of the alkanol hydroxyl group. The order of strong interaction in binary liquids between the component molecules is as follows: DMM + 2-methyl-1-propanol > DMM + 2-propanol > DMM + 2-butanol. The intensity increase of the temperature interaction is as follows: (303.15<308.15<313.15<318.15) K.

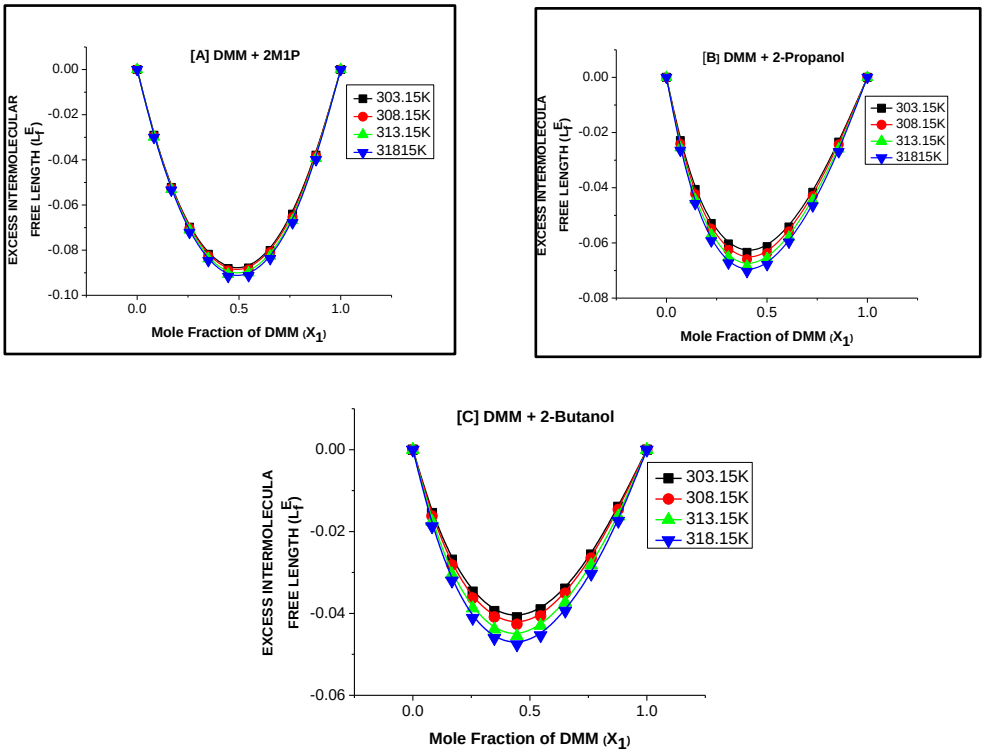

Fig. 3. Variation of Intermolecular Free length with the mole fraction of DMM for the systems [A] DMM + 2-M1-P, [B] DMM +2-propanol and [C] DMM + 2-butanol.

5. Conclusion

The ultrasonic velocities and densities (at 303.15, 308.15, 313.15, and 318.15 K) have been determined over the entire composition range for the binary mixtures of dimethyl malonate with 2-methyl-1-propanol, 2-propanol, and 2-butanol. From the experimental data, deviation in adiabatic compressibility, excess molar volume, and intermolecular free length has been calculated. The excess values and deviations are observed to be negative for all the mixtures at all the temperatures studied. This indicates there exists strong interactions among the binary mixtures.

References

1. W. -L. Weng, J. Chem. Eng. Data, **44**, 63 (1999). https://doi.org/10.1021/je980104d
2. R. Vadamalar, D. Mani, and R. Balakrishnan, Res. J. Chem. Sci. **19**, 79 (2011).
3. O. Redlich and A. T. Kister, Ind. Eng. Chem. **40**, 345 (1948). https://doi.org/10.1021/ie50458a036
4. J. A. Riddick, W. B. Bunger, and T. K. Sakano, Organic Solvents Physical Properties and Method of Purifications (Wiley Interscience, New York, 1986).

5. R. Riggio, H. E. Martinez, and N. Z. De Salas, Can. J. Chem. **70**, 2859 (1992). https://doi.org/10.1139/v92-364
6. A. Krishnaiah and K. N. Surendranath, J. Chem. Eng. Data **41**, 1012, (1996). https://doi.org/10.1021/je950304e
7. B. Jacobson, J. Chem. Phys. **20**, 927 (1952). https://doi.org/10.1063/1.1700614
8. P. S. Nikam, T. R. Mahale, and M Hasan, J. Chem. Eng. Data **43**, 436 (1998). https://doi.org/10.1021/je970253g
9. M. V. P. Rao, Ph. D. Thesis, Sri Venkateswara University, Tirupathi, India (1974).
10. N. A. Dokhe and J. Dokhe, Int. J. Eng. Res. Appl. **11**, 18 (2021).
11. A. Jahan, M. A. Alam, M. Mahbubul, H. Hasan, and S. Akhtar, J. Chem. Chem. Sci. **9**, 115 (2021).
12. K. P. Krishna, P. B. S. Sri, and R. R. Raju. J. Eng. Sci. **11**, 1191 (2020).
13. V. N. S. R. Venkateswararao, P. B. S. Sri, G. R. Satyanarayana, and C. Rambabu, J. Pharm. Chem. Biol. Sci. **5**, 297 (2017).
14. D. G. Prakash and K. Krishan, J. Chem. Eng. Data **61**, 1967 (2016). https://doi.org/10.1021/acs.jced.5b00216
15. R. Sharma, R. C. Thakur, and B. Saini, Asian J. Chem. **28**, 2331 (2016). https://doi.org/10.14233/ajchem.2016.20010
16. D. Archana and S. Mukthar, Int. J. Chem. **46**A, 789 (2007).
17. M. Gowrisankar, P. Venkateswarlu, K. Sivakumar, and S. Sivarambabu, Kor. J. Chem. Eng. **30**, 1131 (2013). https://doi.org/10.1007/s11814-013-0014-y
18. R. Forte and W. R. Moore, Trans Faraday Soc. **62**, 1112 (1966). https://doi.org/10.1039/tf9666201112
19. B. Jacobson, Acta Chem. Scand. **5**, 1214 (1951). https://doi.org/10.3891/acta.chem.scand.05-1214
20. A. M. E. Raj, L. B. Resmi, V. B. Jyothy, M. Jayachandran, and C. Sanjeeviraja, Fluid Phase Equlib. **281**, 78 (2009). https://doi.org/10.1016/j.fluid.2009.04.009
21. M. S. K. Nayeem, M. Kondaiah, K. Sreekanth, and D. K. Rao. Arabian J. Chem. **12**, 3129 (2019). https://doi.org/10.1016/j.arabjc.2015.08.005

Original article International Journal of Dental Materials 2022;4(3) ISSN:2582-2209

Simulations of silicon nanowire sensor and an integrated smart bio-nano sensor

K. K. J. Chakravarthy[1], P. S. Brahmanandam[2,*], D. M. Potukuchi[3], G. Anil Kumar[4], N. S. Subba Rao[5]

[1]Department of Physics, B V Raju College, Vishnupur, Bhimavaram- 534202, India.

[2]Department of Physics, Shri Vishnu Engineering College for Women (A), Vishnupur, Bhimavaram-534202, India.

[3]Department of Physics, JNT University, Kakinada- 533001, India.

[4]School of Renewable Energy and Environment, JNT University, Kakinada-533001, India.

[5]Physics, Govt. Junior College, Tallarevu- 533463, India

Article History

Received *27th July 2022*

Received revised *9th August 2022*

Accepted *15th August 2022*

Available online *25th August 2022*

*Correspondence

P. S. Brahmanandam

Professor,

Department of Physics, Shri Vishnu Engineering College for Women (A), Vishnupur,

Bhimavaram-534202, India.

E-mail: *dranandpotula@svecw.edu.in*

DOI: *http://dx.doi.org/10.37983/IJDM.2022.4302*

Abstract

Background: Simulation-based nano biosensors have been introduced in recent times that will provide a model for the researchers to verify various critical functions of them, which could effectively save time, money, and effort.

Materials and Methods: In this study, we have performed simulations of a silicon nanowire (Si-NW) biosensor, and its various parameters were evaluated. This silicon sensor was designed using the BiosensorLab tool, a simulator from the nanohub website. This paper also presented an Integrated Smart Bio-nano Sensor. The motivation behind this smart sensor was that an incident happened in one of the southern states of India, in the year 2020; the leakage of styrene gas (C_8H_8) from the Polymers industry caused 12 deaths and several people hospitalized. Most people died after they inhaled styrene gas because they thought the pungent smell (of styrene gas) was also part of their kitchen's emissions. This incident prompted us to propose an Integrated Smart Bio-nano Sensor.

Results: The proposed sensor was capable of classifying the origin of sources of emissions dynamically (smart), even under lower concentrations of gas levels (25 ppm) and could alert the habitants in case of untoward danger.

Conclusions: After verifying settling time vs. analyte concentration, the density of captured target molecules concentration with time vs. time, and the signal-to-noise ratio (SNR) of the biosensor in the presence of parasitic molecules vs. receptor density, it was concluded that these three parameters have helped in identifying the characteristics of the proposed bio-nano sensor.

Keywords: Bio-nano Sensors, Volatile Organic Compounds, Integrated Smart Nano sensor, Simulations.

1. Introduction

A biosensor, like any other sensor, is a transducer that converts the biological response to the corresponding electrical signal. Nevertheless, unlike conventional sensors, a biosensor must be highly specific, independent of physical parameters including stirring, temperature, pH, etc. It must also be tiny, bio-degradable, and bio-compatible, which is highly sought after, particularly, in tissue engineering and regenerative medicine [1]. The word biosensor was first coined by Leland C. Clark Jr. [2], an American scientist who is considered the 'Father of Biosensors'. A Clark electrode is a device used to measure oxygen levels in the blood, water, and other liquids.

The combination of nanomaterials and biosensors provides opportunities for building up a new generation of biosensor technologies. Nanomaterials improve mechanical, electro-chemical, optical, and magnetic properties of biosensors and are developing towards single-molecule biosensors with high throughput biosensor arrays. However, because biological molecules have unique structures and properties, it is currently difficult to fully combine these properties with those of nanomaterials and biomolecules to create single-molecule multifunctional nanocomposites, nanofilms, and nanoelectrodes. Other significant challenges for the currently available techniques include processing, characterization, interface issues, the availability of high-quality nanomaterials, tailoring of nanomaterials, and the mechanisms governing the behaviour of these nanoscale composites on the surface of electrodes.

Nano biosensors will play a significant role in combating various grim infections since nanoscience-based materials have different interesting properties than their macro-sized counterparts. Nano-based biosensors would offer excellent avenues as they have unique properties such as enhanced absorption and scattering, relatively profound biocompatibility, facile synthesis [3], and other important characteristics.

In addition, silicon-based biosensors have been recognized as the most relevant sensors to detect DNA, proteins, pH levels, etc. [4]. Various critical features of nano biosensors such as self-powering, re-usability, and long-term stability have been reported in the literature. It has been reported that it has become possible to detect specific sequences of DNA (double-stranded) and RNA (single-stranded) with nanowire biosensors [5]. Kumar and Rao [6] critically evaluated biosensors' physical parameters, including planar biosensors, cylindrical nanowire, nanosphere, extended gate, magnetic particle, pH, and Flexure FET sensors. It was found that the silicon nanowire (Si-NW) average response time is much higher than the ion-sensitive field-effect transistor (ISFET) [7].

Recently, simulation-based nano biosensors were introduced, and they provide a model for the researchers to verify various critical functions. They could effectively save time, money, and effort. This research has, therefore, relied on such simulations to design biosensors. Later, various physical parameters of biosensors were evaluated. This study also proposed an integrated bio-nano sensor.

2. Materials and methods

2.1 Si-NW sensor design

Silicon nanowire sensor was designed using the biosensorLab tool, a simulator from nanoHub.org, developed by the Purdue University (USA) researchers available for research activities at. www.nanoHub.org. Figure 1 depicts a Si-NW sensor. Apart from nanowire (cylindrical) biosensors, there are 'n' of biosensors simulated by researchers from Purdue University, and it is also possible to access various physical parameters of the biosensors. Table 1 shows the different sets of parameters that have been selected for the nanowire sensor simulations.

As far as the nano-based DNA biosensor working principle is concerned, the sensor consists of a field-effect device with a functionalized surface with capture probe (receptor) molecules [8]. If the target molecules diffuse through the solution and reach the so-called field-effect device and get captured by the receptors thereby binding close to the surface. Many biomolecules carry an electrostatic charge under normal physiological conditions. For example, DNA is negatively charged while the net charge of a protein molecule depends on the pH of the solution. The Coulomb interaction between the charge of the target biomolecule and the field device can result in a change in conductivity of the latter and such changes can be measured at the output of the biosensor.

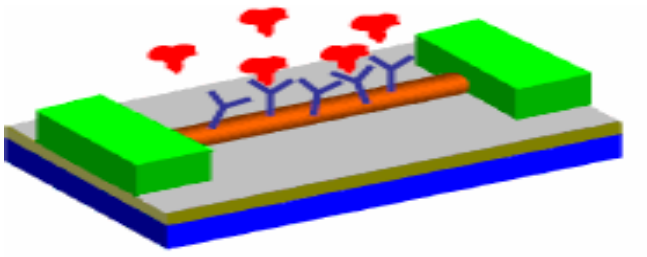

Figure 1. Simulated Si-NW DNA biosensor

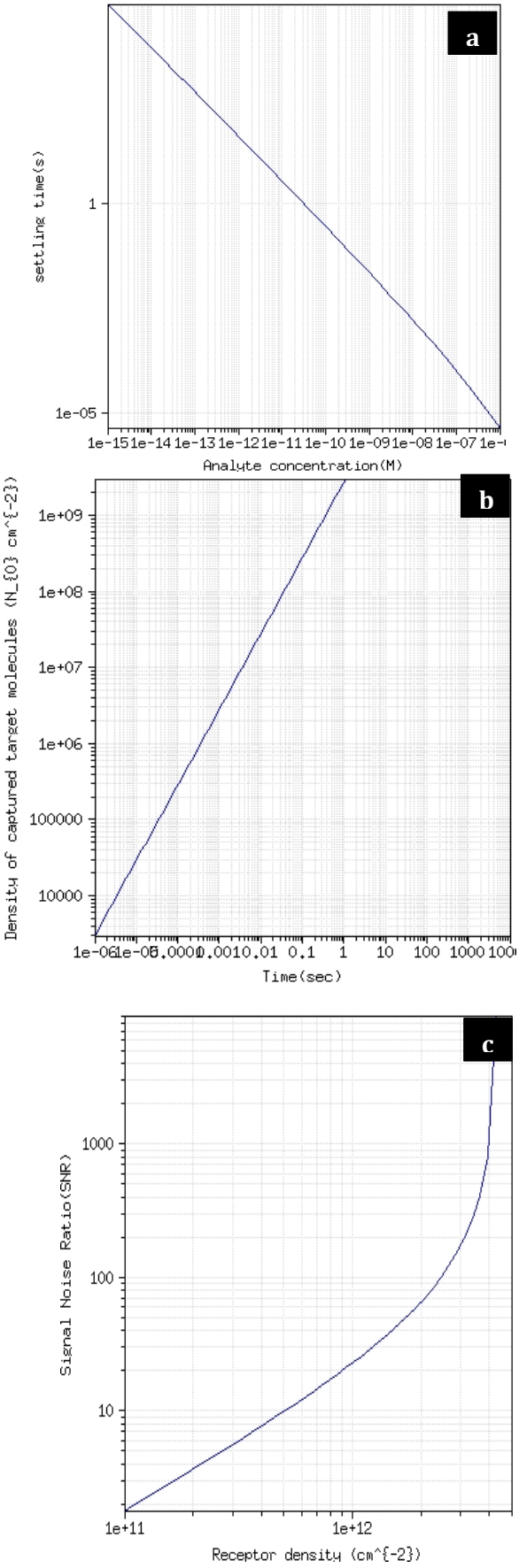

Figure 2. Various physical parameters of the nano biosensor

2.2 Integrated Smart Bio-nano Sensor

Though most of the scientific fraternity is aware of outdoor pollution, which is due to rapid urbanization, indoor pollution would also pose a great threat to the general public. According to the World Health Organization (WHO), the deaths due to both outdoor and indoor pollution are more than double what was documented [9]. Here, we proposed a sensor that can detect three volatile organic components (VOCs including, radon, benzene, and styrene) with higher sensitivity and selectivity, which will, mostly, be used indoors.

3. Results and Discussion

3.1 Si-NW Sensor Design

Based on the experimental model of a nano biosensor, it is required to analyze various properties of the sensor. Figure 2 shows settling time vs analyte concentration (2a), the density of captured target molecules concentration with time vs time (2b), and signal-to-noise ratio (SNR) of the biosensor in the presence of parasitic molecules vs receptor density (2c). These three parameters have helped us in identifying the characteristics of this bio-nano sensor. Further, various iterations (up to 3 steps) of these parameters have been obtained that show the decrease in settling time when concentration increased, and similar trends were also observed in other parameters. The optimum parameters would be, therefore, taken into account in the design of a nanowire-based biosensor.

The simulation of the nanowire sensor has provided a clear view of the pros and cons that would be set as a model for us to overcome various technical glitches while executing a major project. It is also recommended to the scientific community that the scientists at nanoHub have even simulated sensors that might combat recent pandemics i.e., COVID-19, and a serious look at that website may help to create reliable sensors.

3.2 Evaluation of Integrated Smart Bio-nano Sensor

The proposed sensor will consider radon as a template and also choose the radon-related functional device as a monomer, and later Ag-doped LaFeO3 (metal oxide semiconductor perovskite nanomaterial) will be prepared to detect radon gas. Similarly, other gas sensors will be prepared and kept in the same layout, as shown in Figure 3. It can also be observed from the bottom panels of the figures that the response of the sensors in terms of resistivity and concentration. The exciting component concerning this integrated sensor is that it'll have a Field Programmable Gate Array (FPGA), which changes its modus operandi in line with the chaotic state of affairs. The chaotic state of affairs might be an unexpected launch of butane within side the kitchen, risky gas leakage from a chemical factory, and a few unknown stinky chemical emissions.

The large specific surface areas (which increase the interaction between the sensor surface and the surrounding gases), the high porosity, and the useful thickness of the depletion layer are a few advantages of nanomaterials [10]. The proposed sensors work as conventional mere chemiresistive- gas sensors [11]. However, more than a 10-detector array design has already been presented by [12]. But, a sensor that could detect extremely low levels of the emitted gas concentrations has not yet been developed, to the best of the author's knowledge. Nonetheless, an FPGA-type gas sensor (system-on-chip (SoC)) category has already been proposed [13].

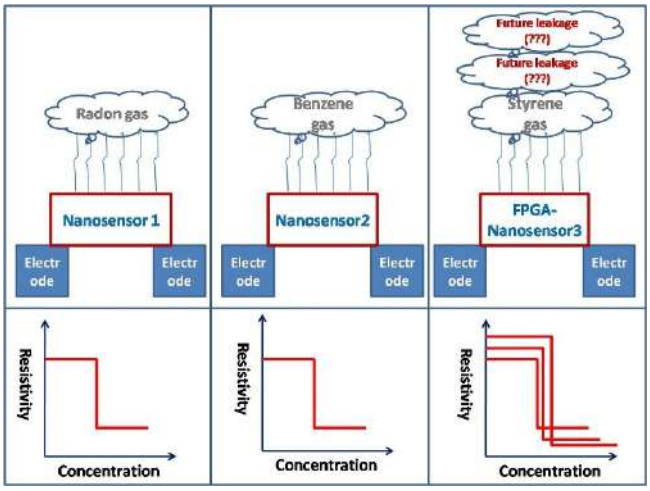

Figure 3. Fabrication schematic of the integrated nano sensor, in which it is also shown an FPGA-based Nano sensor (top right panel), and their responses in terms of resistivity vs concentration.

Figure 4. Dental students working with gas burners in the pre-clinical laboratory.

An unfortunate incident occurred in the early morning hours of 07 May 2020 in one of the southern states of India. There was a leakage of styrene gas from a Polymers firm that led to several deaths and a big number of casualties [14]. Establishing the proposed kind of nano sensors at the industries would be helpful for the early detection of release of any kind of toxic gasses.

These kinds of nano sensors may also be helpful if they are established in dental laboratories, especially in prosthetic labs where large group of students, technicians, and faculty are engaged in making various dental appliances with the usage of gas burners (Figure 4). The leakage of gas may lead to a chaotic situation in the labs. Therefore, this study suggests evaluating the scope of these nano sensors in the dental laboratories.

Future work will be focusing on clarifying the mechanism of interaction between nanomaterials and biomolecules on the surface of electrodes or nanofilms. By using novel properties and emergence of new kind of diseases, it is planned to simulate and later fabricate a new generation of biosensors that could produce results in less time.

4. Conclusion

This study performed simulations of a silicon nanowire biosensor and we also present an Integrated Smart Bio-nano Sensor. The proposed integrated Bio-nano sensor is capable of classifying the origin of sources of emissions dynamically (smart), even under lower concentrations of gas levels (25 parts per million, ppm), and could alert the habitants in case of untoward danger. Various parameters including, settling time vs analyte concentration, the density of captured target molecules concentration with time vs. time and the signal-to-noise ratio (SNR) of the simulated silicon nanowire biosensor have helped in identifying the characteristics of the proposed bio-nano sensor.

Conflicts of interest: Authors declared no conflicts of interest.

Financial support: None

Acknowledgements

The authors to wish to express their sincere gratitude towards the management (Shri Vishnu Educational Society) of Shri Vishnu Engineering College for Women (A), Vishnupur, Bhimavaram, India for their logistic facilities, without which it would have not been possible for us to carry out this work.

References

1. Mehrotra P. Biosensors and their applications–A review. J Oral Biol Craniofac Res. 2016; 6(2):153-9. https://doi.org/10.1016/j.jobcr.2015.12.002
2. Heineman WR, Jensen WB. "Leland C. Clark Jr. (1918–2005)". *Biosensors and Bioelectronics*. 2006; 21 (8):1403–1404. doi:10.1016/j.bios.2005.12.005
3. Burda C, Chen X, Narayanan R, El-Sayed MA. Chemistry and properties of nanocrystals of different shapes. Chemical Reviews. 2005; 105(4):1025-102. https://doi.org/10.1021/cr030063a
4. Zhang GJ, Zhang G, Chua JH, Chee RE, Wong EH, Agarwal A, et al. DNA sensing by silicon nanowire: charge layer distance dependence. Nano Letters. 2008; 8(4):1066-70. https://doi.org/10.1021/nl072991l
5. Ambhorkar P, Wang Z, Ko H, Lee S, Koo KI, Kim K, Cho DI. Nanowire-based biosensors: from growth to applications. Micromachines. 2018; 9(12):679. https://doi: 10.3390/mi9120679
6. Kumar S D R and P V Rao. Modeling and analysis of biosensors for evaluation of its mechanicaland electrical properties. Intl J Nanotechnology Appl. 2017; 11(2):213-35. https://www.ripublication.com/ijna17/ijnav11n3_02.pdf
7. Munna M, Islam MO, Kabiruzzaman M, Mahmood ZH. Performance analysis of a Si-NW biosensor for detection of charged biomolecules. In 2014 International Conference on Informatics, Electronics & Vision (ICIEV) 2014; May 23:1-5. https://doi:10.1109/ICIEV.2014.6850717
8. Nair PR, Alam MA. Design considerations of silicon nanowire biosensors. IEEE Transactions on Electron Devices. 2007; 54(12):3400-8. https://doi: 10.1109/TED.2007.909059
9. Farmer SA, Nelin TD, Falvo MJ, Wold LE. Ambient and household air pollution: complex triggers of disease. Am J Physiol Heart Circ Physiol. 2014; 307(4):H467-76. https://doi:10.1152/ajpheart.00235.2014
10. Kierny MR, Cunningham TD, Kay BK. Detection of biomarkers using recombinant antibodies coupled to nanostructured platforms. Nano Reviews. 2012; 3(1):17240. https://doi:10.3402/nano.v3i0.17240
11. Chiu SW, Tang KT. Towards a chemiresistive sensor-integrated electronic nose: a review. Sensors. 2013; 13(10):14214-47. https://doi.org/10.3390/s131014214
12. Peng DK, Ahmadi AA, Lahann J. A synthetic surface that undergoes spatiotemporal remodeling. Nano letters. 2008; 8(10):3336-40. https://doi.org/10.1021/nl8017669
13. Feng S, Farha F, Li Q, Wan Y, Xu Y, Zhang T, et al. Review on smart gas sensing technology. Sensors. 2019; 19(17):3760. https://doi.org/10.3390/s19173760
14. Naga Sridhar G. Vizag: Gas leak from LG Polymers plant kills 11. The Hindu. https://www.thehindubusinessline.com/news/national/styrene-gas-leaks-from-lg-polymers-in-vizag/article31523261.ece. Accessed on 07.07.2022

How to cite this article: Chakravarthy KKJ, Brahmanandam PS, Potukuchi DM, Anil Kumar G, Subba Rao NS. Simulations of silicon nanowire sensor and an integrated smart bio-nano sensor. Int J Dent Mater. 2022;4(3):58-61. DOI:*http://dx.doi.org/10.37983/IJDM.2022.4302*

Investigation of Sensing Ability of Double-Slot Hybrid Plasmonic Waveguide for Liquid Analyte

Lokendra Singh, Prakash Pareek, Bahija Siddiqui, and Eswara Prasad Konakalla

Abstract This paper focuses on studying the potential of plasmonic technology for sensing liquid analyte. In this work, a double-slot hybrid plasmonic waveguide on SiO_2 substrate layer is considered. The waveguide consists of two narrow slots between metal (silver) and dielectric (silicon) blocks. The width of slots is chosen to facilitate quasi-transverse electric mode. The mode field distribution of proposed waveguide structure with SiO_2 filled slots revealed that this hybrid plasmonic waveguide can serve as a reliable candidate for sensing liquid analyte effectively. Effective mode area for propagating optical signal is obtained as 0.025 per square at operating wavelength of 1550 nm. Moreover, peak sensitivity of 910 nm/RIU was achieved for 150 nm thick liquid and 300 nm thick silicon filled slots.

Keywords Plasmonic waveguide · Effective mode area · Optical sensors · Optical energy · Sensitivity

1 Introduction

Nowadays, an increase in the requirement as well as feasibility of compact devices with low power consumption and broad bandwidth is the reason for the origin of photonic integrated circuits (PICs) [1]. In this perspective, to allow the device integration on nanoscales, for the confinement and better results, beyond the diffraction limit is one of the prime issues in the current scenario [2, 3].

L. Singh · B. Siddiqui
Department of Electronics and Communication Engineering, Koneru Lakshmaiah Educational Foundation, Vaddeswaram, Andhra Pradesh, 522302, India

P. Pareek (✉)
Department of Electronics and Communication Engineering, Vishnu Institute of Technology, Vishnupur, Bhimavaram, Andhra Pradesh, 534202, India
e-mail: prakash.p@vishnu.edu.in

E. Prasad Konakalla
Department of Physics and Electronics, B.V. Raju College, Vishnupur, Bhimvavaram, Andhra Pradesh, 534202, India

D. Gupta et al. (eds.), *Pattern Recognition and Data Analysis with Applications*,
Lecture Notes in Electrical Engineering 888,
https://doi.org/10.1007/978-981-19-1520-8_34

Although few geometries of waveguides are proposed to realize the confinement of surface plasmons (SP) beyond the diffraction limit [4]. The diffused filled properties of surface plasmons at the interface of metal and dielectric are capable of reducing the propagation loss, which further enhances the possibility of fabrication of nanoscale all optical devices [5]. SP-based pure metallic waveguides are capable of confining the optical field to subwavelength scale, but their susceptibility to ohmic loss again limit their further applications [6, 7].

Hence, in order to alleviate these issues, a new kind of waveguide geometry has been proposed named as hybrid plasmonic waveguide (HPWG). A HPWG is a combination of dielectric and plasmonic waveguide, which has been designed to attain subwavelength confinement of SPs with longer propagation length. Some waveguides were also proposed for better optical confinement or infiltrating materials as to increase the sensitivity such as dielectric waveguide, hollow core waveguide, and plasmonic slot waveguide [8].

Recently, optical sensing is of huge interest and hence, various geometries were analyzed to implement it such as dielectric and subwavelength-based grating sensors, hollow core waveguide sensors, and slot waveguide-based sensors [9]. Nanoslots waveguides-based sensors are capable of providing the larger optical sensitivity to the infiltrating materials of the waveguide. The scheme of nanoslot plasmonic waveguides is somewhat different than those of normal index guiding waveguide geometries.

In a dielectric slot waveguide, high–low–high index structure provides the optical confinement where as in plasmonic, the optical confinement occurs in low index medium and confinement gained by plasmonic optical increment. Moreover, in plasmonic waveguides, propagation, and excitation of modes take place at metal surface.

Plasmonic waveguide has better optical confinement properties than its dielectric counterpart but at a cost of high propagation loss. Hence, a double-slot hybrid plasmonic waveguide (DSHPWG) has been proposed to utilize the benefits of both plasmonic as well as dielectric waveguide. DSHPWG waveguide structure shows the benefits of less propagation loss, high optical confinement over the conventional silicon on insulator (SOI) technologies.

Hence, in this paper, DSHPWG studied for its possible application as liquid analyte sensor. The rest of the paper is organized as follows. Section 2 briefly describes proposed waveguide structure along with its design considerations. It also provides theoretical formulation to obtain the key parameter for assessing the potential of considered waveguide as an optical sensor. Section 3 highlights obtained salient results supported by discussions. Finally, Sect. 4 provides conclusions and future scope of this work.

2 Device Structure and Theoretical Formulation

The cross section view of waveguide is shown in Fig. 1. The dielectric slots between the Au and Si ring are narrow enough that the quasi-transverse electric (TE) mode can be supported. It consists of dielectric material in between the metal and silicon to guide and confine the hybrid plasmonic mode. Initially, air is treated as dielectric material between the slots of metal and dielectric, silicon dioxide (SiO_2) is used as the substrate layer.

A block of silicon (Si) is sandwiched between the two nanoslots. The width and height of Si block are denoted by $w_{si} = 300$ nm and $h_{Si} = 250$ nm, respectively. Then, to create the nanoslots, the blocks of gold are placed on both sides of silicon block.

The mode field distribution through the waveguide is shown in Fig. 2, which is captured when silicon dioxide (width and height of slot are 150 nm and 300 nm) is taken as dielectric material in the slots sandwiched between the gold and silicon.

In order to verify the nature of localized field, the effective mode area of guided fundamental mode is plotted as a function of wavelength in Fig. 3 [10]. The mode area can be calculated by using Eq. (1), where x and y are representing the longitudinal and direction of propagation of the field, respectively. The power distribution of power is integrated over the region of length of waveguide.

$$A_m = \frac{\int_{-\infty}^{+\infty} p(x, y)\mathrm{d}x\mathrm{d}y}{\max[p(x, y)]}\left(\frac{1}{\mu m^2}\right) \tag{1}$$

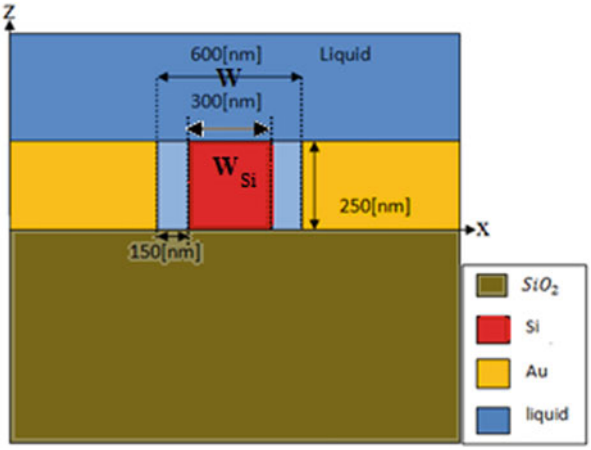

Fig. 1 Cross section view of double-slot hybrid plasmonic waveguide

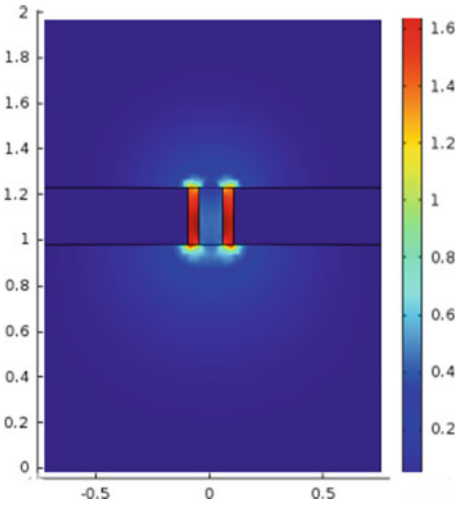

Fig. 2 Propagation of optical fields through the double slots of Au

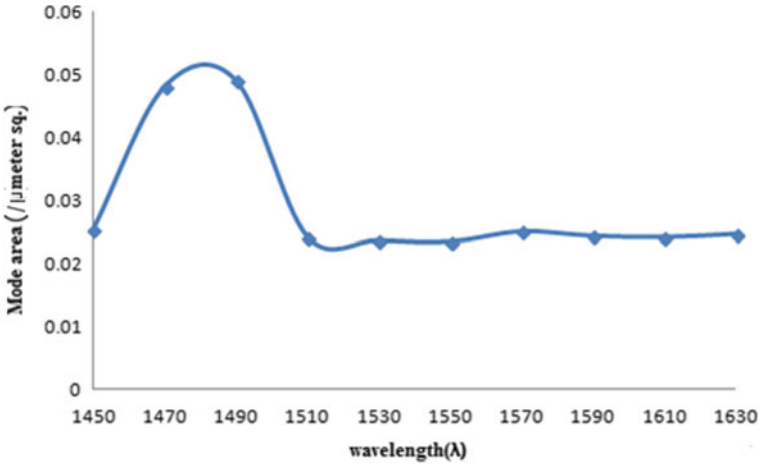

Fig. 3 Effective mode area with respect to wavelength when SiO_2 is used as dielectric material

3 Results and Discussion

The confinement of optical signal for the designed double-slot waveguide-based sensor structure as shown in Fig. 2, satisfied the mathematical formulation given in Eq. (1). Therefore, the analysis of proposed sensor structure was done in terms of evaluation of effective mode area and sensitivity with respect to the width of slots.

The trend of effective mode area with respect to operating wavelength under the presence of SiO_2 as dielectric material is presented in Fig. 3. It represents that for the

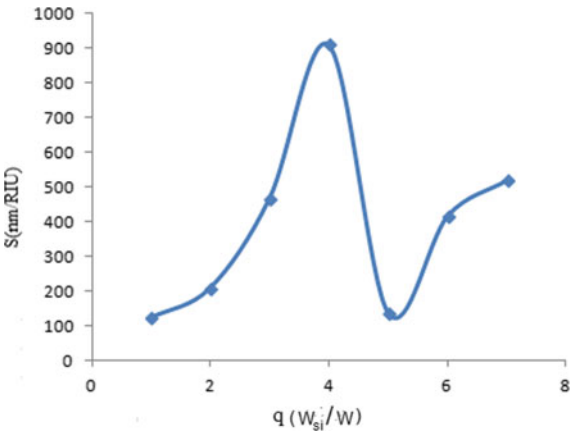

Fig. 4 Variation sensitivity with respect to *q*-parameter when liquid is used in the nanoslots

operating wavelength of 1550 nm, the effective mode area for propagating optical signal is 0.025 per square meter. Thereafter, the analysis of sensitivity was carried out with respect to slot widths. The slot width was considered in the ratio of width of silicon to the width of liquid filled slots.

The attained results are presented in the form of plot as shown in Fig. 4. The maximum sensitivity of 910 nm/RIU was attained at the slot width of liquid and silicon filled slots were considered 150 nm and 300 nm, respectively. The calculation of sensitivity of proposed sensor structure was evaluated in terms of effective mode area, and its mathematical formulation is given in Eq. (2).

The sensitivity evaluation was done in terms of figure of merit (FOM) of the developed sensor model with respect to working wavelength. The working wavelength for the proposed sensor structure was set to equal to third window of telecommunication because of its low loss characteristics. The quality factor denotes the working capabilities of the sensor model.

$$S = \frac{\text{FOM}\,\lambda}{Q} \tag{2}$$

4 Conclusion

This work investigates the viability of the double-slot hybrid plasmonic waveguide for sensing liquid analyte. In the waveguide, dielectric slots between the Au and Si ring are narrow enough that the quasi-transverse electric (TE) mode can be supported. It consists of dielectric material in between the metal and silicon to guide and confine the hybrid plasmonic mode. Simulation-based analysis of proposed sensor structure was done in terms of evaluation of effective mode area and sensitivity with respect to the width of slots. Effective mode area for propagating optical signal is obtained

as 0.025 per square at operating wavelength of 1550 nm. Maximum sensitivity of 910 nm/RIU was achieved at dimension of 150 nm and 300 nm, which are widths of liquid and silicon filled slots, respectively. The proposed structure can be fabricated in the future and may prove to be vital for sensing quality of liquid analyte like water, blood, etc.

References

1. Soref, R.A.: Silicon-based optoelectronics. In: Proceedings of the IEEE, vol. 81, pp. 1687–1706. IEEE, USA (1993)
2. Gramotnev, D.K., Bozhevolnyi, S.I.: Plasmonics beyond the diffraction limit. Nat. Photon. **4**, 83–91 (2010)
3. Schörner, C., Lippitz, M.: Single molecule nonlinearity in a plasmonic waveguide. Nano Lett. **20**, 2152–2156 (2020)
4. Kim, S., Yan, R.: Recent developments in photonic, plasmonic and hybrid nanowire waveguides. J. Mater. Chem. C **6**, 11795–11816 (2018)
5. Kim, H.-M., Park, J.-H., Lee, S.-K.: Fabrication and measurement of optical waveguide sensor based on localized surface plasmon resonance. Micro Nano Syst. Lett. **7**, 7 (2019)
6. Zhang, Y., Zhang, Z.: Ultra-subwavelength and low loss in V-shaped hybrid plasmonic waveguide. Plasmonics **12**, 59–63 (2017)
7. Desiatov, B., Goykhman, I., Levy, U.: Experimental demonstration of locally oxidized hybrid silicon-plasmonic waveguide. In: CLEO 2011-Laser Applications to Photonic Applications, p. JTuI53, OSA, Baltimore, Maryland (2011)
8. Melikyan, A., Alloatti, L., Muslija, A., Hillerkuss, D., Schindler, P.C., Li, J., et al.: High-speed plasmonic phase modulators. Nat. Photon. **8**, 229–233 (2014)
9. Barrios, C.A., Gylfason, K.B., Sánchez, B., Griol, A., Sohlström, H., Holgado, M., et al.: Slot-waveguide biochemical sensor. Opt. Lett. **32**, 3080–3082 (2007)
10. Mere, V., Muthuganesan, H., Kar, Y., Kruijsdijk, C.V., Selvaraja, S.K.: On-chip chemical sensing using slot-waveguide-based ring resonator. IEEE Sens. J. **20**, 5970–5975 (2020)

Journal of Science and Technology
ISSN: 2456-5660 Volume 7, Issue 02 (MAR-APR 2022)

www.jst.org.in *DOI: https://doi.org/10.46243/jst.2022.v7.i02.pp139-145*

FLUID-STRUCTURE INTERACTION IN WATER TANKS: DYNAMIC ASSESSMENT

Mr.K.A.S.V.R.Sai Phani Kumar [1], Dr.A.Padmanabham [2], Mr.V.N.V.Radha Krishna Murty [3,]
Assistant Professor[1],Assistant Professor[2,3,]
Mail id:saifanikumar@gmail.com, Mail Id:apnabham@gmail.com, Mail Id:radhakrishna.veluri@gmail.com,
Department of Physics and Chemistry,
B.V.Raju College,Vishnupur, Bhimavaram,
DNR College of Engineering and Technology, Bhimavaram,

To Cite this Article

Mr.K.A.S.V.R.Sai Phani Kumar, Dr.A.Padmanabham , Mr.V.N.V.Radha Krishna Murty , " Fluid-Structure Interaction In Water Tanks: Dynamic Assessment", *Journal of Science and Technology, Vol. 07, Issue 02, March-April 2022.*

Article Info
Received: 24-02-2022 *Revised: 04-03-2022* *Accepted:15-03-2022* *Published: 24-03-2022*

ABSTRACT
Due to increased population and growth of cities, the number of raised water tanks servicing the demand urban \swater system is on the rise. As it has been indicated in the Iranian code of practise for Earthquake /2800 due \sof the necessity of sanitation and hygiene water tanks have been recognised as vital constructions during the unforeseen occurrences such as earthquake. There is a high anticipation not to observe any phase out for their serviceability following the earthquake. Because of the presence of fluid with various behavioural features of structures containing it Because the most part of mass of tanks are positioned in a great distance from their foundation, the behaviour of these sorts of structures in comparing with conventional structures are more sophisticated. In this study, cylindrical concrete water tanks, which feature a central shaft, have been examined with consideration the influence of the structure's contact with water via accurate execution of boundary constraints on the interface between fluid and structure. Also considering the volume of water in the tank and their response under recorded acceleration of varied earthquakes utilising finite element approach. The findings were then compared with proposed ways by Iranian code /2800, which shows a significant variation between the approaches given.

1. INTRODUCTION

The behaviour of liquid storage tanks during earthquakes is more significant than the economic worth of the tanks and their contents, which are crucial buildings in the water, oil and gas industries. Firefighting water, for example, must be available in the event of an earthquake, and utility infrastructure must be operable to satisfy these needsor satisfy the needs of the public as a source of drinking water. In light of these factors, serviceability is now the primary design consideration is taken into account in the majority of these constructions. It is crucial to have a clear grasp of how seismically vulnerable these buildings are.Safety goals and construction and maintenance expenses must be balanced.The interaction between fluids and these structures is a key issue in the understanding and design of these systems. And organisation. It is very difficult to predict the analytical response of coupled field systems. Most of the time, Numerical approaches, such as the finite element method, are at the heart of many research. Concrete water tanks with central shafts are analysed numerically in this work by employing finite elements. Software component that takes into account fluid-structure interaction.

2.THEORY

There is a wide range of methods for analysing the fluid-structure interaction. a) Added mass technique, b) The Eulerian-Lagrangian method, and c) The Lagrangian-Lagrangian method are all examples of these

approaches.The fluid mass is introduced to the structure at the contact, and the structure is subjected to stress.a dynamic examination This approach considers the fluid's compressibility and stiffness as well as the structure's lexibility.are often overlooked. In 2- and 3-dimensional constructions, this approach is straightforward to employ, however the outcomes areFrequently, there are significant mistakes.The major goal of the second technique is to solve the governing equation for the fluid and structural domains. governing equation of fluid domain for an ideal, homogenous, inviscid, compressible and irrotational flow in term of velocity potential variable, φ , is:

$$\nabla^2\phi = \frac{1}{C^2}\frac{\partial^2\phi}{\partial t^2} \quad (2.1)$$

where C is the velocity of acoustic waves. By this assumption that fluid is incompressible, the Eqn.1 is conformed to Laplace Eqn.2.

$$\nabla^2\phi = 0 \quad (2.2)$$

It is possible to represent fluid dynamics in terms of time by solving Eqn.1 or Eqn.2 for fluid domains in terms of variables P and/or, which are pressure variables.Equations for the coupled field system of nodal displacement are required for the structural domain since the needed variable is nodal displacement.There will be an asymmetrical relationship between fluid and structure, making a simple solution difficult.Third, a particle has been taken into account in terms of time and variables for fluid and structural domains isIn the finite element approach, there is a nodal displacement. There is a major benefit to using this strategy because of the utilisation of the same toolssolving just this motion equation, we get displacement, pressure, and stress values for the fluid and the structure domain.Figures have been drawn out for both fluid and structure.The Langrage-Lagrange approach is being utilised to simulate fluid-structure interaction in this study.In the ANSYS programme, the Fluid80 and Shell63 elements are utilised for fluid and structural analysis.contains eight nodes with three degrees of freedoms in each node and Shell63 element has four nodes with six degrees ofEach node has flexibility.This study is based on the following assumption:1-The foundation of construction is supposed to be sturdy, 2-The tank and the water are assumed to have a linear andThe ability to change shape. Material qualities of concrete and water are presented in Table.1 and the finite element characteristicsFigure 1 shows the reservoir's geometry.Table shows that there are 1.The number of fluids and structures is shown in Table 2.sensitivity analysis of displacement is used for both static and dynamic analysis in order to acquire the elements.

Table 1 Material properties

water			Concrete		
Kinematics viscosity (m^2/s)	Specific mass (kg/m^3)	Bulk modulus (N/m^2)	Poison ratio	Specific mass (kg/m^3)	Modulus of Elasticity (N/m^2)
0.005	1000	2.2e9	0.27	2400	2e10

.pp139-145

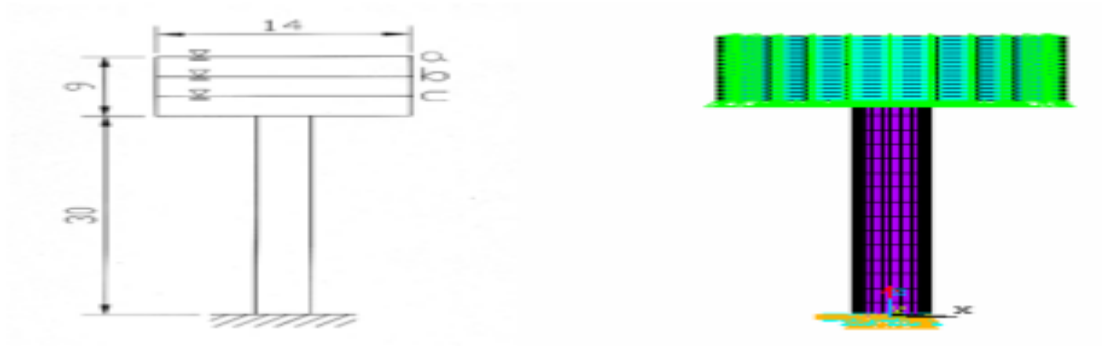

Figure 1 Finite element model of elevated water tanks.

Table 2 Geometric characteristic of tank

Reservoir of tank			shaft			Number of elements		Number of nodes	
thickness of wall (m)	diameter of wall (m)	height of wall	thickness of wall	diameter of wall	height of wall	Fluid	tank	Fluid	tank
0.3	14	9	0.5	3	30	3135	929	25080	3716

STATIC RESULT AND DISCUSSION

In order to study of modeling proportion, displacement and hydrostatic pressure are compared by using of theoretical and finite element methods. Eqn.3 and Eqn.4 are used to calculate the result of fluid weight as shown in Figure .2. To compare of this result with finite element one, the wall of tank are assumed to be rigid. The results are shown in Figures 3 and 4, which show a relatively compatibility between numerical and theoretical methods.

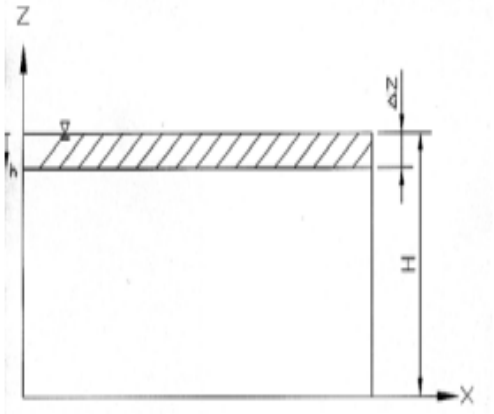

Figure 2 Tank with water

$$U_z = \frac{1}{k}\int_H^h \gamma z dz = \frac{\gamma}{k}\left[\frac{z^2}{2}\right]_H^h = \frac{-\rho g}{2k}\left[H^2 - h^2\right] \quad (3.1)$$

$$P = \gamma h \quad (3.2)$$

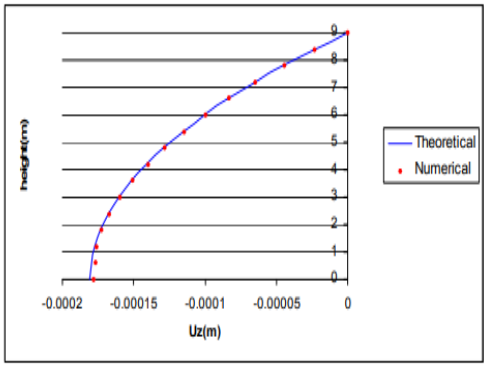

Figure3 Displacement variation along the height of water for theoretical and numerical methods

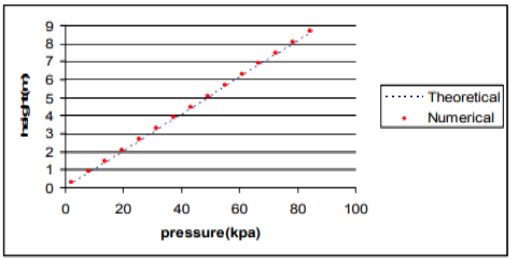

Figure4 Hydrostatic pressure variation along the height of water from theoretical and numerical methods

By solving eigen-value Eqn.5 for tank with different elevation of water (Empty, 3 1 Full, 3 2 Full, Full), the natural periods of system are obtained. A summary of the calculation results is listed in Table 3. While the mode shapes are shown in Figure.5.

$$[k][\phi] = [M][\phi][\Omega^2] \quad (4.1)$$

www.jst.org.in DOI: https://doi.org/10.46243/jst.2022.v7.i02.pp130-138

Table 3 periods of system with different elevation of water

Mode number	Period (sec)			
	Empty	$\frac{1}{3}$ Full	$\frac{2}{3}$ Full	Full
1	1.608	2.42	2.95	3.175
2	1.608	2.42	2.95	3.175
3	0.626	0.669	0.67	0.466
4	0.626	0.669	0.67	0.2
5	0.491	0.491	0.49	0.2
6	0.336	0.36	0.48	0.05

Using Eqn.7 and Eqn.8 with the assumption that the damping ratio is 0.05 for the two initial modes, the damping matrix and may be derived using the equations Eqn.6 and Eqn.7. Table.4 summarises these findings.

$$[c] = \alpha[M] + \beta[k] \quad (4.2)$$

$$\beta = \frac{2(\xi_i w_i - \xi_j w_j)}{(w_i^2 - w_j^2)} \quad (4.3)$$

$$\alpha + \beta w_i^2 = 2 w_i \xi_i \quad (4.4)$$

Whereα,β are coefficients related to mass and stiffness matrices i wj w , are periods of i and j modes. i j ξ ,ξ are damping ratio of i and j nodes.

PERIOD OF SYSTEM RELATED TO IRANIAN CODE/2800 In Iranian

Table.4 Data for α and β with $(\xi = 0.05)$

water elevation	Empty	$\frac{1}{3}$ Full	$\frac{2}{3}$ Full	Full
α	0.281	0.203	0.177	0.152
β	0.0072	0.0086	0.009	0.0093

PERIOD OF SYSTEM RELATED TO IRANIAN CODE/2800

In Iranian code/2800, elevated water tanks are modeled with lumped mass in the end of slender cantilever. These results are summarized in Table.5.

Empty	$\frac{1}{3}$ Full	$\frac{2}{3}$ Full	Full
1.25	1.75	2.138	2.466

From Table.5, It is observed that periods calculated by Iranian code/2800 for elevated storage tank are less than those by using of finite element method.

To understand how a building responds to earthquakes, it is necessary to know the magnitude and direction of these forces. A structure exposed to seismic excitations cannot be observed in terms of precise characteristics like period, vibration amplitude and so on since the acceleration of ground motion is arbitrary and contains many frequencies.Fourier Integration, however, may transform these accelerations into harmonic functions. As a result of this,to investigate the behaviour of structures exposed to harmonic stimulation and the effects of various factorsin place of a seismic shock.

Using harmonic analysis, tanks of varying sizes were examined.As an illustration, consider the case of a water level of 3 metres.One full glass.

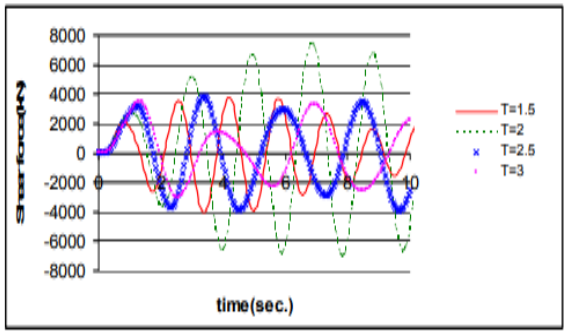

Conclusion:

The base shear force resulting from the structure in pseudo static analysis according to Iranian code/2800 for Empty was found to be:tank is four times as large as those from linear dynamic analysis, and the tank with water is seven times as large.R, the response modification factor, is responsible for the differences.According to the Iranian code/2800, the durations of vibrations are less than in dynamic analysis using finite elements.These discrepancies amount to 27% for an empty tank and 22% for a full tank in this study.with3Water, 2%, for tank with 3 percent2 gallons of water and 27% of the tank's capacity.3. Based on the findings of the analyses of three earthquakes, the base shear force andmagnitude of earthquake displacement is strongly influenced by its frequency content and big earthquakes.This challenge has resulted in a distinction between static and dynamic analysis.In pseudo dynamic analysis, the base shear force is substantially stronger than in static analysis. So that it's more than just a one-time thingThere is no doubt about that.Base shear force and maximum displacement are affected by the vertical component of three accelerograms.We don't need to account for the storage tank since its impact on our calculations is minimal.

9. REFERENCE

Housner, G.W. (1963). The Dynamic Behavior of Water Tanks. Bulletin of Seismological Society of America 53, 381-387. Hamdi, M.E. (1978). A Displacements for the analysis of vibrations of coupled fluid- structures systems. Int. J. Num. Meth., 13, 139-150.

Wilson, E.L. and Khalvati.M. (1983). Finite Elements for Dynamic Analysis of fluid- structure systems. Int. J. Num. Meth. En 19, 1657-1668.

Sharan, S.K., Gladwell, G.M. (1985). A general method for the dynamic response analysis of fluid-structures systems. Comput and structures, 21:5, 937-943.

Olson, L.G., Bathe, K.J. (1985). Analysis of fluid-structure interaction. A direct symmetric coupled formulation based on the fl velocity potential.

Comput. Struct., 21:1/2, 21-32. Ministry of Housing and urban development (Iran), (2006). Iranian code for seismic resistant design of building, (in Persian).

Journal of Science and Technology
ISSN: 2456-5660 Volume 6, Issue 04 (Jul-Aug 2021)

www.jst.org.in *DOI: https://doi.org/10.46243/jst.2021.v6.i04.pp244-250*

Experimental Study of Earth Batteries

Mr.V.N.V.Radha Krishna Murty [1], Dr.A.Padmanabham [2], Mr.Kiran Bachina[3,]
Associate Professor[1, 2,] Head of the Department[3,]
Mail Id:radhakrishna.veluri@gmail.com, Mail Id:apnabham@gmail.com,
Department of Physics,
B.V.Raju College,Vishnupur, Bhimavaram,
DNR College of Engineering and Technology, Bhimavaram,

To Cite this Article

Mr.V.N.V.Radha Krishna Murty , Dr.A.Padmanabham , Mr.Kiran Bachina, *" **Experimental Study of Earth Batteries**", Journal of Science and Technology, Vol. 06, Issue 04, July-Aug 2021.*

Article Info
Received: 01-04-2021 *Revised: 09-04-2021* *Accepted:15-06-2021* *Published: 04-08-2021*

Abstract
Earth batteries have been successfully built and operated as an alternative source of low-power electric supply. Different electrode configurations were tested for the greatest possible variation in potential. The most appropriate combinations of frequently accessible metals were chosen for more thorough characteristic investigations in light of robust and cost-effective application of this natural power technology by untrained village customers. Each cell produced a voltage of 2.05, 1.40, 1.10, and 0.9 volts when the anode and cathode were made of Magnesium, Zinc, Aluminum, and Carbon, respectively. One Zn-Cu cell was found to have an average rated power of a few tens of microampere. When it came to low-power electronic products like mobile phones and white-light LED calculators and wristwatches, the site had them all. Using many earth battery cells in series like a commercial lead acid battery resulted in a linear rise in the voltage. The load current was found to rise by connecting earth cells in parallel. Furthermore, increasing the electrode surface area was shown to boost source current capacity. However, single cell voltage was shown to stay consistent independent of the electrode diameters. According to this research, the most cost-effective metal electrodes for earth batteries have been studied. Operation of earth batteries as a free power source was proved effectively.

INTRODUCTION

Reported free energy holy grails may include electrostatic motors, geo-magnetic generators [1-2], air [3], sea [4] and earth batteries [5-8]. Some free energy proponents have frequently been concentrating on the perpetual motion machines employing scientifically unfeasible theories such as over unity devices, millennium motors, resonance based self-charging and free wheeling devices. There exists nothing as free energy source such as mutual powering motor-generator set without any net input or gravity based free running machines or negative resistance based amplification. However, earth soil chemical processes and electron affinity based earth batteries may be researched for low to high voltage DC potential to drive small scale white emission LED lighting loads in remote mountainous places or small scale electronic equipment. They may also be considered to replace high voltage low current charging power sources or ionisation power supplies. Like earth batteries the marine batteries likewise may be explored for comparable uses. However, air batteries may be employed for bulk power generation and grid system operation [3]. In light of global energy crisis to be triggered by natural end of oil and gas during next 50 to 60 years time [9-11], it has become extremely vital to seek for alternative energy sources to hold back the human race from involvement to a major energy war [12-13] Although, uranium [14] and coal [9] would continue to exist for few millennia but they can not replace oil and gas despite dangers of radiation hazards (plutonium) and greenhouse gases (CO2) (CO2). Either, we can halt global warming at danger of nuclear radiation or make the earth nuclear free at risk of global warming owing to increasing temperatures from1.4 to 5.8ºC from 1990 to 2100 by exponentially rising CO2 concentrations. Rise in earth surface temperature in last 10 hot years (1997-2007) was roughly 0.6ºC. Maximum temperature has been reported to

be 52ºC in major cities of Pakistan and 46ºC in Greece. Cool the house and heat the world or adapt to natural ways of existence. We must halt usage of excessive energy for amusement and retune ourselves to new lifestyles demanding least amount of energy in the form of cooling or heating. The scientists must work hard to investigate new sources of energy otherwise be prepared to be died soon in a major energy war or global greenhouse impact none knows which triumphs sooner. This study is a very honest attempt to examine the possibilities of utilising earth batteries for distant village lights, communication signalling and running small scale electronic loads when there is no other source of power or easy to preserve electricity. Assuming uniform electrode profile the potentials of various typical metals electrode pairs in soils are presented in Table 1. [15-17].

Table 1 Potential of Common Metals Suitable for Earth Battery

Anode materials		Cathode materials		Battery
Material	E^o(V)	Material	E^o(V)	Volts
magnesium	-1.75	coke	+0.30	2.05
zinc	-1.10	graphite	+0.30	1.40
zinc	-1.10	copper	+0.20	0.90
aluminium	-0.80	carbon	+0.30	1.10
iron	-0.50	coal	+0.30	0.80

A few large-sized C, Mg, and Al electrodes are being built or tested to see whether greater currents and voltages are possible. Earth batteries, in contrast to automotive air batteries, have very low Wh capacity. It is unable to run even the most basic motorised toys for children. Due to a lack of voltage, the above-ground battery was unable to power even a 0.7mA LED. It averaged 0.63 watts of output power. Except for an electronic digital clock, it was still too tiny to operate any motorised load. These two materials are all that is needed to make a basic air battery (or iron). Aluminum reacts with oxygen from the air that seeps through saltwater-soaked paper. Aluminum and carbon electrodes may be able to generate enough usable voltage. The voltage of an air battery cell is affected by the reduction potential of the battery. As a rule of thumb,

Table 2 Standard Reduction Potentials of Elements at 25ºC

Anode materials		Cathode materials		Battery
Material	E^o(V)	Materials	E^o(V)	Volts
Li^+(aq)	**-3.045**	**F_2(g)**	**+2.870**	**5.915**
Na^+(aq)	-2.710	H_2O_2(aq)	+1.780	4.490
Mg^{2+}(aq)	-2.370	MnO_4^-(aq)	1.510	3.880
K^+(aq)	**-2.925**	**Au(aq)**	**+1.500**	**3.425**
Al^{3+}(aq)	-1.660	Cl_2(g)	1.360	3.020
Zn^{2+}(aq)	**-0.760**	**Cu^{2+}(aq)**	**0.340**	**1.100**

Air batteries' per cell voltage ranges are much lower than those of air batteries. While the best Li+ (aq)-F2(g) air battery has 5.915 volts, Mg-C has a maximum of 2.05 volts. Nevertheless, for commercial application, air battery design must take into account a number of other economic factors. In compared to a 22kWh NiCd battery, a typical Zn Air battery can provide 312kWh of power. Using bigger capacity batteries, they are capable of supplying 200HP of traction drive at 20mph or 35mph. The recent tendency is to increase the speed to 55mph in order to save energy. Several nations have been using this technology for a long period of time. 200-250Wh/kg and 300-375Wh/L are the air battery energy to weight and energy to size ratios.

EXPERIMENTAL SETUP

The precise voltage and currents of an earth battery cell made up of zinc and copper electrodes were measured in an experiment. Simple pricking of pointed electrodes on the Earth's surface is used to place electrodes on the planet's

surface in an open air setting. Small-scale lighting and electrical loads may be powered by the electrode soil

reaction voltage of 0.92V. At smaller distances between the cathode and anode, currents and voltages were greater, whereas at wider distances they were lower. The voltage and current measurements on the digital multimeter were found to be unreliable. When the electrodes were swapped from north to south, the voltages and currents rose significantly. For several electrodes, the average voltage and current magnitudes were 0.910.15V and 0.70.25mA. Electrode materials and their typical reduction potentials determine the Earth battery's potential. An increase in earth battery voltage is possible by selecting materials with greater positive and negative reduction values. Zn-Cu earth battery voltage is theoretically 0.92V, however our readings with the UNI T professional digital VOAM # 1050444792 (Korea) were roughly 0.900.25V. Efficient electrodes are needed to build a high voltage battery. Common metals behave similarly, with the exception of the fact that the amplitude of the current is dependent on the electrode surface area. Figure 1 depicts the fluctuation of the observed voltages and currents.

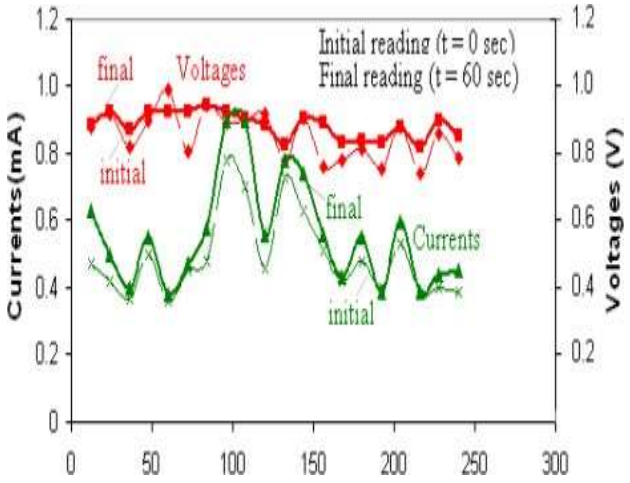

Fig.1 Copper (south)-Zinc (north) earth battery voltages and currents

After repeating the experiment using insulated box mud cells, the voltage and current were found to be very steady. In addition to the typical earth battery currents, it was hypothesised that measurements taken on bare ground would have additional telluric earthcurrents attached to them. For the purpose of determining whether or not telluric earth currents influence the natural direction of measured currents and voltages, the zinc electrode was fixed in the ground and the copper electrode was rotated for multiple directions between 0o (north), 90o (east) and 180o (south) and 270o (north) (west). As shown in Fig. 2, the voltage and current magnitudes at a fixed radius of 9 feet circle were observed

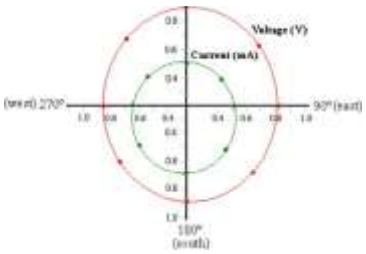

to slightly fluctuate in magnitudes.

Voltage/Impact (V/I) curves for fixed zinc and movable copper electrodes are shown in Figure 2.
Even after 8 to 9 hours of continuous usage, the electrode did not rust. From south to north, the currents are stronger,

while from east to west, the currents are lesser. Electrodes with a positive north and a negative south were similarly more powerful. South-to-North currents were discovered. Although it was feasible to link earth battery cells in series to enhance the voltage, the electrodes from the bottom short circuited via earth electrolyte materials. Parallel

connections of cells, on the other hand, resulted in higher currents because of larger surface areas. The current magnitudes are increased by the spiral electrode design because of the huge surface areas. To get the best results, the maximum voltage recorded was 0.9 0.35 V, with currents in the range of 3–0.25 A. A 15-fold increase in current was seen when the same experiment was carried out in the open air. It seemed as though some random potential source, in addition to the typical soil reaction voltage, was altering the DC earth battery voltage.

III. SERIAL OPERATION OF EARTH BATTERIES

The voltage on the bare ground surface cannot rise due to electrode shorting. To sum the voltage, we must first separate individual cells. Thirteen DC battery cells were made in separate paper boxes to illustrate serial accumulation of voltages. In order to boost the voltage, the separated earth battery cells were linked in series as illustrated in Fig. 3. From 8 to 10cm to 0.5 to 1cm, the distance between Zn and Cu electrodes in various cells changed (b). The DC voltage ranged from 10 to 12 volts, and the current was modest, yet an LED could still be lit using this setup. There was a mud resistance of tens of millions of Ohms between the electrodes. As indicated in Fig.4, copper and zinc plates of 16 inches square and I mm thick were coated with mud to minimise the resistance.

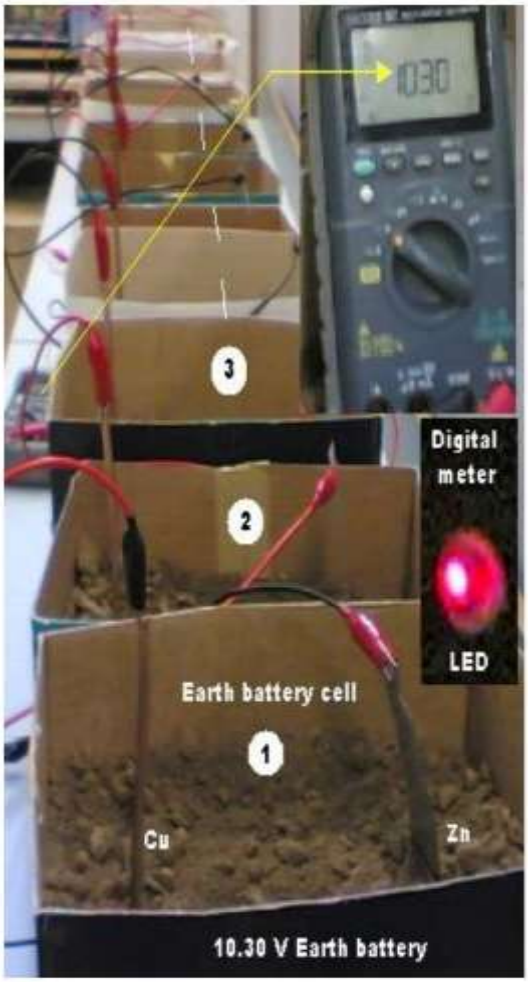

a. A twelve cells 10.30V/45mA earth battery

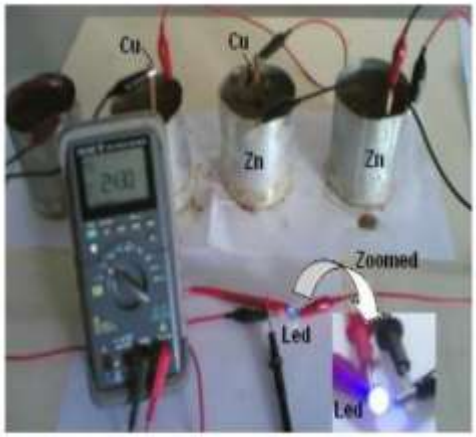

b. A four cells 2.43V/0.20mA earth battery

Fig.3. Experimental demonstration of serial connection of earth batteries

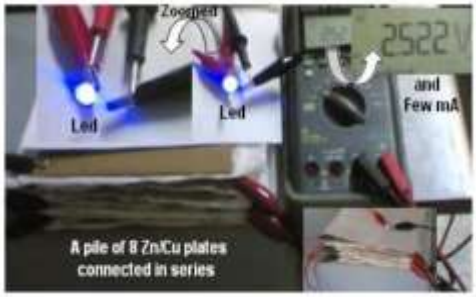

Fig.4 Four inch square Zn/Cu plate electrodes 2.5V/30 A earth battery

Using four cells in series resulted in 2.5 to 3.25V DC and a current of 30 A. It is important to remember that the voltage and current in dry much are affected by the moisture content. The high resistance between the electrodes causes the current to drop to zero when the system is completely dry. Moisture is necessary for the interaction between metal and soil. Instead of just using dry mud, we should use mud electrolyte. After prolonged use, the batteries' electrodes begin to corrode partly. A few studies on rusting have previously been done [20]. Investigations into electrodes with enormous surface areas are now underway.

CONCLUSIONS

Experiments on earth batteries with copper and zinc electrodes have shown promising results. Earth batteries have showed a good amount of potential for signalling, charging mobile phones, and providing white light lighting in distant regions after a month of operation. This fascinating investigation was carried out as part of a HEC-funded study on renewable energy. As a UET Lahore graduate (1984), it gives me great pleasure to present my study at ICEE 2008, which will take place at UET Lahore.

REFERENCES

[1] Gish, O. H., “The Natural Electric Currents in the Earth's Crust,” The Scientific Monthly, Vol. 32, pp. 5-2, 1989.

[2] G. M. Hopkins, “Experimental Science:Elementary, Practical and Experimental Physics. Munn &Co.,. pp. 437 – 451, 1902. [1] J. Cooper, “Powering Future Vehicles with Refuelable Zinc/Air Battery,” Science & Technology Review, pp. 6-13, October 1995.

[3] Lord Kelvin, Sea Battery: Method and Apparatus, US Pat. No. 4153757, End of 1800s. [1] Ryeczek, "U.S. Patent 4,457,988 Earth battery". July 3, 1984. [1] Daniel Drawbaugh, "U.S. Patent 211,322 Earth battery

for electric clocks". 1800s.

[4] M. Emme, "U.S. Patent 495,582 Ground generator of electricity". 1900s.

[5] Dieckmann, George F., "U.S. Patent 329,724 Electric Earth Battery". November 3, 1885. [1] K.S. Deffeyes, "Hubert's Peak: The Impending World Oil Shortage," Princeton University Press. 2002: ISBN 0-691-09086-6.

[6] D. Goodstein," Out of Gas: The End of the Age of Oil. W. W. Norton' Book 2005 ISBN 0-393-05857-3.

[7] H.H. Rogner," An Assessment of World Hydrocarbon Resources," Annu. Rev. Energy Environ, Vol. 22, pp. 217-262, 1997.

[8] M.C. Ruppert," Crossing the Rubicon: The Decline of the American Empire at the End of the Age of Oil," New Society. 2005: ISBN-13: 978- 0865715400.

[9] L.C. Kleveman," The New Great Game: Blood and Oil in Central Asia," Atlantic Monthly Press. 2004: ISBN 0-87113-906-5.

[10] K.S. Deffeyes, I.D. MacGregor, " World Uranium Resources, Scientific America," Vol. 242, pp. 66-67. 1980. [1]

[11] James Napier, "A manual of electro-metallurgy," pp. 48-49, 1876

[12] A. A. Fesquet, "Oliver Byrne, and John Percy," The Practical Metal-worker's Assistant. H.C. Baird & Co., pp. 529-530, 1878.

[13] E. Katz, "Alexander Bain". The history of electrochemistry, electricity and electronics; Biosensors & Bioelectronics.

[14] R. J. Edward," Measurement of Soil Resistivity & Calculation of Earth Electrode Resistance. 15th February 1998.

[15] N. Khan, N. Mariun, Z. Saleem, N. Abas, "Fossil Fuels, New Energy Sources, and the Great energy crisis.

Journal of Science and Technology
ISSN: 2456-5660, Volume 6, Issue 6 (NOV-DEC 2021)

www.jst.org.in DOI: https://doi.org/10.46243/jst.2021.v6.i6.pp19-30

The Osteogenic Potential of Titanium Dioxide Nanoparticles of Different Sizes and Shapes.

Dr.A.Padmanabham[1],Mr.V.N.V.Radha Kishna Murty[2],
Associate Professor[1,2],
Mail Id:apnabham@gmail.com,Mail Id:radhakrishna.veluri@gmail.com,
Department of Physics,
DNR College of Engineering and Technology,
Bhimavaram,
B.V.Raju College of Engineering and Technology,Vishnupur,
Bhimavaram,

To Cite this Article

*Dr.A.Padmanabham ,Mr.V.N.V.Radha Kishna Murty"**The Osteogenic Potential of Titanium Dioxide Nanoparticles of Different Sizes and Shapes**", Journal of Science and Technology, Vol.6, Issue 6, NOV-DEC 2021, pp.:19-30.*

Article Info

Received: 18-11-2021 Revised: 24-11-2021 Accepted: 01-12-2021 Published: 10-12-2021

Introduction

For example, nanoparticles (NPs) are increasingly being used in healthcare, antimicrobial materials, optical and electrical devices, and medication delivery systems [1, 2]. NPs have a greater specific surface area than tiny particles, which increases their reactivity, making them more attractive to researchers. Nanoparticle bioactivity is considered distinct from that of its fine-size equivalent because of surface features such as energy level, electronic structure and reactivity [3]. As a result, several studies [4–10] have examined the possible effects of NPs on cells and tissue. Because TiO2 NPs are NPs, they have the same surface characteristics as the rest of the NPs. TiO2 NPs are extensively employed as a photocatalyst in solar cells, a pigment in paints, a corrosion-protective coating on bone implants, and more because of their unique physicochemical features [11–14]. TiO2 NPs have recently come under scrutiny for their potential impact on human health. A study by Ferin et al. [15] found that ultrafine TiO2 (20 nm) reached the pulmonary interstitium in the rat lung and produced inflammation compared to fine TiO2 at the same mass burden. In vitro and in vivo, Kumazawa et al. [16] found that neutrophils phagocytized Ti par ticles (1-3 m) and concluded that the cytotoxicity of Ti particles was size dependant. After then, TiO2 NPs have been extensively studied to identify their potential toxicity to different cells, including human fibroblasts, macrophages, and cutaneous microvascular endothelial cells [17, 18]. Particle sizes, surface coatings, crystal shapes, and dosages were all used in these research to highlight the cell toxicological effects of TiO2 NPs. It is unknown how TiO2 NPs affect osteogenic differentiation in cells. The human body's bone tissue is one of the most active and versatile types of tissue there is. Trauma, damage, infection, and loss of bone extracellular matrix are among the most serious health threats to humans [22]. [23] Bone tissue engineering is a novel strategy to repairing bone abnormalities and designing bone tissue transplantation. It's been shown in several research on bone tissue engineering that a variety of materials, stress or other variables may impact bone tissue cell proliferation, differentiation or mineralization. Osteoblasts, in particular, populate the bone defect during bone repair. It is the Golgi apparatus of osteoblasts that allows them to release a huge number of proteins onto the surface of the bone matrix [34]. Research into whether or not TiO2 NPs may promote osteogenic differentiation in cells is significant since osteoblasts are critical in bone production. By coculturing MC3T3-E1 cells with TiO2 NPs, we investigated how the concentration, shape, and size of NPs affected the proliferation and osteogenic differentiation of preosteoblasts. The CCK-8 kit is used to monitor MC3T3-E1 cell proliferation. Flow cytometry is used to study cell death and reactive oxidative species (ROS). Analysis of ALP, OCN, and Alizarin Red staining of mineralized osteoblast nodules helps determine the differentiation and proliferation of osteoblasts.

Materials and Methods

In this investigation, R2 (Wan Jing New Material Co. Ltd.; purity > 99:8 percent) and rutile TiO2 NPs (A2; Beijing Nanchen Technology Develop ment Co. Ltd.) without any coating were utilised. It was bought from Gibco Invitrogen's Minimum Essential Medium Eagle (MEM) (USA). MDgenics supplied the foetal bovine serum (FBS)

www.jst.org.in DOI: https://doi.org/10.46243/jst.2021.v6.i6.pp19-30

(New Zealand). INALCO supplied penicillin G and streptomycin for use in this study (USA). Beyotime Institute of Biotechnology provided the cell counting kit-8 (CCK-8), ALP assay kit, 2,7-dichlorodihydrofluorescein diacetate (DCFH-DA), total glutathione assay kit, total superoxide dismutase (SOD) assay kit with WST-1, lipid peroxidation product (malondialdehyde, MDA) assay kit, cell lysis buffer, and BCA protein assay kit (Jiangsu, China). Roche Co. Ltd. provided phenylmethanesulfonyl fluoride (PMSF). AMRESCO supplied the trypsin (USA). Nanjing Jiancheng Bioengineering Institute supplied the mouse bone gla protein/osteocalcin (BGP/OCN) ELISA kit. Bellancom Chemistry provided the company with Alizarin Red S. To get dexamethasone and -glycerophosphate, we went to Sigma-Fluka. AMRESCO bought L-ascorbic acid (USA). For the remainder of this experiment, only analytical-grade chemicals were employed. In anhydrous ethanol, TiO2 NPs were suspended and ultrasonically agitated at 200 watts for 5 seconds ten times. The silicon wafer was dipped into the suspension. SEM revealed the TiO2 NPs' size and form (Hitachi S-4800 SEM). The structural profile of TiO2 NPs was characterised by TEM (FEI Tecnai G2 F20 S Twin). Quanta chrome Instruments, USA, used the Quadrasorb SI analyzer (N2 absorption at 77.3 K) to measure the surface parameters of TiO2 NPs, such as the surface area, average pore diameter, and pore volume. An analyzer that measures particle size and zeta potential was used to determine the dispersion and aggregation of TiO2 NPs in aqueous solution (Zetasizer Nano ZS90, Malvern Instruments, UK). Suspended PBS-TiO2 NPs Sedimentary Observations The sediment of the TiO2 NP suspension was studied in a series of studies. Fresh sterilised PBS solution was used to disseminate the TiO2 NPs at the following concentrations: 10, 30, and 100 g/mL each. TiO2 NPs were dispersed by ultrasonicating the sus pension for 5 s at 200W for 10 times (ultrasonic cell disruptor system, Jiangsu, China). After that, the suspension of TiO2 NP was permitted to stand for 12 hours. A digital camera was used to document the sediment's current condition (Canon PowerShot S95, Japan). For the next step, PBS was used to create nano-TiO2 suspensions containing 5, 10, 20, and 30 ng/mL of TiO2. In order to improve NP dispersion, 2 mg/mL bovine serum albumin (BSA) was added to PBS (40 : 1 compared with the weight of TiO2 NPs). As a counterpoint, MEM was infused with TiO2 NPs at a concentration of 20 g/mL. After a 48-hour period, all TiO2 NP suspensions were analysed for sediment. Cultivation of cells (section 2.4). The National Platform of Experimental Cell Resources for Science and Technology provided the MC3T3-E1 mouse preosteoblast cells (Beijing, China). The cells were incubated at 37°C in a humidified environment containing 5% CO2 in MEM supplemented with 10% FBS, 100 U/mL penicillin, and 100 g/mL streptomycin. When the cells achieved 80% to 100% confluence, the culture media was replaced every three days. A density of 8:0 103 cells per well in 100 L culture media was used to measure cell activity in the 96-well plates. Seeding cells at a density of 2/5 105 cells/well in culture media was used for further investigations, which took place in 6-well plates. The cells were treated to four different nano-TiO2 suspensions after they had reached 70% confluence. BSA was added to a PBS solution containing the TiO2 NP suspension (1mg/mL). Ultrasonication was performed for 30 minutes to prevent agglomeration of the suspensions. MEM was used to dilute the suspension to a concentration of 20 ng/mL. When 10% FBS was added, the TiO2 NP suspension had a concentration of 20 ng/mL.

Table 1: Characterization of TiO_2 NPs.

Original no.	No.	Crystal	Shape	Size (nm)	Specific surface area (m^2/g)	Average pore diameter (nm)	Total pore volume (cc/g)	Z-Ave (d·nm)	Zeta potential (mV)
1	A1	Anatase	Red blood cell like	D: 45.87 ± 7.75	97.75	1.79	0.56	166.6	5.7
6	A2	Anatase	Sphere	D: 79.39 ± 22.58	10.37	1.93	0.05	653.3	-18.7
2	R1	Rutile	Long rod	D: 52.37 ± 7.35 L: 86.55 ± 12.13	21.51	2.17	0.22	408.7	2.3
4	R2	Rutile	Long rod	D: 25.46 ± 9.65 L: 75.34 ± 13.28	28.27	2.44	0.17	183.6	-22.0

used MC3T3-E1 cells as a culture medium. In each experiment, the control was culture medium without TiO2 NPs. 2.5. The CCK-8 Assay is performed. We used a concentration of NPs of 20 g/mL on MC3T3-E1 cells exposed for 24 hours to four different varieties of nano-TiO2. A second round of washing with PBS was followed by incubation with 100 L MEM and 10 L CCK-8 for 2 h, at 37°C. The negative control was MEM and CCK-8 without cells. Microplate reader Varioskan Flash (3001, USA) was used to measure the intensity at 450 nm. As a proportion of viable cells, cell viability was measured. All trials were carried out in at least three separate instances. 2.6. Measurement of ROS and Superoxide Production. In order to measure ROS generation, DCFH-DA fluorescence was used. MC3T3-E1 cells were collected after 24 hours of coculture with four kinds of 20 g/mL TiO2 NPs. In order to verify that the probe had a complete response with the cells, the cells were treated with 10 M DCFH DA in the dark for 20 minutes at 37° C and reverse mixed every 3–5 minutes. After that, the cells were rinsed three times

www.jst.org.in DOI: https://doi.org/10.46243/jst.2021.v6.i6.pp19-30

using a serum-free media. A positive control was performed using cells that had been grown with 1 L of Rosup. Fluorescent chemical 2′,7′-dichlorofluorescein (DCF) is produced via ROS-induced oxidation of DCFH (BD FACSCalibur, USA). DCF fluorescence was measured using 20,000 cells in each experiment group that were excited at 488 nm and emitted at 530 nm. In the presence of superoxide, WST-1 was reduced to an orange soluble formazan that could be read at 450 nm. Catalase and SOD were employed in this kit to ensure that H2O2 was not interrupted, and the results were corrected. MC3T3-E1 Cells were examined by TEM. MC3T3-E1 cells cocultured with or without TiO2 NPs were scraped and immediately submerged in 2.5 percent glutaraldehyde overnight at 4° C for the TEM examination. Using PBS as a pre-treatment, the samples were fixed with 1 percent osmium tetroxide before being dehydrated in a succession of ethanols, embedded in araldite, and polymerized for 24 hours at 37 degrees Celsius. We used a Hitachi H-600 TEM (Japan) with the Cell Apoptosis Assay to examine the ultra-thin sections (60nm) stained with uranyl acetate and lead citrate. By using Annexin V-FITC and PI assays, as well as flow cytometric analyses, apoptosis was determined. The detection kit's instructions on how to use Annexin V-FITC/PI were strictly followed. A concentration of 20 g/mL of TiO2 NPs was applied to the cultured cells for 24 hours. Trypsinization was used to extract cells, which were rinsed with PBS, then centrifuged for 5 minutes at 1,000 rpm. Finally, the cells were resuspended in Annexin V binding buffer solution at a concentration of 1 106 cells/mL. A 5 L aliquot of Annexin V-FITC was incubated with 100 L of cells in a tube for 15 minutes at room temperature and in the dark. Necrotic cells may be identified by the presence of the dye PI. Flow cytometry was used to evaluate the cells after just one hour of labelling, and 400 L binding buffer was added to each tube. Assessment of ALP and OCN activity. In the alkaline buffer, p-nitrophenol was released from p-nitrophenyl phosphate (pNPP). After three PBS washes, cell layers on a 6-well plate were treated for 40 minutes on ice with 100 L of cell lysis buffer containing 1 percent Triton X-100. An EP tube was used to collect the cell lysates using a cell scraper. Following a 10-minute centrifugation at 12,000 rpm at 4°C, the supernatant was utilised to measure activity of the enzyme. In addition, the BCA technique was used to determine the protein concentration. ELISA was used to determine the concentration of OCN products in the culture medium. According to the manufacturer's instructions, the tests were carried out exactly as specified. An ELISA microplate was coated with a purified anti-mouse OCN antibody. The lyophilized culture medium was reconstituted in PBS and pipetted into the wells, which were then incubated. Each

www.jst.org.in DOI: https://doi.org/10.46243/jst.2021.v6.i6.pp19-30

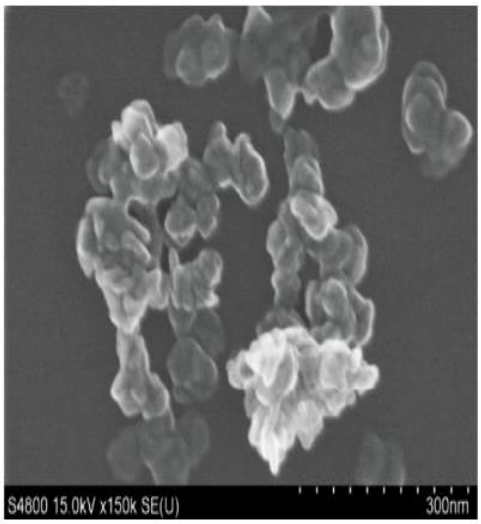

(a)

and every one of the OCN present had to abide by the

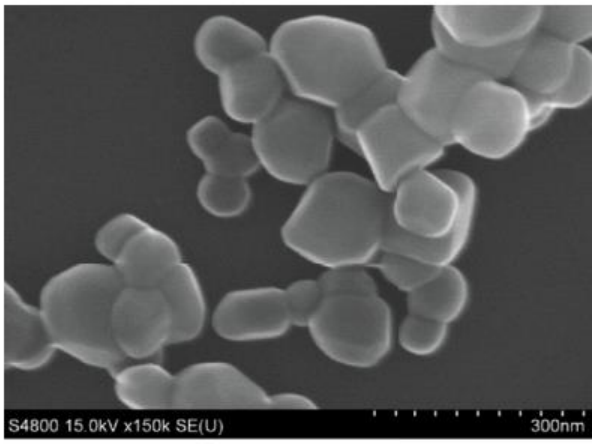

(b)

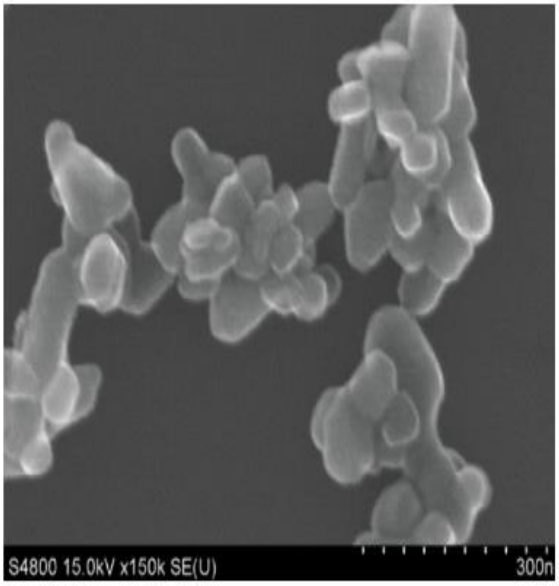

(c)

Journal of Science and Technology
ISSN: 2456-5660, Volume 6, Issue 6 (NOV-DEC 2021)

www.jst.org.in DOI: https://doi.org/10.46243/jst.2021.v6.i6.pp19-30

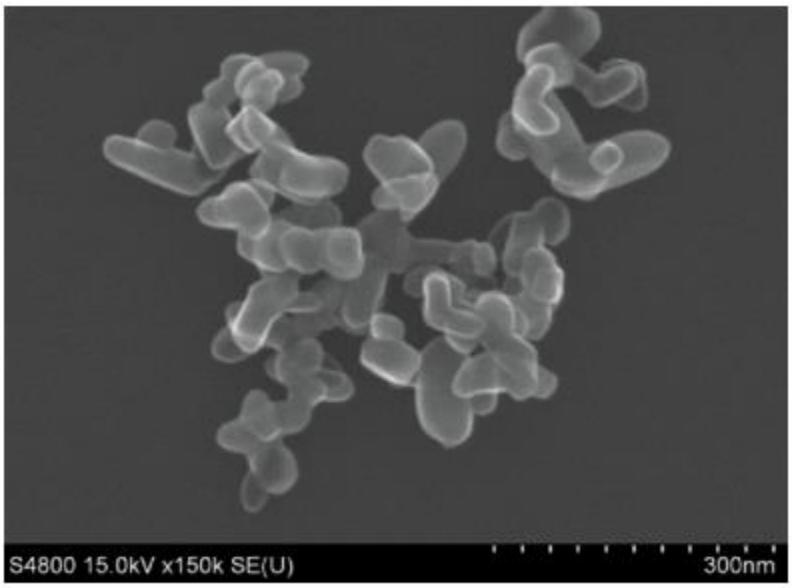

(d)

SEM images of TiO2 NPs are shown in Figure 1. A1 TiO2 NPs have a diameter of 45:87 7:75 nm. Its diameter is 79:39 to 22:58nm for A2 TiO2 nanoparticles. (b) In terms of size, the R1 TiO2 NPs had a diameter and length of 52:37 nm and 86:55 nm, respectively. (d) R2 TiO2 NPs have a diameter of 25:46 nm and a length of 75:34 nm. s. Staining of Mineralized Nodules. Cell mineralization in MC3T3-E1 cells was studied using Alizarin Red S staining. An osteogenic medium comprised of MEM medium, 10 mmol/L beta-glycerophosphate, and 0.05 mmol/L ascorbic acid was used to expose the cells to four different kinds of TiO2 nanoparticles. Every three days, the osteogenic media was replaced. After 28 days, the cell layers were rinsed three times with PBS and fixed in 95 percent ethanol for 10 minutes, as shown in Figure 1. The cells were then stained for 30 minutes with 0.1 percent Alizarin Red S after three washes with water. Images and counts of the mineralized nodules were obtained using microscopy. Analysis of statistical data. The SPSS 13.0 statistical software was used to examine all of the data (SPSS Inc., USA). One-way analysis of variance was used to analyse the experimental data (ANOVA). Results with a p-value of 0.05 or less were deemed significant..

Results

3.1. TiO2 NP characterization. A detailed description of both anatase and rutile TiO2 was supplied and described. Figures 1 and 2 show images of TiO2 NPs taken under SEM and TEM conditions. Figure 1(a) shows that the anatase TiO2 A1 had an average diameter of 45:87 7:75 nm, similar to that of red blood cells (Figure 2(a)). For A2, we found that it had an average diameter of 79:39 nm (Figure 1a). R1 and R2 were long rods of various diameters for the rutile TiO2 (Figures 2(c) and 2(d)). As shown in Figure 1(c), the average length and diameter of R1 were 86:55 nm and 52:37 nm, respectively. For R2, these values were 75:34 nm and 13:28 nm, respectively (Figure 1(d)). Table 1 summarises and lists the physical parameters of TiO2 NPs. In order to study the aggregation of TiO2 NPs in solution, DLS was applied. Figure 3 shows the distribution of TiO2 NPs' hydrodynamic diameters in an aqueous solution. Rutile TiO2 revealed a peak at 408 7.7 nm (size distribution from 141 to 1106 nm) with a Zeta potential of 2.3 mV, suggesting that R1 was readily agglomerated and aggregated in solution. Due to the R2 suspension's zeta potential value of -22.0 mV, the R2 peak at 183.6 nm (size distribution from 105 to 396 nm) indicated that the R2 suspension was stable (Table 1). It was found that anatase A1 had an average diameter of 166.6 nm, whereas A2 had a high peak of 235.3 nm and a lower peak of 5.01 nm. Table 1 lists the zeta potentials of the anatase and rutile

www.jst.org.in DOI: https://doi.org/10.46243/jst.2021.v6.i6.pp19-30

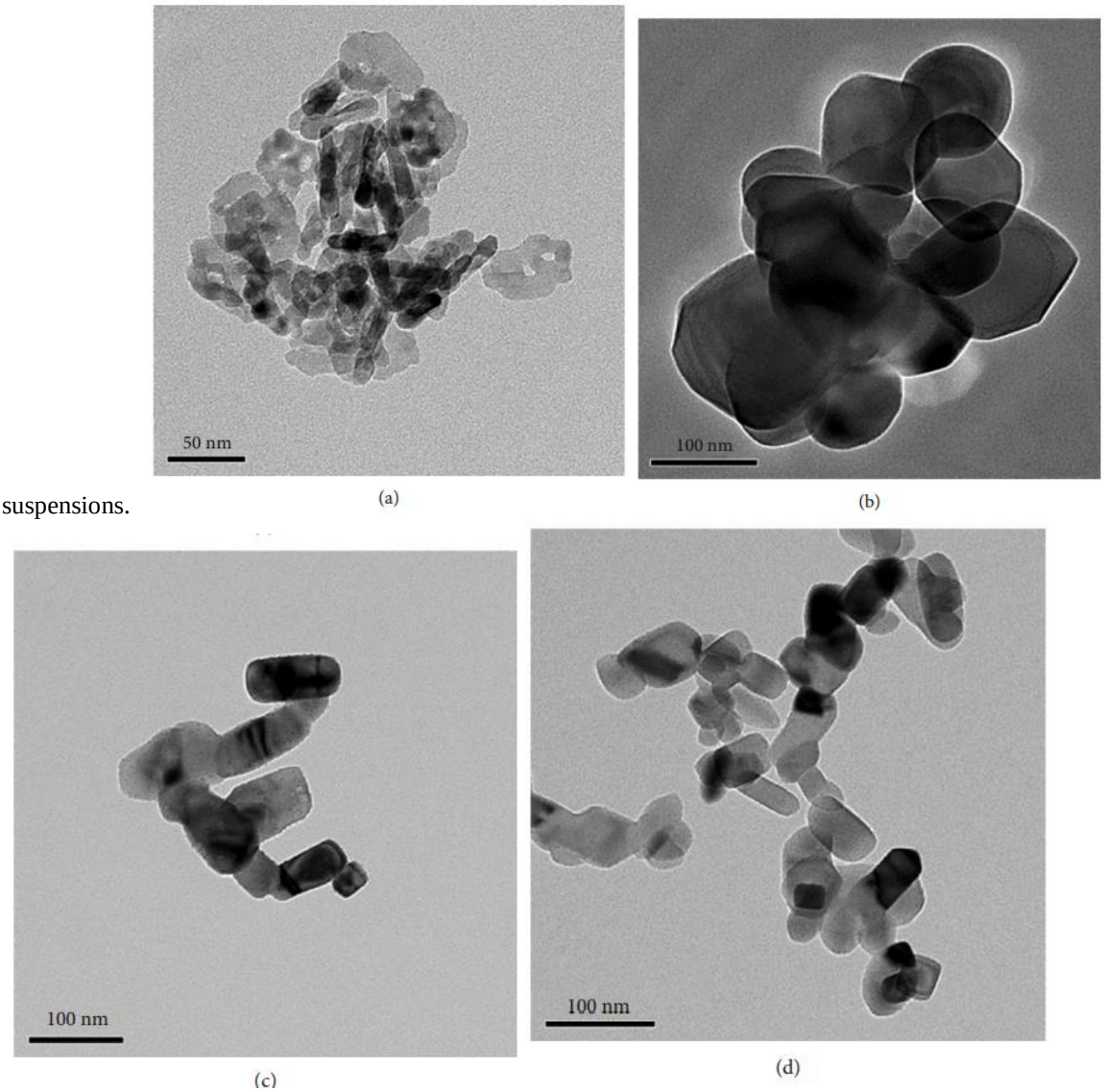

suspensions.

Figure 2: Micrographs of TiO2 NPs by TEM: (a) A1 is erythrocyte like; (b) A2 is spherical; (c) R1 is a long rod; (d) R2 is a long rod.

3.2.Determination of TiO2 NP Concentration.

Using a camera to film the TiO2 NPs sedimentation, we were able to determine the concentration of the NPs to utilise. Figure S1 illustrates the 12-hour sedimentation of TiO2 in PBS containing BSA at concentrations of 10, 30, and 100 g/mL. After two hours of standing, the 100 g/mL TiO2 NP group was allowed to settle. Flocculated precipitations were seen after 12 hours of incubation with TiO2 NPs in the presence of 30 g/mL TiO2 NPs. After settling for 12 hours at a concentration of 10 g/mL, no sediment was found in the suspension. In PBS and culture media for 48 hours, TiO2 NPs lower than 30 g/mL sedimented in Figure S2. As a reference, we used culture media containing 20 g/mL TiO2 NPs as a control. Precipitates were observed in the 30 g/mL group 12 h after incubation, however no precipitates were identified in the TiO2 NPs less than 20 g/mL after 48 h. Both in PBS and in culture media, a suspension of less than 20 g/mL demonstrated excellent stability and dispersion. MC3T3-E1 Cell Viability (3.3) TiO2 NPs were added to the culture. Different concentrations of A1 and R2 TiO2 NPs in MC3T3-E1

www.jst.org.in DOI: https://doi.org/10.46243/jst.2021.v6.i6.pp19-30

preosteoblast cells were used to measure cell viability (Figure 4). After 24 hours of incubation, cell viability was reduced by more than 50% when the concentration of TiO2 NPs exceeded 50 g/mL (Figure 4(a)). TiO2 NPs concentrations between 30 and 50 g/mL substantially decreased cell viability compared to the control group (Figure 4(c)). Cell viability was unaffected by TiO2 NP concentrations lower than 10 g/mL (Figure 4(b)). TiO2 NPs are similarly effective at 20 g/mL.

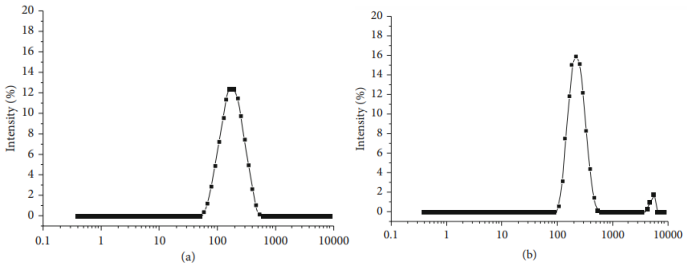

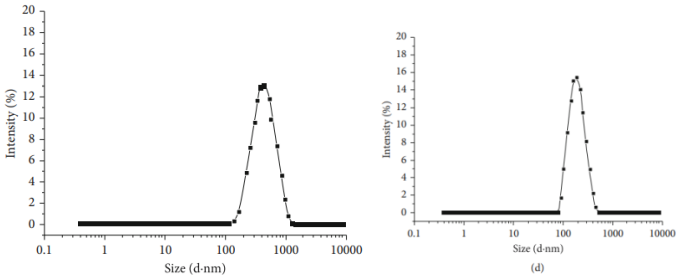

Using the DLS approach, we determined the hydrodynamic diameter distribution of nano-TiO2 in water. (a) A1 has a maximum diameter of 166.6 nm on average. In (b), A2 displays an extremely high, narrow peak at 235.3 nm. At 408.7 nanometers, R1 exhibits a peak. Cell survival was unaffected by R2's small peak at 183.6 nm. TiO2 NPs were found to be cytotoxic at concentrations above 20 g/mL, according to these results, which indicated a critical threshold for cell viability. 3.4. MC3T3-E1 Cells Express ALP and OCN. The MC3T3-E1 cells were cocultured with A1 and R1 TiO2 NPs at concentrations of 20, 50, and 100 g/mL for 7 and 14 days to examine the effect of NPs on ALP expression. The osteogenic differentiation capacity of all experimental groups was dramatically reduced in comparison to the blank control group (Figure 5(a)). Furthermore, A1 and R1 TiO2 NPs had varied effects on osteoblast differentiation, depending on the concentration. R1's inhibitory impact on cell differentiation is less than A1's at low concentrations. While anatase and rutile materials had similar inhibitory effects on cell differentiation, as NP concentration increased, rutile materials were more effective in inhibiting cell differentiation. Figure 5 depicts the 14-day ALP levels of cells cocultured with A1 and R1 materials (b). In comparison to the control, the ALP level decreased by 64.30% when A1 concentration was 20 ng/mL. The ALP level reduced by 43.01 percent and 47.69 percent when the concentration was 50 and 100 g/mL, respectively. R1 had a comparable impact on cell differentiation to A1 in terms of inhibiting cell proliferation. A1 and R1 were shown to have a detrimental effect on preosteoblast cell development. Of course, the experiment groups and the control group did not vary significantly when it came to OCN findings (Figure S3). Assessment of ROS Production and Antioxidant Level 3.5 ROS generation has been implicated with TiO2 NP toxicity in several studies. Figure 6 shows the findings of the ROS generation and antioxidant levels in MC3T3-E1 cells examined in this research. TiO2 NP treatment enhanced the fluorescence of oxidised DCF in cells (Figure 6(a)), particularly in the A1, R1, and R2 groups (p 0:05). Figure 6. This indicated that the treatment with 20 g/mL TiO2 NPs created ROS. It was also possible to measure cell superoxide generation using WST 1. Four different varieties of TiO2 NPs produced considerably more superoxide

www.jst.org.in DOI: https://doi.org/10.46243/jst.2021.v6.i6.pp19-30

when compared to the control group (Figure 6(b)). The primary glutathione (T-GSH)

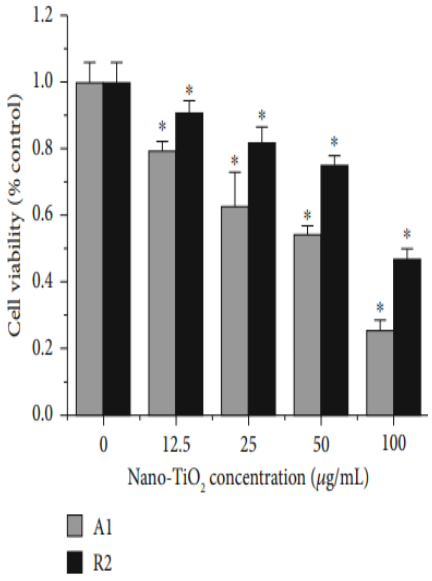

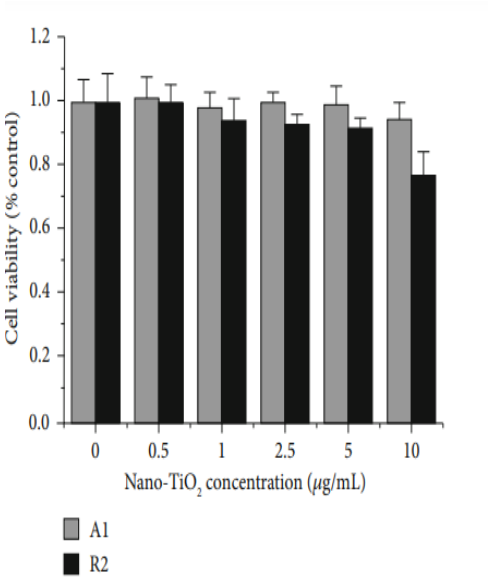

www.jst.org.in DOI: https://doi.org/10.46243/jst.2021.v6.i6.pp19-30

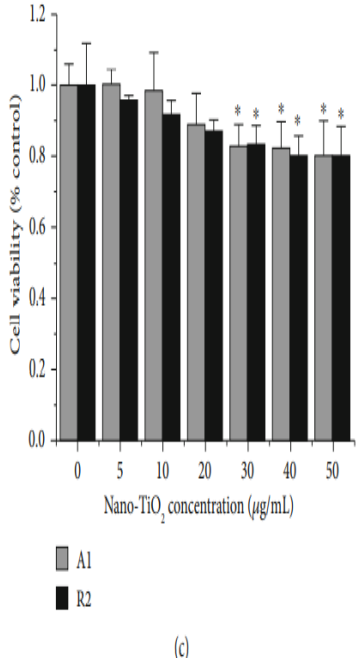

Figure 4: Cell viability of MC3T3-E1 cells cocultured with different concentrations of TiO2 NPs. ∗p < 0:05 significantly different from the corresponding control group

The A1 and R1 groups had considerably reduced levels of T-GSH (Figure 6(c)). MC3T3-E1 cells were also found to have high levels of SOD and MDA, which indicated oxidative stress. Figures 6(d) and 6(e) show that SOD and MDA activity was marginally greater in the TiO2 NP-treated group than in the control group (p 0:05) after the treatment (Figures 6(d) and 6(e)). The TEM is at 3.6. MC3T3-E1 Cell Characterization TiO2 NPs were added to the culture. The membrane of MC3T3-E1 cells was deformed and caved in after coculturing with TiO2 NPs, enclosing the aggregated TiO2 NPs. TiO2 NPs were shown to be grouped around the nucleus inside the plasma membrane of cells (Figure 7(b)). This ultrastructural alteration was triggered by the internalisation of TiO2 NPs, some of which were found in the mitochondria of MC3T3-E1 cells. Although the nucleus was clearly visible, the nuclear envelope was deformed. The nuclear chromatin was in the meanwhile compressed and dispersed throughout the nucleus' periphery. It was shown that when the number of mitochondria and lysosomes rose, the lamellar cristae began to become more irregular. At the same time, the architecture of mitochondria were inflated and void, indicating that the organelle had been damaged by the storage of nano-TiO2. The enlargement of the golgi complex (Figure 7(c)) further revealed that the golgi complex had been damaged. Disintegration and an apoptotic body formed after exposure to A2 and R2 for 24 hours (Figures 7(d) and (e)). Because of their absorption into cells and subsequent subcellular damage, TiO2 nanoparticles were shown to be toxic according to TEM analysis. This section focuses on

cell death and mineralization in MC3T3-E1 cells TiO2 NPs were added to the culture. Apoptosis and necrosis in

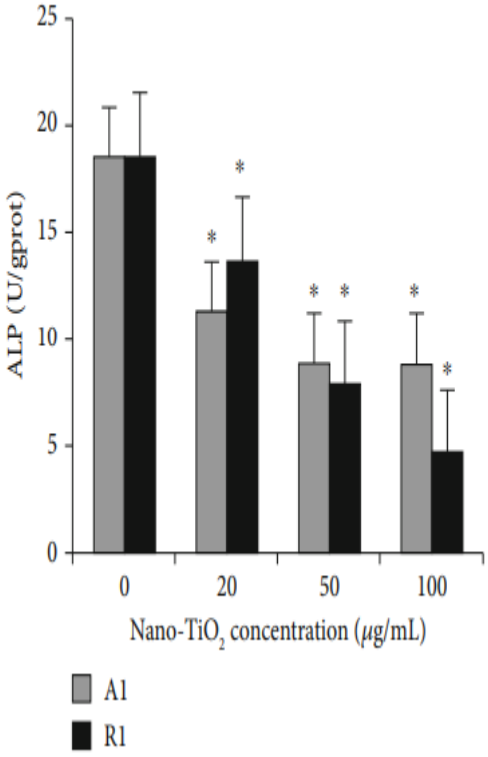

MC3T3-E1 cells were detected by flow cytometry.

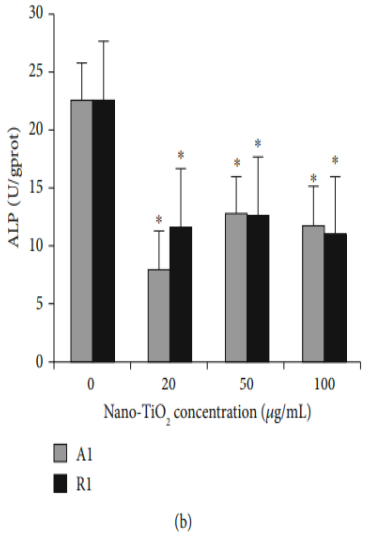

(b)

Conclusion

Bone formation is negatively affected by TiO2 NPs. Nano-TiO2 concentrations, geometries, and coculture periods all affect bone cell proliferation and differentiation in distinct ways, as seen below. According to a general rule,

nano-TiO2 in tissues may lead to a reduction in osteoblast activity as well as blocked bone formation if the presence of nano-TiO2 is present.

References

[1] J. Jeevanandam, A. Barhoum, Y. S. Chan, A. Dufresne, and M. K. Danquah, "Review on nanoparticles and nanostructured materials: history, sources, toxicity and regulations," Beilstein Journal of Nanotechnology, vol. 9, pp. 1050–1074, 2018.

[2] H. Shi, R. Magaye, V. Castranova, and J. Zhao, "Titanium dioxide nanoparticles: a review of current toxicological data," Particle and Fibre Toxicology, vol. 10, no. 1, p. 15, 2013.

[3] S. Silva, H. Oliveira, A. M. S. Silva, and C. Santos, "The cytotoxic targets of anatase or rutile + anatase nanoparticles depend on the plant species," Biologia Plantarum, vol. 61, no. 4, pp. 717–725, 2017.

[4] A. Hasan, M. Morshed, A. Memic, S. Hassan, T. Webster, and H. Marei, "Nanoparticles in tissue engineering: applications, challenges and prospects," International Journal of Nanomedicine, vol. Volume 13, pp. 5637–5655, 2018.

[5] X. Li, J. Wei, K. E. Aifantis et al., "Current investigations into magnetic nanoparticles for biomedical applications," Journal of Biomedical Materials Research Part A, vol. 104, no. 5, pp. 1285–1296, 2016.

[6] A. Jimeno-Romero, M. Oron, M. P. Cajaraville, M. Soto, and I. Marigomez, "Nanoparticle size and combined toxicity of TiO2 and DSLS (surfactant) contribute to lysosomal responses in digestive cells of mussels exposed to TiO2 nanoparticles," Nanotoxicology, vol. 10, no. 8, pp. 1168–1176, 2016.

[7] T. H. Kim, M. S. Kang, N. Mandakhbayar, A. El-Fiqi, and H. W. Kim, "Anti-inflammatory actions of folatefunctionalized bioactive ion-releasing nanoparticles imply drug-free nanotherapy of inflamed tissues," Biomaterials, vol. 207, pp. 23–38, 2019.

[8] I. Pujalte, D. Dieme, S. Haddad, A. M. Serventi, and M. Bouchard, "Toxicokinetics of titanium dioxide (TiO2) nanoparticles after inhalation in rats," Toxicology Letters, vol. 265, pp. 77–85, 2017.

[9] S. Vial, R. L. Reis, and J. M. Oliveira, "Recent advances using gold nanoparticles as a promising multimodal tool for tissue engineering and regenerative medicine," Current Opinion in Solid State & Materials Science, vol. 21, no. 2, pp. 92–112, 2017.

[10] K. Zhang, Y. Fan, N. Dunne, and X. Li, "Effect of microporosity on scaffolds for bone tissue engineering," Regenerative Biomaterials, vol. 5, no. 2, pp. 115–124, 2018.

[11] A. J. Haider, Z. N. Jameel, and I. H. M. Al-Hussaini, "Review on: titanium dioxide applications," Energy Procedia, vol. 157, pp. 17–29, 2019. [12] M. H. Hamzah, S. Eavani, and E. Rafiee,"CoAl2O4/TiO2 nano composite as an anti-corrosion pigment," Materials Chemistry and Physics, vol. 242, p. 122495, 2020.

[13] I. Narkevica, L. Stradina, L. Stipniece, E. Jakobsons, and J. Ozolins, "Electrophoretic deposition of nanocrystalline TiO2 particles on porous TiO2-X ceramic scaffolds for biomedical applications," Journal of the European Ceramic Society, vol. 37, no. 9, pp. 3185–3193, 2017.

[14] T. V. S. S. P. Sashank, B. Manikanta, and A. Pasula, "Fabrication and experimental investigation on dye sensitized solar cells using titanium dioxide nano particles," Materials Today: Proceedings, vol. 4, no. 2, pp. 3918–3925, 2017.

[15] J. Ferin, G. Oberdörster, and D. P. Penney, "Pulmonary retention of ultrafine and fine particles in rats," American Journal of Respiratory Cell and Molecular Biology, vol. 6, no. 5, pp. 535– 542, 1992.

[16] R. Kumazawa, F. Watari, N. Takashi, Y. Tanimura, M. Uo, and Y. Totsuka, "Effects of Ti ions and particles on neutrophil function and morphology," Biomaterials, vol. 23, no. 17, pp. 3757–3764, 2002.

[17] T. Brzicova, J. Sikorova, A. Milcova et al., "Nano-TiO2 stability in medium and size as important factors of toxicity in macrophage-like cells," Toxicology In Vitro, vol. 54, pp. 178– 188, 2019.

[18] M. Ibrahim, J. Schoelermann, K. Mustafa, and M. R. Cimpan, "TiO2 nanoparticles disrupt cell adhesion and the architecture of cytoskeletal networks of human osteoblast-like cells in a size dependent manner," Journal of Biomedical Materials Research Part A, vol. 106, no. 10, pp. 2582–2593, 2018.

[19] K. Hattori, K. Nakadate, A. Morii, T. Noguchi, Y. Ogasawara, and K. Ishii, "Exposure to nano-size titanium dioxide causes oxidative damages in human mesothelial cells: the crystal form rather than size of particle contributes to cytotoxicity," Biochemical and Biophysical Research Communications, vol. 492, no. 2, pp. 218–223, 2017.

[20] M. J. Bessa, C. Costa, J. Reinosa et al., "Toxicity of rutile TiO2 nanoparticles immobilized in nanokaolin nanocomposites on HepG2 cell line," Toxicology and Applied Pharmacology, vol. 316, pp. 114–122, 2017.

Trends in Biomaterials and Artificial Organs
www.biomaterials.org.in/tibao

Review Article

Toxicity Associated with Gold Nanoparticles: A Review

K.K.J. Chakravarthy[1], P.S. Brahmanandam[2*], G. Uma[2], D.M. Potukuchi[3], N.S. Subba Rao[5], G. Anil Kumar[4], A. Rama Krishna[5]

[1]*Department of Physics, BV Raju College, Vishnupur, Bhimavaram 534202, India*
[2]*Department of Physics, Shri Vishnu Engineering College for Women (A), Vishnupur, Bhimavaram 534202, India*
[3]*Department of Physics, 4.School of Renewable Energy and Environment, JNT University, Kakinada 533001, India*
[5]*Physics, Govt. Junior College, Tallarevu 533463, India*
[6]*Dental Materials, Vishnu Dental College, Vishnupur, Bhimavaram 534202, India*

Received: *2 June 2022*
Accepted: *26 July 2022*
Published online: *30 September 2022*

Keywords: : *nanotechnology, gold nanoparticles, toxicity, green synthesized gold nanoparticles, in vivo and in vitro studies*

Gold nanoparticles (AuNPs) are by far the most studied nanomaterials by the scientific fraternity, possibly due to their immense potential in medical applications. Nevertheless, there is a disparity of opinion that prevailed concerning the toxicity of AuNPs. This study, therefore, presents a systematic review concerning toxicity related to AuNPs with the help of recently published databases. The disparity is due to the fact that the adoption of various protocols in the assessment of toxicity over the years that led to divergent views about the actual safety of AuNPs. This paper has considered a few recent research works and their databases to assess the toxicity of AuNPs *in vivo* and *in vitro*. Further, this paper also discussed the possible approaches that could effectively minimize the lethal effects of AuNPs and elaborated on the future scope of this interesting and highly useful research. For time being, it is concluded here that nanomaterial safety data are scarce, and it is not even an exaggeration to say that that is even scarcer than reported.

Introduction

Ever since the term nanotechnology was coined by Norio Taniguchi, a professor at Tokyo University, Japan in the year 1974, several prominent research and development (R&D) organizations, academic and non-academic institutions, and others have ventured their efforts across the globe to gain benefits out of this ever-growing field. The growth of nanomaterials and nano-products synthesized (engineered) using nanoscience and nanotechnology has been phenomenal and non-linear, as rightly predicted by Richard Feynman in his speech at the American Physical Society (1959) at Caltech that 'There's Plenty of Room at the Bottom'. Nanomaterials' widespread use and success can be attributed to their distinct qualities compared to their bulk counterparts, such as lightweight, low cost, small size, and more durability, to mention a few.

Other properties such as chemical (reactivity and reaction rates), electrical (conductivity), magnetic, optical (colour and transparency), and physical (hardness and boiling point) have altered significantly as a result of nanoscience and nanotechnology and are now extremely valuable in the manufacture of high-end products. It may not be an exaggeration that there are no scientific, research, medical, aerodynamics, space, and other industrial fields that have not used nano-enabled products. For instance, engineered nanomaterials (ENMs) find potential applications in medicine, pharmaceutics, biotechnology, energy production, environmental sciences, crop protection, transportation, housing, and electronics. Still, there is a considerable proliferation of ENMs and nanocomposites in the market, thanks to this ever-increasing field on a day-by-day basis. The nanoscience enabled nanomaterials/products were successfully used in the eradication of corona virus disease-2019 (COVID-19) [1].

Researchers, on the other hand, have proposed two schools of thought. One school believes there are no risks related to nanomaterials, while the other institution disagrees. Certain characteristics of anthropogenic origin nanomaterials, such as their size, mobility, and significant interaction with the host where they are deposited and dispersed, may make them dangerous. After recognizing this potential distinction, a few research groups have

* *Coresponding author*
E-mail address: *dranandpotula@svecw.edu.in* (Dr P. S. Brahmanandam)

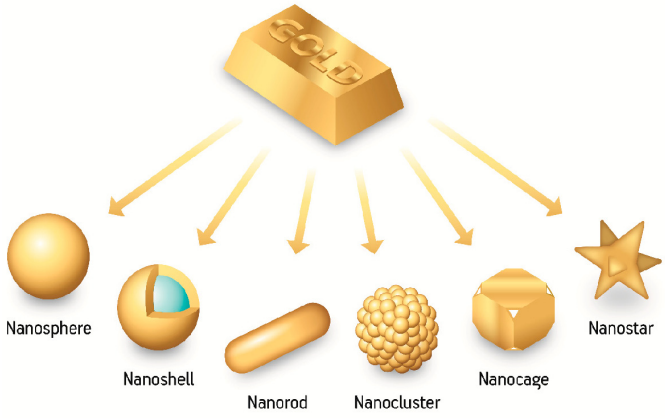

Figure 1: Most common gold nanoparticle assemblies and morphologies (After Freitas et al., 2018, Reference [11])

already initiated significant research under the name of "nanotoxicology research". In order to adequately address nanotoxicology and its detrimental implications, if any, on humans, animals, the environment, and other living species, it is necessary to examine and understand recent technical advancements in the field of nanotechnology.

Nanomaterials found in the human environment may have the potential for toxicological effects. However, the current literature on the toxicological effects of nanomaterials is diverse. The current data are presented from studies without harmonization [2]. These studies have used different in vitro and in vivo test models, different sources of test nanomaterials, different methods for nanomaterial characterization, and different experimental conditions. Therefore, these data are hard to interpret. More research on nanomaterial characterization, biological interaction, bio distribution, toxicity, and health effects are needed. The test methods need to be validated. Positive and negative controls for nanotoxicity need to be identified. Toxicity data harmonization needs to be done. Therefore, general information is not currently available for risk evaluation of certain nanomaterials that might be present in consumer products or that may enter the market in the future. Standardized and validated methods are necessary for the toxicity assessment of nanomaterials. Therefore, in the absence of standardized validated methods, any specific regulatory testing requirements for nanomaterials are currently premature. The benefits of nanomaterials found currently in the human environment are many, but their overall adverse effects on human health are limited [3].

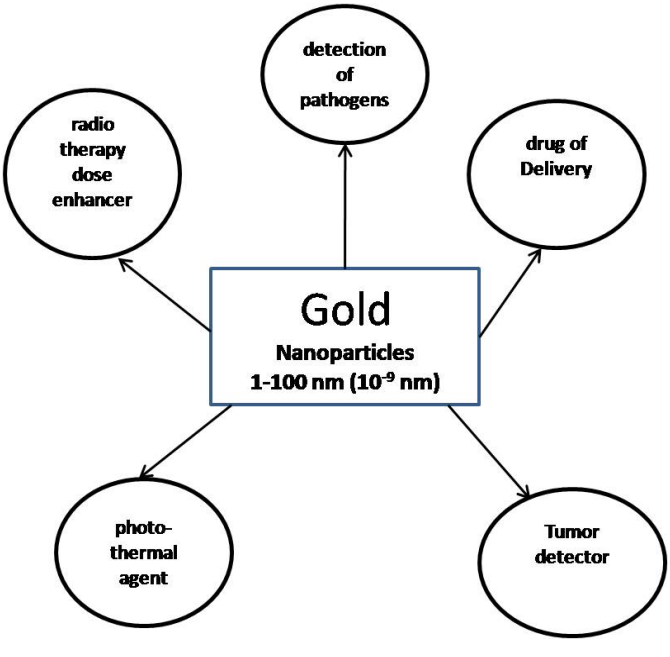

Figure 2: Gold nanoparticles medical applications (After Gerber et al., 2013, Reference [13])

In recent years, various studies have been conducted to determine the potential toxicity of nanoparticles in response to significant concerns regarding nanotechnology's safety. Nanomaterials' distinctive qualities, such as their extremely small size, high reactivity, and unique tensile property, as well as their considerable magnetic properties, have sparked a great deal of interest in their use in biological, environmental, and industrial applications. As a result, concerns regarding the impact on the environment, human health, and safety have been raised. For example, there was a lot of debate about the toxicity of carbon nanotubes (CNTs), which are thought to induce tissue damage in animals [4]. On the other hand, various research investigations on the toxicity of CNTs have come up with conflicting results [5].

Unlike CNTs, the variety of AuNPs and their biomedical uses continues to grow daily. Biosensorics, bioimaging, photothermal treatment, targeted drug delivery, and mushroom growth are some of the applications of AuNPs. Therefore, human safety problems are becoming increasingly prominent. As a result, a deeper understanding of the potential toxicity hazards of current AuNPs and the resulting AuNPs has become critical. With the aforementioned considerations in mind, this research highlighted two crucial issues: a comprehensive recent review of AuNPs nanotoxicity, as well as feasible approaches to reduce or eliminate the lethal consequences of AuNPs toxicity.

Recent Studies of Gold Nanoparticles Toxicity: *In vivo* and *In vitro*

Numerous AuNPs shapes and topologies have been fabricated using various synthetic approaches. Nanospheres, nanoshells, nanorods, nanoclusters, nanocages, and nanostars are some of the diverse shapes of AuNPs [6-10]. The most common gold nanoparticle assemblages and morphologies are depicted in figure 1 (after Freitas et al., 2018, [11]). AuNPs are widely utilized across the medical field due to their excellent biocompatibility, because of their high chemical and physical stability and ease to functionalize with biologically active organic molecules or atoms [12]. Various medical applications of AuNPs can be found in figure 2 (after Gerber et al., 2013 [13]). AuNPs can directly conjugate and interact with diverse molecules containing proteins, drugs, antibodies, enzymes, nucleic acids and fluorescent dyes on their surfaces for diverse medical applications and biological activities [14-16].

Figure 3 shows how various molecules conjugate with AuNPs (after Hu et al., 2013 [10]). As previously indicated, there is a wide divergence of opinion among researchers on the toxicity of AuNPs. This paper initially, therefore, presents the literature survey of AuNPs toxicity, followed by summarizing a few studies associated with AuNPs toxicity (*in vivo* as well as *in vitro*) in table 1 and table 2, respectively.

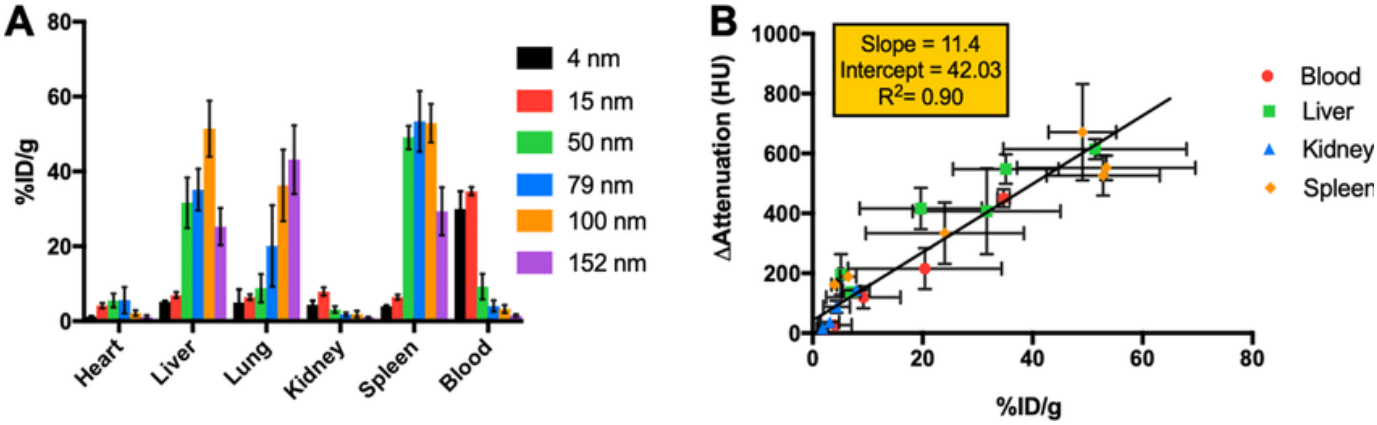

Figure 3: (A) Biodistribution of AuNP in different organs at 2hours post-injection. A Tukey's multiple comparisons test was done to compare the interactions between each AuNP size. (B) Comparison between the attenuation change in different organs derived from CT scans performed at 2hours post-injection and biodistribution of AuNP in different organs at 2hours post-injection (After Dong et al., 2019, Reference [49])

Biological Eeffects of AuNPs: A Comprehensive Viewpoint

As already stated in the introduction**,** as AuNPs have been widely used in various biomedical fields, human health may get affected through nanoparticle-protein interaction, immunogenicity, and cytotoxicity.

It was righteously articulated by Saptarshi et al. [37] that the interaction of nanoparticles with proteins is the basis of nanoparticle bio-reactivity, and this interaction gives rise to the formation of a dynamic nanoparticle-protein corona. The protein corona may influence cellular uptake, inflammation, accumulation, degradation and clearance of the nanoparticles. The nanoparticle surface can induce conformational changes in adsorbed protein molecules, which may affect the overall bio-reactivity of the nanoparticle. In depth understanding of such interactions can be directed toward generating bio-compatible nanomaterials with controlled surface characteristics in a biological environment [37].

Gold nanoparticles synthesized using citrate and *Z. officinale* extract demonstrated very low protein adsorption, as reported by [38]. Both nanoparticles were non-platelet activating and non-complement activating on contact with whole human blood. They also did not aggregate other blood cells. However, nanoparticles synthesized with *Z. officinale* extract were highly stable at

Table 1: Recent studies of AuNPs *in vivo* toxicities

Organism	Possible Effects	Type of synthesis	References
Mice	High concentrated AuNPs induced decreases in body weight, red blood cells, and hematocrit.	Water-soluble gold nanoparticles	[17]
Mice	Alteration in cell shape, inhibition of proliferation, or mutation in DNA	Polyethylene glycol (PEG)-coated AuNPs	[18]
Swiss Mice	Trans-placental size-dependent clastogenic and epigenetic effects	Water-soluble gold nanoparticles	[19]
Rats	DNA damage in the cerebral cortex	Water-soluble gold nanoparticles	[20]
Sprague-Dawley rats	No threats were found	Water-soluble gold nanoparticles	[21]
Wistar Rats	Potentially safe (no cardio toxic effects, echocardiography, arterial pressure, biochemical and histopathological analyses were found)	Biodegradable lipid-core nanocapsules	[22]
Albino rats	Histological changes in the lung tissue	Water-soluble gold nanoparticles	[23]
Rats	Mild changes in kidney, liver and testis	Biological and Fusarium oxysporum	[24]
Rats	Lung retention was found	Bio-persistent gold nanoparticles	[25]
Male albino rats	Ultra-small AuNPs showed low or no toxicity	Green synthesized ultra-small gold nanoparticles (Egyptian propolis extract)	[26]

Table 2: Recent and significant studies of AuNPs *in vitro* toxicities

Organism	Possible Effects	Type of synthesis	References
Cervix carcinoma epithelial cells (HeLa)	Necrosis	Water-soluble gold nanoparticles	[27]
Small airway epithelial cells (SAECs)	Oxidative stress-related cytotoxicity and genotoxicity in SAECs	Water-soluble gold nanoparticles	[28]
Human primary lymphocytes and murine macrophages	Proliferative activity, mitotic, apoptotic, necrotic markers, chromosomal damage	Spherical citrate-capped Au NPs	[29]
Bronchial epithelial cell line BEAS-2B, Human embryonic kidney cell line	Chinese hamster ovary cell line CHO damage	Citrate stabilized gold nanoparticles	[30]
Somatic and tumor cells	No significant cytotoxic effects found	Chitosan based gold nanoparticles	[31]
Chinese hamster ovary cells	No genotoxic effects found	Citrate-stabilized gold nanoparticles	[32]
Heart, kidney and lung	Larger sizes (42.5 and 61.2 nm) and smaller size (6.2 and 24.3 nm) AUNPs induced oxidative stress	Water soluble AuNPs	[33]
Human Cancer Cells	Toxic threat found	Biomimetic gold nanoparticles	[34]
Cholesterol molar ratio, Span 60: Tween 60 M ratio	Showed dose-dependent cytotoxicity and significant up-regulation of mRNA expression	Green synthesis AuNPs	[35]
Gastric buffer	Showed lesser toxicity	Cabotegravir - biodegradable gold nanoparticles	[36]

physiological conditions compared to citrate capped nanoparticles, which aggregated.

Ajdari et al. [39] investigated AuNPs interactions in blood using thromboelastography as a rapid screening tool to monitor their influence on blood coagulation. The 1.2 nM colloidal AuNPs ranging from 12 to 85 nm do not affect the blood. However, 5 nM AuNPs demonstrate pro-thrombogenic concentration-dependent effects with a reduction in clot formation.

To better understand the interaction of AuNPs with common human blood proteins, [40] performed absorbance, fluorescence quenching, circular dichroism, dynamic light scattering, and electron microscopy measurements on surface-functionalized water-soluble AuNPs having a diameter range from 5 to 100 nm in the presence of common human blood proteins: albumin, fibrinogen, ã-globulin, histone, and insulin. It was found that the gold NPs strongly associate with these essential blood proteins where the binding constant, *K*, and the degree of cooperativity of particle"protein binding (Hill constant, *n*), depends on particle size and the native protein structure. Further, is also found tentative evidence that the model proteins undergo conformational change upon association with the NPs and that the thickness of the adsorbed protein layer (bare NP diameter <50 nm) progressively increases with NP size. These effects have potential general importance for understanding NP aggregation in biological media and the interaction of NP with biological materials broadly.

While studying the protein adsorption, blood cell aggregation, and C3 adsorption onto AuNPs to evaluate their complement activation potential and blood compatibility, it has been observed that these nanoparticles do not induce any complement activation or blood cell aggregation [41]. It has also been reported that particles were non-hemolytic, and the adsorptions of proteins were negligible, further validating its significance in drug delivery and gene delivery applications.

An attempt has been made to evaluate the protein adsorption, blood compatibility and complement activation potential of two batches of Swarna bhasma preparation, along with its physicochemical characterization [42]. Red blood cell hemolysis, aggregation studies with blood cells, protein adsorption, complement C3 adsorption, platelet activation and tight junction permeability in the Caco-2 cell line were investigated. It was reported that the Swarna bhasma preparations with a crystallite size of 28-35 nm did not induce any blood cell aggregation or protein adsorption. The activation potential of these preparations towards the complement system or platelets was negligible. These particles were also non-cytotoxic. Swarna bhasma particles opened the tight junctions in Caco-2 cell experiments. The results suggest the application of Swarna bhasma preparations as a therapeutic agent in clinical medicine from a biological safety point of view.

He et al. [43] investigated the possible effects of polyethene glycol-coated AuNPs (PEG@AuNPs) and citric acid-coated AuNPs (CT-AuNPs) on the blood cell function and distribution of those nanoparticles in blood components including erythrocytes, leukocytes, platelets (PLTs) cells and plasma. It was found that the amount of CT-AuNPs engulfed by leukocytes was four folds more compared to PEG@AuNPs, indicating that PEGylation might have the ability to escape the immune system. It is also reported that each leukocyte uptake more AuNPs particles than individual platelet.

Ma et al. [44] described a universal bio-conjugation approach that uses a new recombinant fusion protein combining two distinct domains. These researchers have identified and characterized the remarkable ability to bind gold nanoparticles (GNPs) by forming

gold–sulfur bonds (Au–S). The C-terminal part of this multi-domain construct is the SpyCatcher from *Streptococcus pyogenes*, which provides the ability to capture recombinant proteins encoding a SpyTag. It was shown that SpyCatcher could be immobilized covalently on GNPs through GST without losing its full functionality. It was also demonstrated that GST-SpyCatcher activated particles can covalently bind a SpyTag modified protein by simple mixing through the spontaneous formation of an unusual isopeptide bond.

Once nanoparticles enter the bloodstream, they become in contact with the different components of the blood and can potentially interfere with normal platelet function leading to bleeding or thrombosis [45]. As metallic NPs have already been used for diagnosis and treatment due to their unique characteristics, the potential interactions between metallic NPs and platelets have not been widely studied and reported. This review article focuses on the factors that can affect platelet activation and aggregation by metal NPs and the nature of such interactions, providing a summary of the effect of various metal NPs on platelet function available in the literature [45].

A first-time investigation on the effects of polymeric, metallic and nonmetallic nanoparticles on red blood cells' hemocompatibility was done by Mehrizi [46]. The authors reviewed the reported impacts of polymeric, metallic and carbon-based nanoparticles on Red Blood Cells (RBCs). Their study results have shown that using negatively charged dendrimers, unsaturated/uncharged liposomes, and PEGylated forms of NPs and RBCs are the best approaches to improve the hemocompatibility conditions of red blood cells. However, large cationic dendrimers, liposomes composed of saturated lipid with long acyl chains, and cationic chitosan nanoparticles have less RBC compatibility. In addition, polymeric nanoparticles have more surface modification capacity, making it possible to make more hemocompatible derivatives. Among metallic nanoparticles, gold and iron nanoparticles were more RBC compatible. However, the smaller size, higher concentration and longer exposure time of these nanoparticles can induce hemolysis and morphological changes in RBCs. On the other side, nonmetallic nanoparticles mostly had poor RBC compatibility, but their effects on RBCs strongly depended on their concentration and physicochemical properties and could be controllable. As a result, the use of polyethene glycol (PEG), gold, polymeric, and iron nanoparticles in the design of protocols to maintain the survival, structure and activity of red blood cells for improving hemocompatibility can be more effective.

Is it possible to alter nanoparticles from the toxic nature to make non-toxic nature?

Since nanoparticles have a wide range of applications in biomedicine and as drug delivery carriers, developing biocompatible and non-toxic nanomaterials is critical. Understanding the mechanism of nanoparticle toxicity will help researchers create nanoparticles that are less harmful to the environment. The redesign techniques must be chosen based on the principal mechanism of toxicity, as well as what changes to the nanomaterial can be made without affecting its ability to perform in its intended use. Nanomaterials can be constructed to have a negative surface charge, employ ligands like polyethylene glycol to inhibit protein binding, or have a shape that discourages binding with a cell surface to limit interactions with the cell surface. The toxic species can be replaced by less harmful components with similar characteristics to reduce nanoparticle dissolution to toxic ions. The nanoparticle can be capped with shell material, and the nanoparticle's morphology can be chosen to reduce surface area and therefore disintegration.

In addition, a chelating agent can be co-introduced or functionalized into the nanomaterials' surface. The band gap of the material can be modified either by utilizing various elements or by doping, a shell layer can be added to prevent direct contact with the core, or antioxidant molecules can be attached to the nanoparticle surface to limit the generation of reactive oxygen species. It's critical to examine whether a redesign method minimizes toxicity to species in relevant environmental compartments while redesigning nanoparticles. It's also important to make sure the nanomaterial retains the crucial physicochemical features that led to its inclusion in a product or device.

Conclusion

Undoubtedly, gold nanoparticles (AuNPs) are by far the most studied nanomaterials, primarily due to their immense potential in biomedical applications. As a consequence, it is obvious that huge demands surfaced to evaluate the health impact of these materials. Certain aspects could force us to believe the toxicity threat of AuNPs.

For instance, small-sized AuNPs may have been associated with toxicity, due to fact that their high surface area relative to their volume. This leads to enlarged absorption capacity and may increase the chance of interacting with biomolecules, effectively [47]. Secondly, AuNPs are believed to be the least toxic, and thus the most appropriate for biological/medical applications. However, due to their low rate of clearance from circulation streams and tissues, they may lead to health problems [48]. Further, the toxicological behavior of gold nanoparticles can be influenced by the physicochemical properties, including size, shape, surface charge, and other factors, such as methods used in the synthesis of gold nanoparticles, models used, dose, *in vivo* route of administration, and interference of gold nanoparticles with *in vitro* toxicity assay systems.

Most engineered nanoparticles are far less toxic than household cleaning products, insecticides used on family pets, and over-the-counter dandruff remedies. Certainly, the nanoparticles used as drug carriers for chemotherapeutics are much less toxic than the drugs they carry and are designed to carry drugs safely to tumors without harming organs and healthy tissue. Most importantly, this review points towards the toxicological aspect of AuNPs, albeit a few studies are denying that important fact. For time being, it may be reasonable to conclude here that more *in vivo* studies are necessary to precisely examine the effects of nanoplastics in human physiology, together with accurate quantification of environmental nanoparticle loads and a more standardized methodology to address the confounding variability of in vitro approaches.

Future scope

There is a great scope for this ever-increasing research. To elaborate, the toxicity and biodistribution profile of differently sized AuNPs still remains controversial and incomplete, thus hindering their further applications. But, the positive ray of hope is that several results of the biodistribution show that AuNPs with larger sizes, approximately 42.5 and 61.2 nm, accumulated mainly in liver and spleen while little or none were found in heart, kidney and lung.

On the other hand, smaller ones, approximately 6.2 and 24.3 nm, are distributed not only in liver and spleen but also in other organs. Additionally, most of the AuNPs were excreted out in less than 30 days, whereas there were still bits of remains in liver and spleen up to 90 days, especially for the 42.5 and 61.2 nm Au NPs. These findings are meaningful for the design of the AuNPs in the biomedical fields in the ensuing days.

Acknowledgements

The corresponding author (Dr P S Brahmanandam) wishes express his sincere gratitude towards the management (Shri Vishnu Educational Society) of Shri Vishnu Engineering College for Women (A), Vishnupur, Bhimavaram, India for their logistic facilities, without which it would have not been possible for us to carry out this work.

References

1. P. S. Brahmanandam, K. K. J. Chakravarthy, G. Ramakrishnam Raju, N. S. Rao, M. Satyavani, V. Naveen Kumar, Rama Krishna Alla, K Ganesh Kadiyala, P Vinay, Ch Rao, E Laxmi Narsaiah, L Satish, Feasible Solutions and Role of Nanomaterials in Combating the COVID-19 Pandemic: A Preliminary Study, J Trends in Biomaterials and Artificial Organs, 34(S2), pp. 44-51, (2020).
2. Kus-Liœkiewicz, M., P. Fickers, I. Ben Tahar, Biocompatibility and Cytotoxicity of Gold Nanoparticles: Recent Advances in Methodologies and Regulations, International journal of molecular sciences, 22(20), 10952. (2021).
3. S. C. Sahu, A. W. Hayes, Toxicity of nanomaterials found in human environment: A literature review, Toxicology Research and Application, 1, 1-13, (2017).
4. D. Mohanta, S. Patnaik, S. Sood, N. Das, Carbon nanotubes: Evaluation of toxicity at biointerfaces, J Pharm Anal., 9(5), 293-300. (2019).
5. Meike van der Zande, Rüdiger Junker, X. Frank Walboomers, and John A. Jansen, Carbon Nanotubes in Animal Models: A Systematic Review on Toxic Potential, Tissue Engineering Part B: Reviews, 17 (1), 57-69 (2011).
6. D. P. O'Neal, L. R. Hirsch, N. J. Halas, J. D. Payne, J. L. West, Photothermal tumor ablation in mice using near infrared-absorbing nanoparticles. Cancer Lett., 209, 171–176. (2004).
7. H. Chen, X. Kou, Z. Yang, W. Ni, J. Wang, Shape- and size-dependent refractive index sensitivity of gold nanoparticles. Langmuir 24, 5233–5237 (2008).
8. S. L. Li, T. Zhang, T. Wang, L. Li, C. Wang, Z. Su, The facile synthesis of hollow Au nanoflowers for synergistic chemo-photothermal cancer therapy, Chem. Commun. 51, 14338–14341 (2015).
9. T. J. Xiao, D. Huang, D. Wang, T. Meng, X. Yang, Au and Au-Based nanomaterials: synthesis and recent progress in electrochemical sensor applications. Talanta 206:120210 (2019).
10. X. Hu, Y. Zhang, T. Ding, J. Liu, H. Zhao, Multifunctional Gold Nanoparticles: A Novel Nanomaterial for Various Medical Applications and Biological Activities, Front Bioengineering and Biotechnology, 8 (1), 990 (2020).
11. Freitas de Freitas L, G. H. C. Varca, J. G. Dos Santos Batista, A. Benévolo Lugão, An Overview of the Synthesis of Gold Nanoparticles Using Radiation Technologies, Nanomaterials (Basel), 8(11), 939. (2018)
12. D. Pissuwan, G. Camilla, S. Mongkolsuk, M. B. Cortie, Single and multiple detections of foodborne pathogens by gold nanoparticle assays, *WIREs* Nanomed. Nanobiotechnology, 12, 584 (2019).
13. A. Gerber, M. Bundschuh, D. Klingelhofer, et al., Gold nanoparticles: recent aspects for human toxicology, J Occup Med Toxicol., 8, 32 (2013).
14. J. M. Slocik, M. O. Stone, R. R. Naik, Synthesis of gold nanoparticles using multifunctional peptides, *Small* 1, 1048–1052 (2005).
15. Jazayeri et al., Various methods of gold nanoparticles (GNPs) conjugation to antibodies, Sensing and Bio-sensing Research, 9, 22, (2016).
16. V. Ramalingam, Multi-functionality of gold nanoparticles: plausible and convincing properties, *Adv. Colloid Int. Sci.,* 271, 101989 (2019).
17. Zhang et al., Toxicological effects of gold nanoparticles in vivo by different administration routes, International Journal of Nano-medicine, 5, 771, (2010).
18. X.-D. Zhang, Wu, Shen, Liu, Sun, Zhang, Fan, Size-dependent in vivo toxicity of PEG-coated gold nanoparticles, International Journal of Nano-medicine, 2071, (2011).
19. R. Balansky, R., Longobardi, M., Ganchev, G., Iltcheva, M., Nedyalkov, N., Atanasov, P., Toshkova, R., De Flora, S., and A. Izzotti, Transplacental clastogenic and epigenetic effects of gold nanoparticles in mice, Mutation Research - Fundamental and Molecular Mechanisms of Mutagenesis, *751-752*(1), 42-48 (2013).
20. E. Cardoso, G. T. Rezin, Zanoni ET et al. Acute and chronic administration of gold nanoparticles cause DNA damage in the cerebral cortex of adult rats. Mutat. Res. 766–767, 25–30 (2014).
21. Han et al., Pulmonary Responses of Sprague-Dawley Rats in Single Inhalation Exposure to Graphene Oxide Nanomaterials, BioMed Research International, (full reference) (2015).
22. Fracasso et al., Evaluation of potential acute cardio toxicity of biodegradable nanocapsules in rats by intravenous administration, Toxicology Research, 5(1), 168 (2016).
23. R. H. Elbakary, Okasha EF, Hassan Ragab AM, Ragab MH, Histological Effects of Gold Nanoparticles on the Lung Tissue of Adult Male Albino Rats, J Microsc Ultrastruct, 6(2),116 (2018).
24. Yahyaei, Behrooz et al., Effects of biologically produced gold nanoparticles: toxicity assessment in different rat organs after intraperitoneal injection, AMB Express, 9 (1), 38, (2019).
25. J. K. Kim, Kim, H.P., Park, J.D. et al, Lung retention and particokinetics of silver and gold nanoparticles in rats following subacute inhalation co-exposure, Part Fibre Toxicol 18, 5 (2021).
26. F. S. Aljohani, Hamed, M.T., Bakr, B.A. et al,. In vivo bio-distribution and acute toxicity evaluation of greenly synthesized ultra-small gold nanoparticles with different biological activities, Sci. Rep 12, 6269 (2022).
27. Y. Pan, Neuss, S., Leifert, A., Fischler, M., Wen, F., Simon, U., Schmid, G., Brandau, W. and W. Jahnen-Dechent, Size-Dependent Cytotoxicity of Gold Nanoparticles, Small, 3: 1941-1949 (2007).
28. C-T Ng, Li JJ, Gurung RL, et al., Toxicological profile of small airway epithelial cells exposed to gold nanoparticles. Experimental Biology and Medicine, 238(12), 1355 (2013).
29. Bucchianico Di, Sebastiano et al., Aneuploidogenic effects and DNA oxidation induced in vitro by differently sized gold nanoparticles, International journal of nanomedicine, 9, 2191 (2014).
30. M. A. Vetten MA, Tlotleng N, Tanner Rascher D, et al., Label-free in vitro toxicity and uptake assessment of citrate stabilised gold nanoparticles in three cell lines, Part Fibre Toxicol., 10(1), 50 (2013).
31. Futyra et al., Development of Noncytotoxic Chitosan–Gold Nanocomposites as Efficient Antibacterial Materials, ACS Applied Materials & Interfaces, (Full reference)
32. J. M. George, Millicent Magogotya, Melissa A. Vetten, Antoinette V. Buys, Mary Gulumian, From the Cover: An Investigation of the Genotoxicity and Interference of Gold Nanoparticles in Commonly Used *In Vitro* Mutagenicity and Genotoxicity Assays, *Toxicological Sciences*, 156 (1), 149, (2017).
33. Li Xiaomin Li, Zhenpeng Hu, Jinlong Ma, Xinyu Wang, Yapei Zhang, Wei Wang, Zhi Yuan, The systematic evaluation of size-dependent toxicity and multi-time biodistribution of gold nanoparticles, Colloids and Surfaces B: Bio-interfaces,167, 260 (2018).
34. Jeyarani et al., Biomimetic gold nanoparticles for its cytotoxicity and biocompatibility evidenced by fluorescence-based assays in cancer (MDA-MB-231) and non-cancerous (HEK-293) cells, Journal of Photochemistry and Photobiology B: Biology, 202, (2020).
35. Amale et al., Gold nanoparticles loaded into niosomes: A novel approach for enhanced antitumor activity against human ovarian cancer, Advanced Powder Technology, 32 (12), 4711 (2021).
36. P. Rawat, S. S. Imam, and S. Gupta, Formulation of Cabotegravir Loaded Gold Nanoparticles: Optimization, Characterization to In-Vitro Cytotoxicity Study, J Clust Sci. (2022).
37. Saptarshi, S.R., Duschl, A. and Lopata, A.L. Interaction of nanoparticles with proteins: relation to bio-reactivity of the nanoparticle. J Nanobiotechnol., 11**,** 26 (2013).
38. Kumar et al., Green synthesis of gold nanoparticles with Zingiber officinale extract: Characterization and blood compatibility, Process Biochemistry, 46 (10), 2007 (2011).
39. Ajdari et al., Gold nanoparticle interactions in human blood: a model evaluation, Nanomedicine: Nanotechnology, Biology and Medicine, 13 (4), 1531 (2017).
40. Lacedra et al., Interaction of Gold Nanoparticles with common Human Blood Proteins, ACS Nano, 4(1), 365 (2010).
41. Nimi, N., Paul, W. and Sharma, C.P., Blood protein adsorption and compatibility studies of gold nanoparticles, Gold Bull, 44**,** 15 (2011).
42. Paul W, Sharma CP. Blood compatibility studies of Swarna bhasma (gold bhasma), an Ayurvedic drug. International Journal of Ayurveda Research, 2(1), 14 (2011).
43. He et al., The effects of gold nanoparticles on the human blood functions, Artificial Cells, Nanomedicine, and Biotechnology, 46, 720 (2018).
44. Ma, W., Saccardo, A., Roccatano, D. *et al.* Modular assembly of proteins on nanoparticles. Nat Commun, 9, 1489 (2018).
45. Hante NK, Medina C, Santos-Martinez MJ. Effect on Platelet Function of Metal-Based Nanoparticles Developed for Medical Applications. Front Cardiovasc Med. 18, 139 (2019).

46. Tahereh Zadeh Mehrizi, Hemocompatibility and Hemolytic Effects of Functionalized Nanoparticles on Red Blood Cells: A Recent Review Study, Nano, (full reference)
47. Jain et al., Calculated Absorption and Scattering Properties of Gold Nanoparticles of Different Size, Shape, and Composition: Applications in Biological Imaging and Biomedicine, The Journal of Physical Chemistry B, (2006).
48. K. Murali, M. S. Neelakandan, S. Thomas, Biomedical applications of gold nanoparticles, JSM Nanotechnol. Nanomed., 6, 1064 (2018).
49. Y. C. Dong, Hajfathalian, M., Maidment, P.S.N. et al. Effect of Gold Nanoparticle Size on Their Properties as Contrast Agents for Computed Tomography, Sci Rep 9, 14912 (2019).

INTERNATIONAL RESEARCH JOURNAL OF SCIENCE ENGINEERING AND TECHNOLOGY

ISSN 2454-3195

An Internationally Indexed Peer Reviewed & Refereed Journal

WWW.RJSET.COM
www.isarasolutions.com

Published by iSaRa Solutions

SHALL LITERATURE BE GENDERED?

K. Neelima *, V.Narasimhaswamy Pamarti ** ,

Department of English

B.V.Raju College, Vishnupur, Bhimavaram, West Godavari district, Andhra Pradesh

Abstract :The gender of literature has been explained through the works of some famous writings, such as, Sonnet 116 of Shakespeare; in which love is unchangeable. The gender of the poem is love. Doctor Faustus by Christopher Marlowe where thirst for knowledge becomes folly. The gender in the drama is stupidity. The Rape of the Lock by Alexander Pope which tells the pride of some characters in the poem, gender in the poem is pride. Pride and Prejudice by Jane Austen. It helps the rare men and women who live with great respect and come down for their love. The gender of the novel is living with great respect. Pigmalion by George Bernard Shaw, which tells the change of relationship between teacher and student. The gender in the play is love between creator and creature. The Great Gatsby by F Scott Fitzgerald, which has the inner meaning of mortal love, power and wealth, above which the life is more precious. Finally the literature's gender explained as it is for all.

Introduction

The gender of literature is life. Literature is neither male nor female. But it is more than all the barriers. It is better explained through some of the great works of the English writers. Life indeed has many things to ponder over. But others are individuals by themselves. Literature is the mirror of life, is a saying that simply describes the partiality of literature. It has got nothing with negativity. It stands with everyone and everything in the world. Literature is friend of all. It has no special place for few peoples. It pours praises on saints and guides sinners towards right path. It is a constitution to kings and consolation to the oppressed. For the betterment of the world it stands, and lighthouse to the wandering ships in the darkness.

Literature for few can be gendered as male or female. For it is not fixed to one, but it changes according to time and context; that who, when, what, where and why. Who in the works of literature is speaking, when the person is speaking, what is being spoken, where is it spoken and why is it spoken. The person can be speaking from the male point of view or if female, as the world has many groups like patriots, feminists and anthropologists. Though reason able they are, literature is above them, that it speaks of the world.

Explanation

In the poem Sonnet 116, Shakespeare speaks of the unchangeable love even when there are changes in life. The Love is unmovable and like the lighthouse to the mankind, who all suffer loneliness. Many can be the problems but love cannot be shaken. The world may change as the time moves and the beauty may wither but love will never be shaken. Therefore literature has the gender of love, that explains the reality of life with love. Shakespeare in his words wanted to talk to his lady love. He wished that his lady love would be content by this poem and what he wrote is infact truth. Very few can love without any expectations. Because, many expect something in return for their love. Though a person is wise if he doesn't love, the wisdom of the person is in vain. For love has patience, it is kind, merciful,

never speaks negatively, never was it pride, wasn't a selfish, love respects the person; so, let the world be filled with love. And literature is the only way to express the love.

Doctor Faustus, a play by Christopher Marlowe contemplates the life and death of doctor Faustus. Faustus was unsatisfied after having learnt everything in the world, and wanted to learn more. One day he came across the book of conjuring. He learnt everything from the book. And he subdued Mephistophilis, and with his help he abjured God and heaven for the sake of unnatural powers. He enjoyed all the bliss of the world in the illusion of the demons. Finally he was destroyed by Satan. Though he was a learned man, he has no love for truth. He just wanted the worldly pleasures, which lead his life into wrong path. Most of the people in the world do the same like doctor Faustus. They learn everything for the good cause of the world but after achieving what they wanted; they forget the truth and are addicted to the wealth and lusty for the worldly things. Most of the people in world are busy with earning money. They all wanted to become rich. They don't have any other thoughts. Their education began with a good motif. Once they have achieved the goal, they forgot the motivation and became selfish. Very few in the world did good to society. Everything in the world has become capitalistic. Even service to the poor and the downtrodden has become money minded. The gender of the play is folly towards the end. So, literature through this play says that most of the men in the world are avaricious. They in the beginning think that serving the society is easy. They later found it hard just because of the selfishness grew in them. Literature always enlightens mankind. They are living a life of harshness by being selfish. At first harsh towards themselves and then harsh towards the others. Literature throws awareness in the world, to bring consciousness to what is happening to them. They are killing each other for the sake of wealth which is temporary. They are running all around for it. Being content with what they have is better than dying for the accumulation of wealth.

Alexander Pope wrote "The Rape of the Lock". It tells the story of the aristocrats' pride. They all gather in parties, where they want to showcase the maintenance of new styles in their dressing and cosmetics. A woman among them was Belinda, whose locks were cut by lord Baron. He cut the lock because she did not accept the ball-dance with him. And then the poem begins with all the Ariels and Umbriels, who assisted Belinda while she was sleeping. Pope had added a lot of imagination to the poem, which explains the beauty of physical world and the ugliness of spiritual world in the lifestyle of aristocrats. However, literature is indirectly used to expose the malicious heart of the aristocratic society. People in all generations are self centred. They don't bother about what is happening to others. The riches they enjoy is not theirs, but they feel that they have toiled for that. They just live a life that's filled with fooling themselves, and finally die doing nothing. The folly is, nothing can a man take with him when he was dead. Literature in truth says that, these people live in nothingness. Life is not just parties and fun. It has love, patience, mercy, faith and responsibilities; which are lacking in these fools. Loving whole world is what really meant, having patience towards every individual is what really required, merciful not just for family members but towards all. Do not judge everyone, but try to have faith in them. Responsibility towards not just family and job, but to be a good citizen. All should endure the responsibility of citizenship by being helpful to all those who are weak.

Jane Austen in her Novels mostly exposed the problems women face in family matters and even with the society. She as well brought up some women characters who had overcome such hurdles with their prudence. One of those was the novel 'Pride and Prejudice' which tells the story of a women and a men, who experienced the painful situations where they were degraded eventhough they are great in heart. They were seen as angry and serious characters by others, since they cannot accept the truth of falsehood.

But their goodness was gradually progressive as the novel moved on. However, Jane Austen with this great piece of her work wanted to say that, all men and women are equal; and they have to be happy and loving each other in their equality, but not fighting for the rights. By her novel the world has got a great lesson that, neither women nor men are superior over the other person in their martial relationship. There should not be any patriotism or feminism. Many people think that Jane Austen is a feminist. With this novel in fact she proved her beautiful nature to all the mankind that, she had a heart to bring family in unity. Therefore literature is universal and it is for everyone to love and live in solidarity and fraternity. This may not be acceptable to many but it is the truth to be accepted. Love is truth, so, let us love one another. Never treat a woman with less respect. She can be your mother, sister, daughter or friend. Respect her and don't stop her from thinking for she will be another Jane Austen. Literature has been giving birth to some greats like Jane Austen, and one day it can be one of us. Thanks to literature.

George Bernard Shaw's 'Pygmalion' brings up the love between teacher and disciple. Though it was a gradual growth of love, it has a great impact of both professor Henry Higgins and Eliza Doolittle. This play was about passing Eliza as a duchess though she was not a Duchess perhaps. It was a great challenge from the part of Henry Higgins. Professor and Eliza were always in quarrel on their way to achieve the challenge. Finally the day had come, Higgins presented her in a party where she was assumed to be duchess of a town. And many rich young men of great wealth tried to woo her. Even many rich women spoke of her beauty, that she had become the centre of attraction to all of them. All credit belongs to Higgins but Eliza did not accept it, and said that it is her own hard work. The play is ultimately about the love between creator and creature. It is a fact that the creator kindles love for his work of art. Literature has the gender of portraying the love between parents and children. Parents are the ones through whom children are born, in the same manner the creator loves his created thing. He never let that be taken away or be destroyed. He gives all his life for the being. He cannot bear the pain of his created thing and keeps it endlessly.

F. Scott Fitzgerald, had produced a wonderful novel, 'The Great Gatsby', which speaks about the differences between upper class society and lower class society. Though the lower class are richer than the upper class, the upper class never accept them. The protagonist also have experienced the same with this problem. And he finally died. The upper class had just got the habit of using the lower class for their need. If they are not needed, the upper class don't bother about them. Daisy the upper class woman, fell in love with Jay Gatsby. She spent many happy moments with him, but married Tom Buchanan, a wealthy upper class man. Ones Jay Gatsby had become richer than Tom Buchanan, she returned to him but Tom had him killed by George B Wilson the husband of Myrtle Wilson, who was killed by Daisy Buchanan accidentally. However the upper class prevailed over the lower class. Again Daisy returned to Tom Buchanan. In this novel the gender of literature shows that, how class differences had played role among people who are common in all things. 'Class' is created by human beings to kill eachother. Therefore, literature with the help of F. Scott Fitzgerald tells whole world to be united in love rather divided by wealth. Life is precious than all the mortal love, power and wealth. The love of the woman who wants money is always dangerous. Above all the person who gives importance to his community is too dangerous. More than all these things life is precious and we have to live it more happily by sharing the happiness to all.

Critique :The gender of the literature is such, that it is ultimately universal. Literature belongs to everyone and everything in the world. All that was expressed by literature expressed; has different meanings, experiences and facts; which happen always to every generation and to every individual. They

would surely help the personalities to be aware and to realise their role in the world, that would be careful and selfless towards the world and the situations to come. Literature consoles those who are in distress. It encourages the ones who are fallen. Moralises those who are immoral. Brings unity amidst the broken familys and relationships. It tells men that all are equal. To some loving one another. Whether the world is aware or not, literature always backs the world with its strongest thoughts. Literature as it is said the mirror of life. And it is not the life of one person or one country or one language but belongs to whole world. The ultimate solution for every problem is literature. All those who are weary can rest in the lap of literature.

Conclusion:The gender of literature does not mean that it belongs to one particular gender. But few people think that it is for men. Few say that literature is there to support their gender. Few say that literature is for their people or language. But time brings every solution through literature. Finally it is not just for one but for all.

References

1.https://www.poetryfoundation.org/poems/45106/sonnet-116-let-me-not-to-the-marriage-of-true-minds

2. https://en.m.wikipedia.org/wiki/Doctor_Faustus_(play)

3. https://en.m.wikipedia.org/wiki/The_Rape_of_the_Lock

4. https://en.m.wikipedia.org/wiki/Pride_and_Prejudice

5. https://en.m.wikipedia.org/wiki/Pygmalion_(play)

6. https://en.m.wikipedia.org/wiki/The_Great_Gatsby

International Journal of Science and Research (IJSR)
ISSN: 2319-7064
SJIF (2022): 7.942

Numerical Study of Higher Order Differential Equations Using Differential Transform Method

P. L. Suresh[1], Ch. Satyanarayana[2]

[1]Lecturer, Department of Mathematics, B V Raju Degree College, Bhimavaram, West Godavari Dt. Andhra Pradesh, India
Email: *p.arunasuresh[at]gmail.com*

[2]Lecturer, Department of Mathematics, B V Raju Degree College, Bhimavaram, West Godavari Dt. Andhra Pradesh, India

Abstract: ***In this article the Differential Transform method is working for obtaining solutions for higher order differential equations. This proposed technique gives the series of solutions which can be easily converted to exact ones. The differential transform method was productively applied to higher order differential equations The results of the study has established that the method is easy , effective and flexible. The result of the differential transform method is in good agreement with those obtained by using the already existing ones.***

Keywords: Differential Transform, Higher order differential equations, Taylor's Series

1. Introduction

Nonlinear phenomena have significant effects in applied mathematics, physics and related to engineering; many such physical phenomena are modeled in terms of nonlinear differential equations [3,4,10]. A variety of numerical and analytical methods have been developed to obtain precise approximate and analytic solutions for the problems in the literature [3,7,8,10,11,12]. The classical Taylor's series method is one of the earliest analytic techniques to many problems, especially ordinary differential equations. However, since it requires a lot of symbolic calculation for the derivatives of functions, it takes a lot of computational time for higher derivatives. Here, we introduce the update version of the Taylor series method which is called the differential transform method (DTM)[4,5]. The (DTM) is the method to determine the coefficients of the Taylor series of the function by solving the induced recursive equation from the given differential equation. The basic idea of the (DTM) was introduced by Zhou [5]. In what follows we introduce a few notations for the (DTM).

2. The Differential Transform Method

The transformation of the k th derivative of a function y(x) in one variable is defined as follows

$$Y(k) = \frac{1}{k!}\left[\frac{d^k(y(x))}{dx^k}\right]_{x=0} \quad (1)$$

and the inverse transform of Y(k) is defined as

$$y(x) = \sum_{k=0}^{\infty} Y(k)x^k \quad (2)$$

The following are the important theorems of the one dimensional differential transform method

Theorem 1: If then $Y(k) = M(k) \pm N(k)$

Theorem 2: If $y(x) = \alpha m(x)$, they$(x) = m(x) \pm n(x)$, $Y(k) = \alpha M(k)$

Theorem 3: If $y(x) = \frac{dm(x)}{dx}$, then $Y(k) = (K+1)Y(k+1)$

Theorem 4: If $y(x) = m(x)n(x)$, then $Y(k) = \sum_{r=0}^{k} M(r)N(k-r)$

Theorem 5: If $y(x) = x^l$, then $Y(k) = \delta(k-l) = \begin{cases} 1, \text{if } k = l \\ 0, \text{if } k \neq l \end{cases}$

Theorem 6: If $y(x) = \frac{d^2g(x)}{dx^2}$ then $Y(k) = (k+1)(k+2G(k+2)$

Theorem 7: If $y(x) = \frac{d^m g(x)}{dx^m}$ then $Y(K) = (k+1)(k+2+\ldots+k+mG(k+m)$

Theorem 8: If $y(x) = 1$ then $Y(k) = \delta(k)$

Theorem 9: If $y(x) = x$ then $Y(k) = \delta(k-1)$

Theorem 10: If $y(x) = e^{ax}$ then $Y(k) = \frac{a^k}{k!}$

Theorem 11: $If\ y(x) = (1+x)^m\ then\ Y(k) = \frac{m(m-1)(m-2)\ldots(m-k+1)}{k!}$

Theorem 12: $If\ y(x) = \sin(wx+\alpha)\ then\ Y(k) = \frac{w^k}{k!}sin(k\pi+\alpha)$

Theorem 13: $If\ y(x) = \cos(wx+\alpha)\ then\ Y(k) = \frac{w^k}{k!}cos(k\pi+\alpha)$ *where w and α are constants*

3. Applications

In this section, we apply the (DTM) to some ordinary differential equations

Problem 1: Consider the following initial value problem

$\frac{d^2y}{dx^2} - 2p\frac{dy}{dx} + p^2y = e^{px}, p(\neq 0) is\ a\ real\ number, given\ that\ y(0) = 0, y(1) = 1/p$ (1)

Apply DTM to (1), we obtain

$$(k+2)(k+1)Y - 2p(k+1)Y(k+1) + p^2Y(k) = \frac{p^k}{k!}$$

$$put\ k = 0\ then\ 2Y(2) - 2pY(1) + p^2Y(0) = 1$$

$$2Y(2) - 2p\left(\frac{1}{p}\right) + p^2(0) = 1$$

$$Y(2) = \frac{1+2}{2} = \frac{3}{2}$$

Put k = 1, then $6Y(3) - 2pY(2) + p^2Y(1) = p$

$$6Y(3) - 2p\left(\frac{3}{2}\right) + p^2\left(\frac{1}{p}\right) = p$$

$$6Y(3) - p(3) + p = p$$

$$Y(3) = \frac{3p}{6}$$

And so on.

The solution is

$$y(x) = \sum_{k=0}^{\infty} Y(k)x^k$$

$$y(x) = Y(0)x^0 + Y(1)x^1 + Y(2)x^2 + Y(3)x^3 + \cdots$$

$$y(x) = 0.1 + \frac{1}{p}x + \frac{3}{2}x^2 + \frac{3p}{6}x^3 + \cdots.$$

$$y(x) = \frac{1}{p}x + \frac{3}{2}x^2 + \frac{p}{2}x^3 + \cdots$$

Problem 2: Consider the following initial value problem

$$\frac{d^2y}{dx^2} + l^2y = e^{lx} + sinlx + coslx, l(\neq 0) is\ areal\ number,$$
$$given\ that\ y(0) = 1, y(1) = l \qquad (2)$$

Apply DTM to (2), we obtain

$$(k+1)(k+2)Y(k+2) + l^2Y(k) = \frac{l^k}{k!} + \frac{l^k}{k!}sin(k\pi) + \frac{l^k}{k!}cos(k\pi)$$

Put k = 0, then $2Y(2) + l^2Y(0) = 1 + 0 + 1$

$$2Y(2) + l^2.1 = 2$$

$$Y(2) = \frac{2-l^2}{2}$$

Put k = 1, then $6Y(3) + l^2Y(1) = l + l(0) + l(-1)$

$$6Y(3) + l^2\left(\frac{2-l^2}{2}\right) = l$$

$$Y(3) = \frac{l - l^2\left(\frac{2-l^2}{2}\right)}{2} = \frac{2l - 2l^2 + l^4}{4}$$

And so on.
The solution is

$$y(x) = \sum_{k=0}^{\infty} Y(k)x^k$$

$$y(x) = Y(0)x^0 + Y(1)x^1 + Y(2)x^2 + Y(3)x^3 + \cdots$$

$$y(x) = 1.1 + lx + \frac{2-l^2}{2}x^2 + \frac{2l - 2l^2 + l^4}{4}x^3 + \cdots.$$

Problem 2: Consider the following initial value problem

$$\frac{d^3y}{dx^3} + a^2\frac{dy}{dx} = sinax, a(\neq 0) is\ areal\ number,$$
$$given\ that\ y(0) = 1, y(1) = a, y(2) = a^2 \qquad (3)$$

Apply DTM to (3), we obtain

$$(k+1)(k+2)(k+3)Y(k+3) + a^2(k+1)Y(k+1) = \frac{a^k}{k!}sin(k\pi)$$

Put k = 0, then $6Y(3) + a^2Y(1) = 0$

$$6Y(3) + a^2.a = 0$$

$$Y(3) = -a^3$$

Put k = 1, then $24Y(4) + a^2Y(2) = a.0$

$$24.Y(4) + a^2(-a^3) = 0$$

$$Y(4) = \frac{a^5}{24}$$

And so on.

The solution is

$$y(x) = \sum_{k=0}^{\infty} Y(k)x^k$$

$$y(x) = Y(0)x^0 + Y(1)x^1 + Y(2)x^2 + Y(3)x^3 + Y(4)x^4 + \cdots$$

$$y(x) = 1.1 + ax + a^2x^2 - a^3x^3 + \frac{a^5}{24}x^4 + \cdots.$$

4. Conclusion

The observations of the present study have shown that the (DTM) is easy to apply and effective. As a result, the conclusion comes through this work, is that the Differential Transform Method can be applied to a wide class of differential equations, due to the efficiency in the application to get the possible results.

References

[1] Ayaz.F, Solutions of system of differential equation by Differential Transform Method.Appl.Math.comput 2004.pp147-547-567.
[2] G.Adoman.R.Rack, On linear and nonlinear integro-differential equations. J. Math. Anal. Appl.113(1)(1986), pp. 117-120.
[3] Kaya.N.T. Comparing numerical methods for solutions of ordinary differential equations, Appl.Math. Lett, 17(2004)323-328.
[4] Liu.H and Y.Song, Differential Transform Method applied to higher index differential- algebraic equations. Appl.Math. Comput,2007,184-748-753.

[5] Zhou.J.K. Differential transformation Method and applications for electrical circuits, Huazhong University press, Wuhan, China, (1986)
[6] Onur Kiymaz, An Algorithm for Solving Initial Value Problems, using Laplace Adomian Decomposition Method. Applied Mathematical Sciences, Vol. 3, 2009, no. 30, 1453 - 1459
[7] E. Hesameddini, H. Latifizadeh. A new vision of the He's homotopy perturbation method. International Journal of Nonlinear Sciences and Numerical Simulation. 2009.
[8] E. Hesameddini, H. Latifizadeh. Reconstruction of variational iteration algorithms using the Laplace transform. International Journal of Nonlinear Sciences and Numerical Simulation. 2009.
[9] S.T. Mohyud-Din, M.A. Noor, K.I. Noor. Some relatively new techniques for nonlinear problems. Math. Porb.Eng. Article ID 234849, 25 pages, doi: 10.1155/2009/234849, 2009.
[10] S.T. Mohyud-Din, A. Yildirim. Variational iteration method for solving Klein- Gordon equations. Journal of Applied Mathematics, Statistics and Informatics.2010.
[11] Jagdev Singh, Devendra Kumar and Sushila Rathore, Application of Homotopy Perturbation Transform Method for Solving Linear and Nonlinear
[12] Klein- Gordon Equations, Journal of Information and Computing Science,ISSN 1746-765 England, UK,Vol. 7, No. 2, 2012, pp. 131-139.
[13] A. Yildirim. An Algorithm for Solving the Fractional Nonlinear Schröndinger Equation by Means of the Homotopy Perturbation Method. International Journal of Nonlinear Science and Numerical Simulation. 2009.
[14] Abbasbandy. S., 2006, "Homotopy perturbation method for quadratic Riccati differential equation and comparison with Adomian's decomposition method," Applied Mathematics and Computation, **172** (1), pp.485–490.
[15] Adomian, G., and Rach, R., 1986, "Solving nonlinear differential equations with decimal power nonlinearities," Journal of Mathematical Analysis and Applications, **114** (2), pp.423–425.
[16] Ahmadian, M., Mojahedi, M., and Moeenfard, H., 2009, "Free vibration analysis of a nonlinear beam using homotopy and modified lindstedt-poincare methods," Journal of Solid Mechanics, **1** (1), pp.29–36.
[17] AL-Jawary, M. A., and Al-Razaq, S. G., 2016, "A semi analytical iterative technique for solving Duffing equations," International Journal of Pure and Applied Mathematics, 108 (4), pp. 871–885.
[18] AL-Jawary, M. A., and Raham, R. K., 2016, "A semi-analytical iterative technique for solving chemistry problems," Journal of King Saud University, (In press).
[19] AL-Jawary, M. A., 2017, "A semi-analytical iterative method for solving nonlinear thin film flow problems," Chaos, Solitons and Fractals, **99**, pp.52–56.
[20] Aminikhah, H., 2013, "Approximate analytical solution for quadratic Riccati differential equation," Iranian Journal of Numerical Analysis and Optimization, **3** (2), pp.21–31.
[21] Anderson, B. D., and Moore, J. B., 1999, "Optimal control-linear quadratic methods," Prentice-Hall, New Jersey.
[22] Banach, S., 1922, "Sur les opérations dans les ensembles abstraits et leur application aux equations integrals," Fundamenta Mathematicae, **3**, pp. 133–181.
[23] Barari, A., Ganjavi, B., Jeloudar, M. G., and Domairry, G., 2010, "Assessment of two analytical methods in solving the linear and nonlinear elastic beam deformation problems," Journal of Engineering, Design and Technology, **8**, (2), pp.127–145.
[24] Barari, A., Omidvar, M., Ganji, D. D., and Tahmasebi, A. P., 2008, "An Approximate Solution for Boundary Value Problems in Structural Engineering and Fluid Mechanics**,"** Journal of Mathematical Problems in Engineering, Vol. 2008, pp.1–13.
[25] Lasiecka, I., and Tuffaha, A., 2007, "Riccati equations arising in boundary control of fluid structure interactions," International Journal of Computing Science and Mathematics, **1** (1), pp.128–146.